



Measurement of double-differential charged-current Drell–Yan cross-sections at high transverse masses in pp collisions at $\sqrt{s} = 13$ TeV with the ATLAS detector

The ATLAS Collaboration

This paper presents a first measurement of the cross-section for the charged-current Drell–Yan process $pp \rightarrow W^\pm \rightarrow \ell^\pm \nu$ above the resonance region, where ℓ is an electron or muon. The measurement is performed for transverse masses, m_T^W , between 200 GeV and 5000 GeV, using a sample of 140 fb^{-1} of pp collision data at a centre-of-mass energy of $\sqrt{s} = 13$ TeV collected by the ATLAS detector at the LHC during 2015–2018. The data are presented single differentially in transverse mass and double differentially in transverse mass and absolute lepton pseudorapidity. A test of lepton flavour universality shows no significant deviations from the Standard Model. The electron and muon channel measurements are combined to achieve a total experimental precision of 3% at low m_T^W . The single- and double differential W -boson charge asymmetries are evaluated from the measurements. A comparison to next-to-next-to-leading-order perturbative QCD predictions using several recent parton distribution functions and including next-to-leading-order electroweak effects indicates the potential of the data to constrain parton distribution functions. The data are also used to constrain four fermion operators in the Standard Model Effective Field Theory formalism, in particular the lepton-quark operator Wilson coefficient $c_{\ell q}^{(3)}$.

Contents

1	Introduction	3
2	ATLAS detector	4
3	Simulated event samples	5
4	Event reconstruction and selection	6
4.1	Object reconstruction and selection	6
4.2	Event selection	8
5	Background estimation	8
5.1	Top-quark background contribution	9
5.2	Multijet background estimate via the matrix method	9
5.3	Data and prediction comparisons	12
6	Cross-section measurement	15
6.1	Fiducial definition	15
6.2	Unfolding procedure	15
6.3	Event migration studies	16
6.4	Optimisation of number of iterations	16
6.5	Observed and predicted event yields	17
7	Systematic uncertainties	20
7.1	Electron channel	20
7.2	Muon channel	22
7.3	Common uncertainties	23
8	Results	25
8.1	Separate differential cross-sections in the electron and muon channels	25
8.2	Electron-muon ratios of charge-integrated cross-sections	26
8.3	Combination of electron and muon channels	27
8.4	Charge asymmetry of combined cross-sections	29
9	Interpretation and discussion	30
9.1	Comparison to QCD predictions	30
9.2	Effective Field Theory constraints	32
10	Conclusions	38

1 Introduction

The Drell–Yan process [1] of lepton pair production in hadronic interactions is a powerful tool in understanding the nature of partonic interactions and hadronic structure, and it can be a probe of the electroweak sector of the Standard Model. It has been fundamental in developing perturbative quantum chromodynamics (QCD) with calculations now available at next-to-next-to-next-to-leading-order (N³LO) accuracy [2–5].

Cross-section measurements from the Large Hadron Collider (LHC) of inclusive neutral-current ($pp \rightarrow Z/\gamma^* \rightarrow \ell^+\ell^-$) and charged-current ($pp \rightarrow W^\pm \rightarrow \ell^\pm\nu$) Drell–Yan processes at centre-of-mass energies of $\sqrt{s} = 5.02$ TeV, 13 TeV and at 13.6 TeV have recently been published by the ATLAS [6, 7], CMS [8–10] and LHCb [11] collaborations. These measurements, performed at the resonant peaks where event yields are very large and background contributions are extremely small, reach high experimental accuracy. They provide new constraints on the parton distribution functions (PDFs) of the proton and offer insights into the initial-state QCD radiation dynamics in vector boson production [6]. They are however restricted in the kinematic range of partonic momentum fraction x and four-momentum transfer $Q = m_{\ell\ell}$, where $m_{\ell\ell}$ denotes the invariant mass of the dilepton pair.

Measurements extending to lower or higher invariant masses have been performed in the neutral-current channel only [12–18] and access wider x and Q kinematic regions. At low Q the measurements are sensitive to QCD resummation effects. At large Q they are sensitive to new physics beyond the Standard Model and also provide new constraints on the poorly known high- x anti-quark PDFs.

The charged-current process is highly complementary to the neutral-current process. The charge-separated cross-sections for W^+ and W^- production depend on different flavour combinations, while the Z production depends on same-flavour combinations. The dominant partonic contributions are (u, \bar{d}) and (c, \bar{s}) for W^+ , and (d, \bar{u}) and (s, \bar{c}) for W^- production.

Since the final-state neutrino is not observed, the dilepton invariant mass cannot be experimentally determined, and the transverse mass m_T^W is used instead, defined by $m_T^W = \sqrt{2p_T^\ell p_T^\nu (1 - \cos \Delta\phi(\ell, \nu))}$. Here p_T^ℓ is the charged lepton transverse momentum, p_T^ν is the neutrino or missing transverse momentum, and $\Delta\phi(\ell, \nu)$ is the azimuthal angle between them.

To date no cross-section measurements of the charged-current process above the W -boson resonance region have been made. This kinematic region is of particular interest as at the highest transverse masses accessible at the LHC, the observed m_T^W spectrum in the decay to electron or muon final states is sensitive to new physics. Such effects could manifest as a localised resonance [19, 20], a violation of lepton flavour universality or an enhancement or suppression of the continuum spectrum. Modifications to the Standard Model predictions can be described in terms of an Effective Field Theory (EFT). In this formalism the Standard Model Lagrangian is extended with new operators which are suppressed by an energy cut-off scale. The charged-current Drell–Yan process is sensitive to operators which modify the couplings between fermions and the W -boson, and operators which allow for a direct interaction between four fermions without a mediator. The effects of four-fermion operators grow quadratically with energy, so the measurement of charged-current Drell–Yan at high m_T^W therefore provides strong sensitivity to such effects. This measurement is thus expected to provide electroweak precision tests that surpass LEP in sensitivity [21].

This article reports a first measurement of the cross-section for the process $pp \rightarrow \ell\nu + X$ above the W -boson resonance production region. The measurements are performed using a sample of 140 fb^{-1} of

pp collision data at $\sqrt{s} = 13$ TeV collected by the ATLAS detector at the LHC in both electron and muon channels. The double-differential measurement is reported as a function of m_{T}^{W} and absolute charged-lepton pseudorapidity $|\eta|$. The data are also presented as single-differential cross-sections $d\sigma/dm_{\text{T}}^{\text{W}}$. The data cover the kinematic region of $200 \leq m_{\text{T}}^{\text{W}} \leq 5000$ GeV and access partonic momentum fractions from $x \sim 10^{-2}$ up to $x \sim 1$.

2 ATLAS detector

The ATLAS detector [22] at the LHC covers nearly the entire solid angle around the collision point.¹ It consists of an inner tracking detector surrounded by a thin superconducting solenoid, electromagnetic (EM) and hadronic calorimeters, and a muon spectrometer incorporating three large superconducting air-core toroidal magnets.

The inner-detector system (ID) is immersed in a 2 T axial magnetic field and provides charged-particle tracking in the range $|\eta| < 2.5$. The high-granularity silicon pixel detector covers the vertex region and typically provides four measurements per track, the first hit generally being in the insertable B-layer (IBL) installed before Run 2 [23, 24]. It is followed by the SemiConductor Tracker (SCT), which usually provides eight measurements per track. These silicon detectors are complemented by the transition radiation tracker (TRT), which enables radially extended track reconstruction up to $|\eta| = 2.0$. The TRT also provides electron identification information based on the fraction of hits (typically 30 in total) above a higher energy-deposit threshold corresponding to transition radiation.

The calorimeter system covers the pseudorapidity range $|\eta| < 4.9$. Within the region $|\eta| < 3.2$, electromagnetic calorimetry is provided by barrel and endcap high-granularity lead/liquid-argon (LAr) calorimeters, with an additional thin LAr presampler covering $|\eta| < 1.8$ to correct for energy loss in material upstream of the calorimeters. Hadronic calorimetry is provided by the steel/scintillator-tile calorimeter, segmented into three barrel structures within $|\eta| < 1.7$, and two copper/LAr hadronic endcap calorimeters. The solid angle coverage is completed with forward copper/LAr and tungsten/LAr calorimeter modules optimised for electromagnetic and hadronic energy measurements respectively.

The muon spectrometer (MS) comprises separate trigger and high-precision tracking chambers measuring the deflection of muons in a magnetic field generated by the superconducting air-core toroidal magnets. The field integral of the toroids ranges between 2.0 and 6.0 T m across most of the detector. Three layers of precision chambers, each consisting of layers of monitored drift tubes, cover the region $|\eta| < 2.7$, complemented by cathode-strip chambers in the forward region, where the background is highest. The muon trigger system covers the range $|\eta| < 2.4$ with resistive-plate chambers in the barrel, and thin-gap chambers in the endcap regions.

The luminosity is measured mainly by the LUCID-2 [25] detector that records Cherenkov light produced in the quartz windows of photomultipliers located close to the beampipe.

¹ ATLAS uses a right-handed coordinate system with its origin at the nominal interaction point (IP) in the centre of the detector and the z -axis along the beam pipe. The x -axis points from the IP to the centre of the LHC ring, and the y -axis points upwards. Polar coordinates (r, ϕ) are used in the transverse plane, ϕ being the azimuthal angle around the z -axis. The pseudorapidity is defined in terms of the polar angle θ as $\eta = -\ln \tan(\theta/2)$ and is equal to the rapidity $y = \frac{1}{2} \ln \left(\frac{E+p_z}{E-p_z} \right)$ in the relativistic limit. Angular distance is measured in units of $\Delta R \equiv \sqrt{(\Delta y)^2 + (\Delta \phi)^2}$.

Events are selected by the first-level trigger system implemented in custom hardware, followed by selections made by algorithms implemented in software in the high-level trigger [26]. The first-level trigger accepts events from the 40 MHz bunch crossings at a rate close to 100 kHz, which the high-level trigger further reduces in order to record complete events to disk at about 1.25 kHz.

A software suite [27] is used in data simulation, in the reconstruction and analysis of real and simulated data, in detector operations, and in the trigger and data acquisition systems of the experiment.

3 Simulated event samples

Monte Carlo (MC) simulation samples are used to model the expected signal and background yields, with the exception of certain data-driven background estimates. The MC samples are normalised using higher-order cross-section predictions in perturbation theory.

The neutral and charged current Drell-Yan processes are generated at next-to-leading-order (NLO) using POWHEG BOX v1 [28–31] and the CT10_{NLO} PDF [32], with PYTHIA 8.1 [33] to model the parton showers (PS) and hadronisation. The effect of QED final-state radiation was simulated with PHOTOS++ 3.52 [34, 35]. The EVTGEN 1.2.0 program [36] was used to decay bottom and charm hadrons. This MC sample is hereafter referred to as the POWHEG+PYTHIA sample. Using invariant-mass dependent k -factors [37] these predictions are corrected to account for next-to-next-to-leading-order (NNLO) QCD and NLO electroweak (EW) effects. The QCD corrections are computed using V_{RAP} v0.9 [38] and also weight the predictions to the CT14_{NNLO} PDF set [39]. The EW corrections excluding QED final state radiation (FSR) are computed using MCSANC [40] and vary from about -3% at low m_T^W to about -10% at $m_T^W = 1$ TeV. The additive approach is used to combine the EW and QCD corrections.

An alternative simulation of the signal process is used for the assessment of systematic uncertainties arising from different modelling choices. It is generated using SHERPA 2.2.11 [41] at NLO in QCD for up to two additional partons and at LO for up to five partons, using the NNPDF3.0_{NNLO} PDF set [42]. The sample is then reweighted to the CT18_{NNLO} PDF set [43]. The prediction is corrected to approximate NNLO accuracy with a k -factor of 0.95 calculated using MATRIX v2 [44, 45]. NLO EW corrections are implemented in SHERPA. The exponentiated approach for combining EW and QCD corrections is used, which yields corrections lying between the additive and multiplicative approaches. The differences between all three corrections is however small and typically below 1%.

The background from $t\bar{t}$ production is the dominant background with isolated prompt leptons from electroweak boson decays. It is estimated at NLO using POWHEG BOX v2 [46] with a top-quark mass of $m_{\text{top}} = 172.5$ GeV and the NNPDF3.0_{NLO} PDF set [42], with PYTHIA 8.2 [47] for parton showering and hadronisation. The decays of bottom and charm hadrons were performed by EVTGEN 1.6.0. The $t\bar{t}$ MC samples are reweighted in the p_T of the top quark and in the mass of the $t\bar{t}$ pair to inclusive cross-section calculations at NNLO accuracy in QCD including NLO EW corrections [48]. The single-top-quark background, consisting of s - and t -channel processes and the tW process, is also simulated under the same conditions. The dynamic scale diagram subtraction scheme [49] is used to account for the interference between the tW and $t\bar{t}$ production diagrams.

Further important background contributions are due to diboson (WW , WZ and ZZ) production decaying into final states with at least one charged lepton. The diboson processes are generated with SHERPA 2.2.1 or SHERPA 2.2.2 depending on the process, using the NNPDF3.0_{NNLO} PDF set. They were generated using

matrix elements at NLO accuracy in QCD for up to one additional parton and at LO accuracy for up to three additional parton emissions.

All MC samples used in the analysis include the effects of QED FSR, multiple pp interactions per bunch crossing (“pile-up”), and detector simulation. The QED FSR is simulated using PHOTOS [50], except for samples generated by SHERPA which includes a native FSR simulation. The effect of pile-up was modelled by overlaying the simulated hard-scattering event with inelastic pp events generated with PYTHIA 8.1 using the NNPDF2.3_{LO} PDF set [51] and the A3 set of tuned parameters [52]. The interactions of particles with the detector are modelled using a full ATLAS detector simulation [53] based on GEANT4 [54]. Finally, several corrections are applied to the simulated samples, accounting for differences between data and simulation in the lepton trigger, reconstruction, identification, and isolation efficiencies as well as lepton resolution and muon momentum scale.

4 Event reconstruction and selection

Events are required to be recorded during stable beam condition periods and must pass detector and data-quality requirements [55]. Due to differences in the detector response to electrons and muons the nominal selection is optimised separately for each channel and is described in the following. In addition to the nominal selection two further selections are defined. Both correspond to less stringent selections needed for either the background estimation (“loose”) or in order to veto events with a second lepton (“veto”).

4.1 Object reconstruction and selection

4.1.1 Electrons

Electrons are reconstructed from clusters of energy deposited in the EM calorimeter and matched to tracks reconstructed in the ID [56]. An energy scale correction determined from $Z \rightarrow e^+e^-$, and $J/\psi \rightarrow e^+e^-$ decays is applied to data. Electron candidates are required to have a pseudorapidity within the inner detector tracking region, $|\eta| < 2.4$, excluding a region, $1.37 < |\eta| < 1.52$, where the transition between the barrel and endcap electromagnetic calorimeters is not well modelled in the simulation.

The primary interaction vertex is taken to be the one with the largest sum of squared transverse momenta of all associated tracks [57]. Electrons must originate from the primary vertex and are selected by requiring $|z_0 \sin \theta| < 0.5$ mm, where z_0 is the coordinate of the track at the point of closest approach to the beam-line. The significance of the transverse impact parameter, defined by the distance of closest approach of the track to the beam-spot in the $r - \phi$ projection $|d_0|$, divided by its estimated uncertainty $\sigma(d_0)$, is required to satisfy $|d_0|/\sigma(d_0) < 5$.

Candidates must satisfy the *LooseAndBLayer* likelihood-based identification requirements [56] based on EM shower shapes, track quality, and track–cluster matching.

Leptons produced in the Drell–Yan process are expected to be well isolated from energy depositions not associated with the lepton. Therefore the electron candidates also need to fulfil the *FCLoose* isolation working point [56], which has two distinct definitions of the degree of isolation: one is based on calorimeter information and one is based on tracks in the ID. The calorimeter-based isolation is defined as the scalar sum of transverse energy, $\sum E_T$, contained in a cone of size $\Delta R = \sqrt{(\Delta\phi)^2 + (\Delta\eta)^2}$ around the electron,

omitting the electron transverse energy, E_T . It is given by $\sum E_T(\Delta R = 0.2) < 0.20 \cdot E_T$. The track-based criterion is based on the scalar sum of transverse momenta, $\sum p_T$, of additional tracks around the electron, and is required to be below 15% of the electron p_T , i.e. $\sum p_T(\Delta R) < 0.15 \cdot p_T$. Here, the ΔR cone size shrinks with increasing transverse momentum of the electron, $\Delta R = \min(\frac{10 \text{ GeV}}{p_T}, 0.2)$.

The criteria above define the “loose” and the “veto” level as they are identical for electrons. The nominal selection requires electrons to in addition satisfy the *Tight* likelihood-based identification requirements and an additional electron isolation requirement that uses the *FCHighPtCaloOnly* isolation working point [56], based on calorimeter information only via $\sum E_T(\Delta R = 0.2) < \max(0.015 \cdot E_T, 3.5 \text{ GeV})$.

4.1.2 Muons

Muon candidates are reconstructed from tracks in the muon spectrometer matched to tracks from the ID and satisfy $|\eta| < 2.4$. Muons originating from the primary vertex are selected by requiring $|z_0 \sin \theta| < 0.5 \text{ mm}$ and $|d_0|/\sigma(d_0) < 3$.

Except for the “veto” level the muon identification uses the *High- p_T* working point [58] designed to optimise the resolution for muons with p_T above 100 GeV. This working point requires: agreement in the charge-to-momentum ratio of the muon as measured in the ID and the MS, taking into account their uncertainties; at least three precision space-points in the MS for improved sagitta measurement; and upper limits on the uncertainty of the charge-to-momentum ratio. These requirements cannot be fulfilled in some regions of the MS, for example in the transition region between barrel and endcap with $1.01 < |\eta| < 1.1$. The *Medium* working point [58], which particularly requires only two precision space-points in the MS, is used when vetoing additional muons.

The nominal selection requires muons to in addition fulfil an isolation criteria. It is defined using the scalar sum of transverse momenta, $\sum p_T$, of additional tracks divided by p_T , the transverse momentum of the muon. The selection requires $\sum p_T(\Delta R = 0.2) < 0.06 \cdot p_T$, providing a good discrimination against the background arising from the semileptonic decays of heavy quarks.

4.1.3 Jets

Jets are reconstructed and used in the determination of the missing transverse momentum in the event. A particle flow algorithm [59] is used which optimally combines calorimetric and tracking information. The anti- k_t algorithm [60, 61] is used with radius parameter $R = 0.4$. They are calibrated using in situ measurements and simulation [62]. Jets are required to satisfy transverse momentum $p_T > 25 \text{ GeV}$ and pseudorapidity $|\eta| < 2.5$. Jets with $p_T < 60 \text{ GeV}$ and $|\eta| < 2.5$ are also required to pass the *tight* jet vertex tagger criteria [63]. Identification of jets containing b -hadrons is performed with the DL1r algorithm [64] with an average tagging efficiency of b -jets from simulated dileptonic $t\bar{t}$ events of 70%.

4.1.4 Overlap removal

Particles identified by the ATLAS detector may be reconstructed as multiple different objects. Ambiguities for electrons are resolved by applying a sequential algorithm to select the best choice for each object. If a pair of electron candidates share a track, the lower p_T object is removed. Any jet within $\Delta R = 0.2$ of an electron candidate is removed. Then, any electron candidates found within $\Delta R = 0.4$ of a jet are removed.

Ambiguities for muons are not resolved at this stage as they are beneficial for the estimation of the amount of non-prompt muons in this measurement (see Section 5.2.2).

4.1.5 E_T^{miss}

The missing transverse momentum, with magnitude E_T^{miss} , is determined from the sum of transverse momenta of reconstructed and calibrated objects in the event. A so-called soft term accounts for the p_T of all remaining tracks associated to the primary vertex [65].

4.2 Event selection

The electron data are collected by a set of triggers which use calorimetric information to identify a compact electromagnetic energy deposition [66]. Identification algorithms use calorimeter shower shape information to find candidate electrons with a minimum transverse energy of 60 or 120 GeV in 2015. *Medium* identification criteria [56] are applied at the lower threshold and *loose* criteria for the higher threshold. In the remaining years the higher transverse energy threshold was changed to 140 GeV. To validate backgrounds two additional low-threshold triggers were used with trigger thresholds 24 GeV and *medium* identification criteria in 2015, and a 26 GeV threshold with *tight* identification in subsequent years. In the muon channel data are collected using a single muon trigger with a transverse momentum above 50 GeV [67].

Events are required to have exactly one reconstructed electron with $E_T > 65$ GeV or exactly one reconstructed muon with $p_T > 65$ GeV. The electron or muon has to satisfy the nominal selection criteria. In both cases the lepton is required to match a corresponding trigger. Events containing additional muons or electrons with $p_T > 20$ GeV fulfilling the “veto” level criteria are rejected. The E_T^{miss} is required to be greater than 85 GeV and the reconstructed m_T^W must exceed 200 GeV. It is determined from the relationship given in Section 1 using the reconstructed E_T^{miss} , lepton p_T , and the azimuthal angle between them.

5 Background estimation

The background from processes with one prompt isolated final-state lepton is estimated from MC simulation and includes: $Z \rightarrow \ell\ell$ where one lepton is not reconstructed due to detector acceptance or efficiency effects; $W \rightarrow \tau\nu$ and $Z \rightarrow \tau\tau$ where a τ -lepton decays leptonically; diboson production of ZZ , WZ and WW in which one boson decays leptonically; and $t\bar{t}$ and single top production (hereafter termed the top-quark background). The MC predictions for some of the major contributions are validated in dedicated kinematic regions.

A further background contribution arises from light- and heavy-flavour multijet production in which non-prompt leptons are produced or form the misidentification of jets as fake electrons. In the following the multijet background is defined as the sum of both contributions. This background is not well modelled in simulation and is determined using data-driven techniques described in detail below.

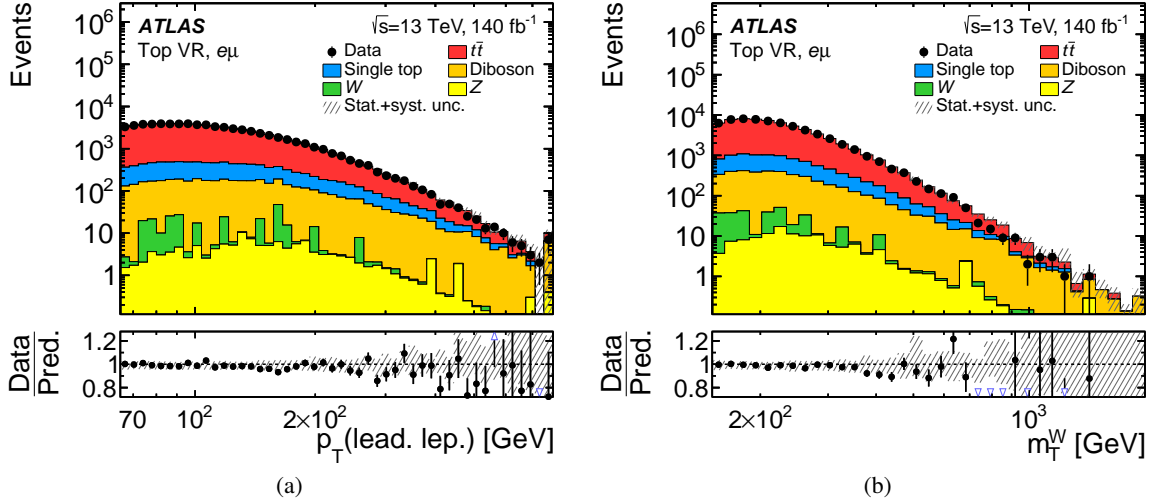


Figure 1: Comparisons of the data and prediction in the top validation region for the (a) p_T of the leading lepton and the (b) transverse mass of the W boson. Statistical and systematic uncertainties of the prediction are included in the uncertainty band. A blue triangle in the bottom panel indicates data points outside the vertical range shown.

5.1 Top-quark background contribution

The background contribution from top-quark production is estimated using the MC simulation, and is expected to be large in the phase space of this measurement. It is therefore important to check the validity of the MC simulation using data. As the dominant contribution stems from dileptonic decays of the $t\bar{t}$ pairs, a top-quark-enriched sample of events is selected by requiring two “tight” leptons – one electron and one muon both with $p_T > 30$ GeV. The leading lepton is further required to have $p_T > 65$ GeV matching the signal region selection, and this lepton is used with E_T^{miss} in the calculation of the m_T^W observable. The E_T^{miss} is required to be above 85 GeV, and the m_T^W is required to exceed 150 GeV. This validation region closely matches the kinematic region of the measurement and is found to be highly enriched in $t\bar{t}$ and single-top production with fractions of 85% and 9% respectively, where the single-top production is dominated by the tW process. The signal and multijet contributions are negligible in this sample. All kinematic observables are found to be well described in shape and in normalisation by the sum of MC expectations. Examples are shown in Figure 1 for the leading lepton p_T and the m_T^W observable.

The top-quark background is further cross checked in two variations of the validation region where the E_T^{miss} requirement is removed or where an additional b-jet is required. The former validation region allows a check of the region of small E_T^{miss} used in the multijet estimate, while the latter is a pure (> 99%) top-quark control region. The simulation is again found to describe the data well in both regions.

5.2 Multijet background estimate via the matrix method

The matrix method [14] is used to estimate the multijet background in the electron and muon channels. The method makes use of the different sets of selection criteria described in Sections 4.1.1 and 4.1.2. It relates the number of observed leptons satisfying the nominal (“tight”) requirement, N_T , or only the less stringent (“loose”) requirements, N_L , to the number of prompt (“real”) leptons, N_R , and to the number of non-prompt

leptons or jets (“fake”), N_F . They are connected by a pair of linear equations, using MC estimates of the real efficiency, ϵ_r , and data-driven estimates of the fake efficiency, ϵ_f . The real efficiency is defined to be the fraction of prompt leptons satisfying at least the loose selection which also pass the tight selection, $\epsilon_r = N_R^T / (N_R^L + N_R^T)$. The fake efficiency is analogously defined as the fraction of non-prompt leptons and jets satisfying at least the loose selection which also pass the tight selection $\epsilon_f = N_F^T / (N_F^L + N_F^T)$. The relationship is given as:

$$\begin{pmatrix} N_T \\ N_L \end{pmatrix} = \begin{pmatrix} \epsilon_r & \epsilon_f \\ 1 - \epsilon_r & 1 - \epsilon_f \end{pmatrix} \begin{pmatrix} N_R \\ N_F \end{pmatrix}.$$

The equation can be inverted to derive the multijet background as

$$N^{\text{multijet}} = \epsilon_f N_F = \frac{\epsilon_f}{\epsilon_r - \epsilon_f} [\epsilon_r (N_L + N_T) - N_T].$$

This general method is used to derive the distribution of multijet events as a function of any variable of interest for both the electron and the muon channels.

5.2.1 Multijet background estimate in the electron channel

The real efficiency is determined using the signal MC sample in which the reconstructed prompt electron is matched to the corresponding Born-level particle. The E_T^{miss} and m_T^W criteria described in Section 4.2 are not applied. The ϵ_r are determined in 132 two-dimensional bins of electron p_T and $|\eta|$. The resulting factors are found to vary between 90 – 95% except at the largest $|\eta|$ and close to the transition region between the barrel and endcap calorimeter.

The fake efficiency is measured using a data sample enriched in fake electrons by removing the m_T^W criterion and requiring the E_T^{miss} to be below 65 GeV, which also ensures orthogonality between the signal and fake enriched selections. The residual real electron contribution is subtracted using the MC predictions. The fake efficiency has the same binning in p_T and $|\eta|$ as the real efficiency, but depends simultaneously also on the difference in azimuthal angle between the electron and the E_T^{miss} , $\Delta\phi(e, E_T^{\text{miss}})$, leading to 660 three-dimensional bins. The fake efficiencies are found to be typically below 50% with a marked reduction at larger p_T . The resulting efficiencies are validated by comparing the simulation and predicted multijet background contribution to the data in a wider fake enriched region in which the E_T^{miss} condition is removed completely. Figure 2 shows the data and the predicted event yields for the m_T^W and η spectra in this region for the e^- measurement channel. The data are described by the prediction given the multijet and statistical uncertainties shown in the figure. The dominant uncertainty, particularly at low E_T^{miss} , arises from the choice of calibration applied to loose objects in the E_T^{miss} calculation as discussed in Section 7.1.

5.2.2 Multijet background estimate in the muon channel

The multijet background estimation in the muon channel largely follows that of the electron channel described above. The real efficiency is determined from the signal Drell–Yan MC simulation from events in which the reconstructed muon is matched to the Born-level particle. The E_T^{miss} and m_T^W selection criteria are dropped. The real and fake efficiencies, ϵ_r and ϵ_f , are determined in only 18 two-dimensional bins of

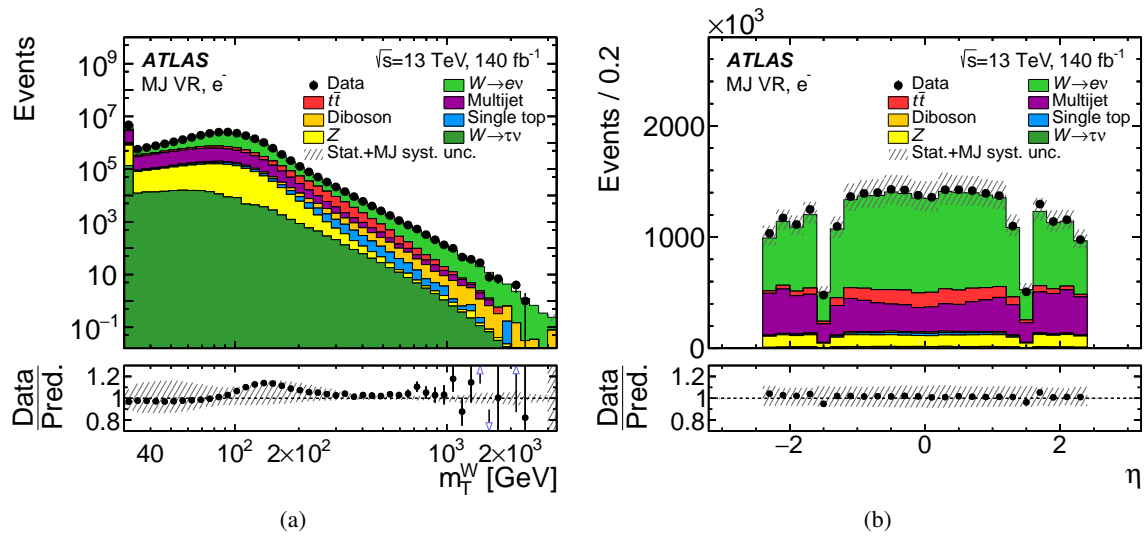


Figure 2: Comparisons of the data and prediction in the multijet validation region for the (a) transverse mass of the W boson and the (b) pseudorapidity of the electron for the e^- final state. The grey shaded band represents the statistical uncertainty of the prediction and the systematic uncertainties on only the multijet estimate. A blue triangle in the bottom panel indicates data points outside the vertical range shown.

reconstructed muon p_T and $|\eta|$ due to the limited sample size available to the fake efficiency estimate when compared to the case of electrons. The real efficiencies are found to exceed 99% in all bins.

The fake enriched region in the muon channel is created by first removing the m_T^W requirement and requiring $E_T^{\text{miss}} < 65$ GeV, as described in Section 5.2.1. Since the dominant source of fake muons arises from heavy flavour b - and c -hadron decays within jets, further selections are used to enhance the yield of this class of events. Dijet topologies are targeted in which an additional jet is required (see Section 4.1) which is back-to-back in the azimuthal angle with respect to the muon, $\Delta\phi(j, \mu) > \frac{5}{6}\pi$. The azimuthal angular separation between the muon and the E_T^{miss} is required to be less than $\frac{\pi}{6}$. This criterion efficiently suppresses the signal contribution. Finally, the transverse impact parameter significance $|d_0|/\sigma(d_0)$ is required to be greater than 1.5. The remaining contributions from EW processes and the signal process are subtracted using the predictions from MC simulation.

An algorithm similar to the one used to resolve particle object ambiguities in the electron channel within an event as described in Section 4.1 is not applied in the muon channel as non-prompt muons arise predominantly from within jets. Therefore, the contribution from non-prompt muons is increased in the fake enriched region while these muons are efficiently suppressed by the isolation requirement for muons which is part of the tight selection.

The efficiency for selecting fake muons is found to be about 10% at low p_T , rising to between 30% for central pseudorapidity and 65% at the highest pseudorapidity. It is validated by estimating the multijet background in an enlarged kinematic region with respect to the region used to estimate the fake efficiency. This is achieved by first removing the E_T^{miss} selection criterion. Figure 3 shows the data and the predicted event yields for the extrapolation in E_T^{miss} and for η for the μ^+ measurement channel. Up to $E_T^{\text{miss}} \approx 150$ GeV where the multijet contribution is large, the data are well described by the predictions within the systematic uncertainty of only the multijet estimate and the statistical uncertainty of the prediction. However, the region of high m_T^W cannot be validated as the requirement on $\Delta\phi(\mu, E_T^{\text{miss}})$ suppresses the event yield.

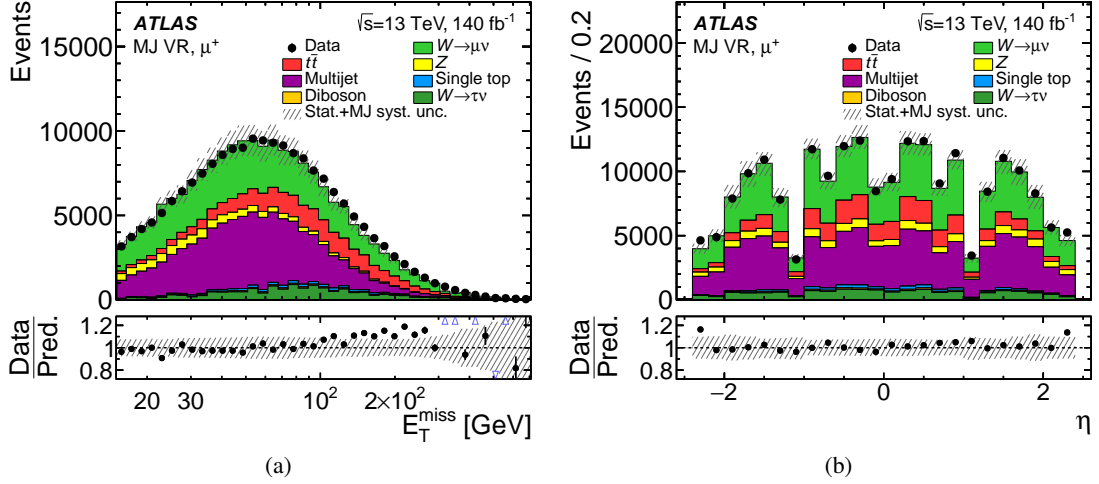


Figure 3: Comparisons of the data and prediction in the multijet validation region for the (a) missing transverse energy and the (b) pseudorapidity of the muon for the μ^+ final state. The grey shaded band represents the statistical uncertainty of the prediction and the systematic uncertainties on only the multijet estimate. A blue triangle in the bottom panel indicates data points outside the vertical range shown.

Therefore a second validation region is defined by removing the requirement on $\Delta\phi(\mu, E_T^{\text{miss}})$ and requiring at least three jets instead. The resulting phase space is found to be composed of approximately equal contributions from multijet events, signal, and top quark processes. The data in this phase space are well described by the prediction.

5.3 Data and prediction comparisons

The number of expected events is calculated as the sum of the data-driven and simulated background estimates, and the expected event yield predicted by the signal Drell–Yan MC simulations.

Figures 4 and 5 compare data and expectation for the reconstructed lepton p_T , E_T^{miss} , and m_T^W distributions. In the phase space of the measurement the three largest background contributions in the electron channel are the top-quark ($t\bar{t}$ and single top), multijet and diboson contributions which are found to be approximately 23%, 4%, and 3% respectively in the $W \rightarrow e^+\nu$ channel. The corresponding contributions in the $W \rightarrow e^-\nu$ channel are 33%, 5%, and 4%.

In the muon channel the three largest background contributions are from top-quark ($t\bar{t}$ and single top), Z +jets, and diboson production. They constitute about 20%, 8%, and 2% of the total expectation in the $W \rightarrow \mu^+\nu$ channel. In the $W \rightarrow \mu^-\nu$ measurement the contributions are found to be approximately 31%, 6%, and 3% of the expectation event yield. The multijet contribution in the muon channels is below 2%.

The data event yields and spectra are found to be well described by the expectation in both the $W^\pm \rightarrow e^\pm\nu$ and the $W^\pm \rightarrow \mu^\pm\nu$ channels.

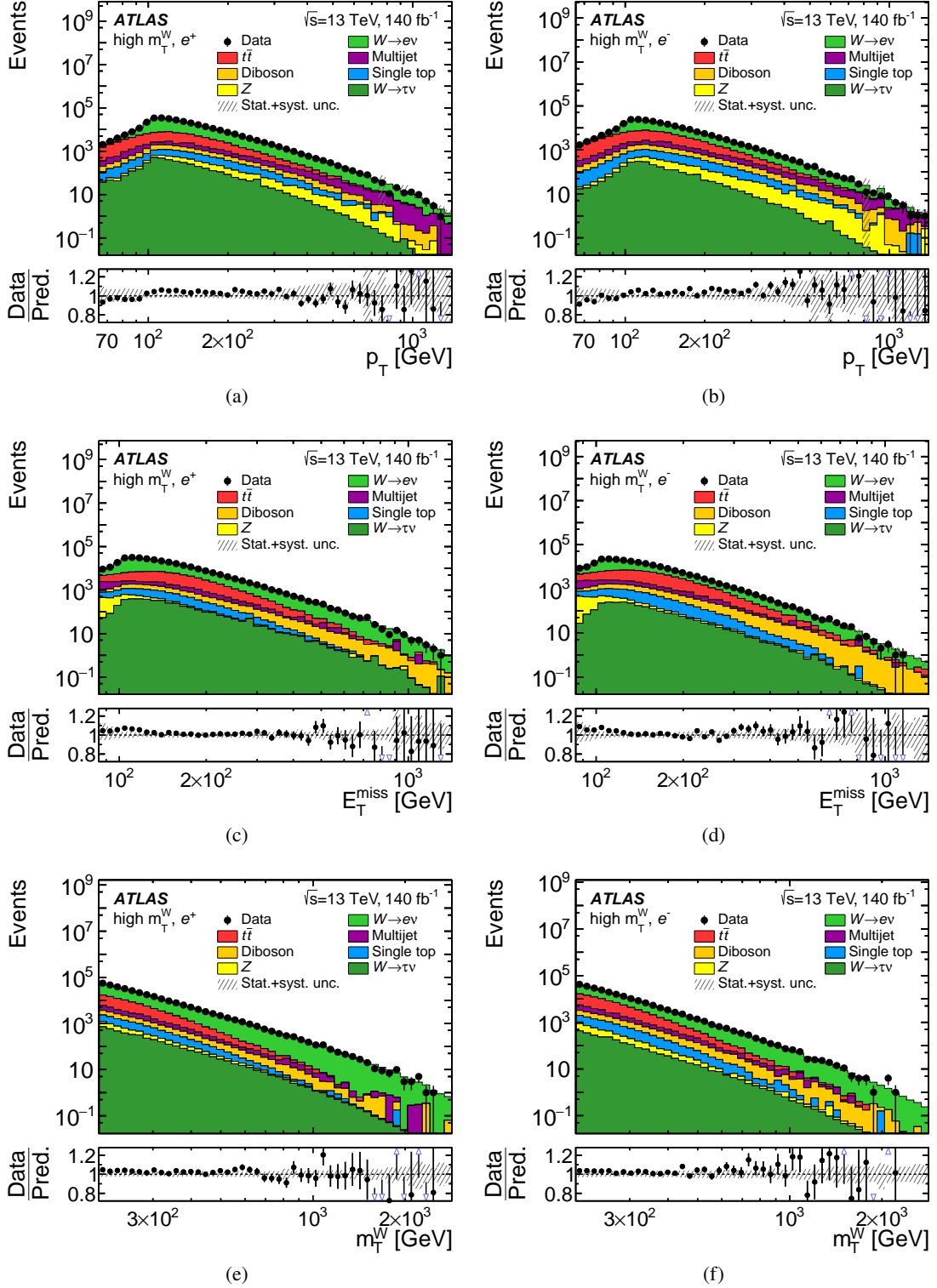


Figure 4: Comparisons of the data and prediction in the signal region for the (a, b) transverse momentum of the lepton, (c, d) missing transverse momentum, and (e, f) transverse mass m_T^W in the (a, c, e) e^+ and (b, d, f) e^- final states. Statistical and systematic uncertainties of the prediction (except for theoretical uncertainties on the signal) are included in the uncertainty band. A blue triangle in the bottom panel indicates data points outside the vertical range shown.

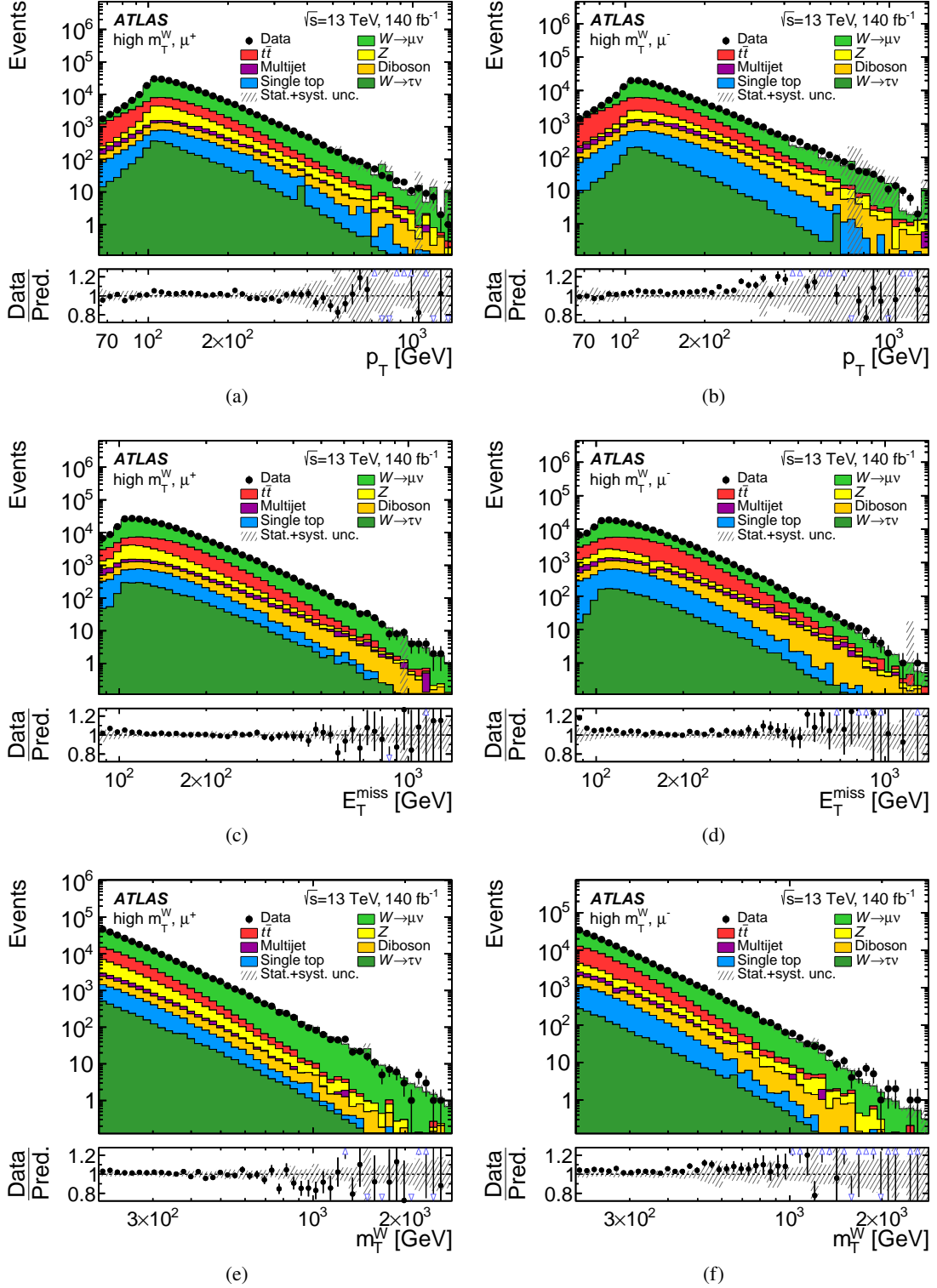


Figure 5: Comparisons of the data and prediction in the signal region for the (a, b) transverse momentum of the lepton, (c, d) missing transverse momentum, and (e, f) transverse mass m_T^W in the (a, c, e) μ^+ (right) and (b, d, f) μ^- final states. Statistical and systematic uncertainties of the prediction (except for theoretical uncertainties on the signal) are included in the uncertainty band. A blue triangle in the bottom panel indicates data points outside the vertical range shown.

6 Cross-section measurement

The charged current Drell–Yan cross-sections are measured for each charge and lepton flavour separately. The differential cross-sections are measured in 12 m_{T}^{W} bins in the range $200 \leq m_{\text{T}}^{\text{W}} \leq 5000$ GeV. Double differential cross-sections in five m_{T}^{W} bins and up to 12 $|\eta|$ bins are also presented covering the region $0 \leq |\eta| \leq 2.4$, and $200 \leq m_{\text{T}}^{\text{W}} \leq 2000$ GeV, as listed in Table 1.

The binning in m_{T}^{W} is chosen such that expected signal event yields have moderate statistical uncertainties, and that bin widths are larger than the detector resolution to minimise migrations between bins. In particular, the muon channel is expected to have worse resolution at high m_{T}^{W} than the electron channel since the muon is fully reconstructed from track-based measurements only. The muon p_{T} dominates the resolution for $m_{\text{T}}^{\text{W}} > 400$ GeV, but below this region it is the $E_{\text{T}}^{\text{miss}}$ which gives the leading contribution. In the fiducial region the single differential bin purity, defined as the yield ratio of particle-level signal MC events to reconstructed signal MC events, is found to be typically 60%. In the muon channel this decreases in the 2 – 5 TeV m_{T}^{W} bin, whereas in the electron channel it increases, reaching unity at the highest m_{T}^{W} .

6.1 Fiducial definition

The measurements are unfolded to a common fiducial region that closely matches the kinematic selection described in Section 4. It is defined at particle level as $|\eta| < 2.4$, $p_{\text{T}}^{\ell} > 65$ GeV, the transverse momentum of the (anti-)neutrino $p_{\text{T}}^{\nu} > 85$ GeV, and $200 \leq m_{\text{T}}^{\text{W}} \leq 5000$ GeV for the single differential measurements, or $200 \leq m_{\text{T}}^{\text{W}} \leq 2000$ GeV for the double differential measurements. The lepton charge is included in the definition of the fiducial region.

The fiducial region is defined at the Born particle level prior to any QED radiation from the final-state charged lepton. The measurements can also be corrected to the “dressed” particle level by multiplying the reported cross-sections by the multiplicative factor C_{fsr} defined as the ratio of the dressed-level cross-section to the Born level, and is provided in the data tables (see Section 8). The dressed particle level is obtained from MC simulation by merging the Born-level leptons with any prompt photons within a cone of $\Delta R < 0.1$ around the charged lepton. The C_{fsr} are close to unity and found to vary weakly with m_{T}^{W} .

6.2 Unfolding procedure

After the signal region selection has been applied and each of the background contributions has been subtracted from the data, the observed distributions are corrected for detector effects in an unfolding procedure [68]. The differential one-dimensional cross-section $d\sigma^j/dm_{\text{T}}^{\text{W}}$ is determined using

$$\frac{d\sigma^j}{dm_{\text{T}}^{\text{W}}} = \frac{1}{\Delta m_{\text{T}}^{\text{W}} \cdot \mathcal{L}_{\text{int}} \cdot \epsilon^j} \sum_i R_{ij}^{-1} \cdot f_{\text{in}}^i \cdot (N_d^i - N_b^i),$$

where $\Delta m_{\text{T}}^{\text{W}}$ is the bin width, \mathcal{L}_{int} the integrated luminosity, and N_d^i and N_b^i are the numbers of observed data and estimated background events in the i -th bin, respectively. The factor f_{in}^i corrects for signal events that pass the detector-level selection but not the fiducial selection, i.e. for events which migrate into the measurement region, also called “in-smearing”. The factor ϵ^j corrects for signal events that pass the fiducial selection but not the detector-level selection, accounting for selection efficiency and acceptance. The matrix R_{ij} is the detector response matrix containing the number of events in the i -th reconstructed

Table 1: Kinematic bin edges for the two-dimensional cross-section measurements.

m_T^W / GeV	200 , 300 , 425
$ \eta $	0.0 , 0.2, 0.4, 0.6, 0.8, 1.0, 1.2, 1.4, 1.6, 1.8, 2.0 , 2.2 , 2.4
m_T^W / GeV	425 , 600 , 900
$ \eta $	0.0 , 0.4, 0.8, 1.2, 1.6 , 2.0 , 2.4
m_T^W / GeV	900 , 2000
$ \eta $	0.0 , 0.8, 1.2, 1.8 , 2.4

measurement bin and the corresponding prediction in the j -th particle-level bin. It gives the probability of a selected event reconstructed in a given bin i to have originated at particle level from the fiducial bin j . The signal MC sample is used to obtain f_{in}^i , ϵ^j and R_{ij} . The equation is trivially extended for the two-dimensional case.

Iterative Bayesian unfolding [69] is used to approximate the inversion of the matrix R_{ij} . The procedure is regularised through the number of iterations in which the particle-level prediction is used as a biased prior. The prior is replaced by the unfolded output of the previous iteration, thereby reducing the bias, but potentially increasing the variance. The measurement is optimised using two iterations.

6.3 Event migration studies

The reconstructed event selection efficiency including acceptance losses, is found to be $\epsilon^j \approx 70\% - 90\%$ in the electron channel and $\epsilon^j \approx 50\% - 75\%$ in the muon channel.

The factors f_{in}^i are used to correct the data for in-smearing in particular from the W -boson resonance production region into the kinematic phase space of this analysis. As the correction is done without iteration it is better to maximise its value, reducing the impact of measurement biases. This was studied by reducing the m_T^W selection to 150 GeV and introducing an additional bin in the iterative unfolding procedure covering the region 150 – 200 GeV. This modification is found to increase the value of f_{in}^i in the measurement bin $200 < m_T^W < 250$ GeV from 70% to 85%, but has no impact at larger m_T^W .

The measurement is not extended down to $m_T^W = 150$ GeV because f_{in}^i is only 40% meaning 60% of reconstructed events in this extended bin are predicted to originate from mainly the W -boson resonance. For this reason the unfolding is performed with (a) a selection cut of $m_T^W > 150$ GeV, and (b) the introduction of a so-called “shadow bin” with $150 \leq m_T^W \leq 200$ GeV which serves to stabilise the unfolding. The final cross-section measurements are only reported for $m_T^W \geq 200$ GeV.

Figure 6 shows the two-dimensional correction factor f_{in}^i for the negatively charged electron and muon analyses. The shadow bin (shaded region) is also shown for comparison. The in-smearing factors are found to be very low in the shadow bin, but reach 85% – 90% in the first measurement bin. They are observed not to depend strongly on $|\eta|$, as expected.

6.4 Optimisation of number of iterations

The robustness of the unfolding procedure is tested in a number of studies using the signal MC. These include using the SHERPA MC as pseudo-data unfolded using the POWHEG+PYTHIA MC sample; unfolding the W^+ MC pseudo-data with the W^- MC sample and vice versa; and applying an arbitrary linear m_T^W

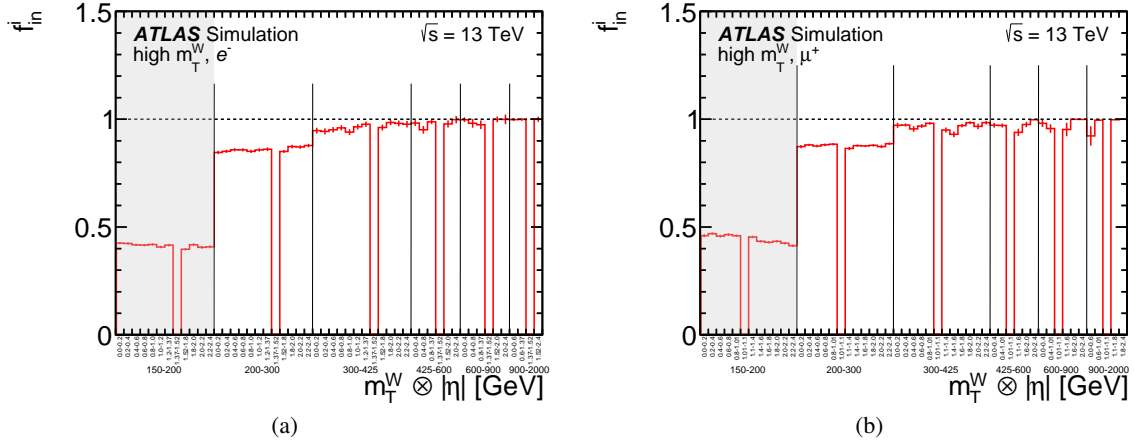


Figure 6: The correction factor f_{in}^i that corrects for events not generated in the fiducial measurement range are shown for a (a) negatively charged electron and (b) positively charged muon. On the horizontal-axis the double-differential measurement binning in the transverse mass of the W boson and the absolute pseudorapidity of the lepton is shown.

dependent event weight to the signal MC which changes the predicted cross-section by $\pm 20\%$ and $\pm 50\%$ at low m_T^W . In all cases the resulting biases and variances were studied for between one and five iterations. The optimum number of iterations is chosen to be two, mainly based on a scan of global correlation coefficients [70] but also on the linear m_T^W dependent reweighting discussed above.

6.5 Observed and predicted event yields

In Figure 7 the predicted event yields are compared to data in the one-dimensional measurement binning separated by charge and lepton flavour. The uncertainty band represents the combined statistical and systematic uncertainties. The overall agreement of data and prediction, taking into account the uncertainty band, is very good.

In Figure 8 the predicted two-dimensional event yields are compared to data separated by charge and lepton flavour. The distributions are shown in the final binning used to report the cross-section measurements. The distribution in the shadow bin is also shown for comparison.

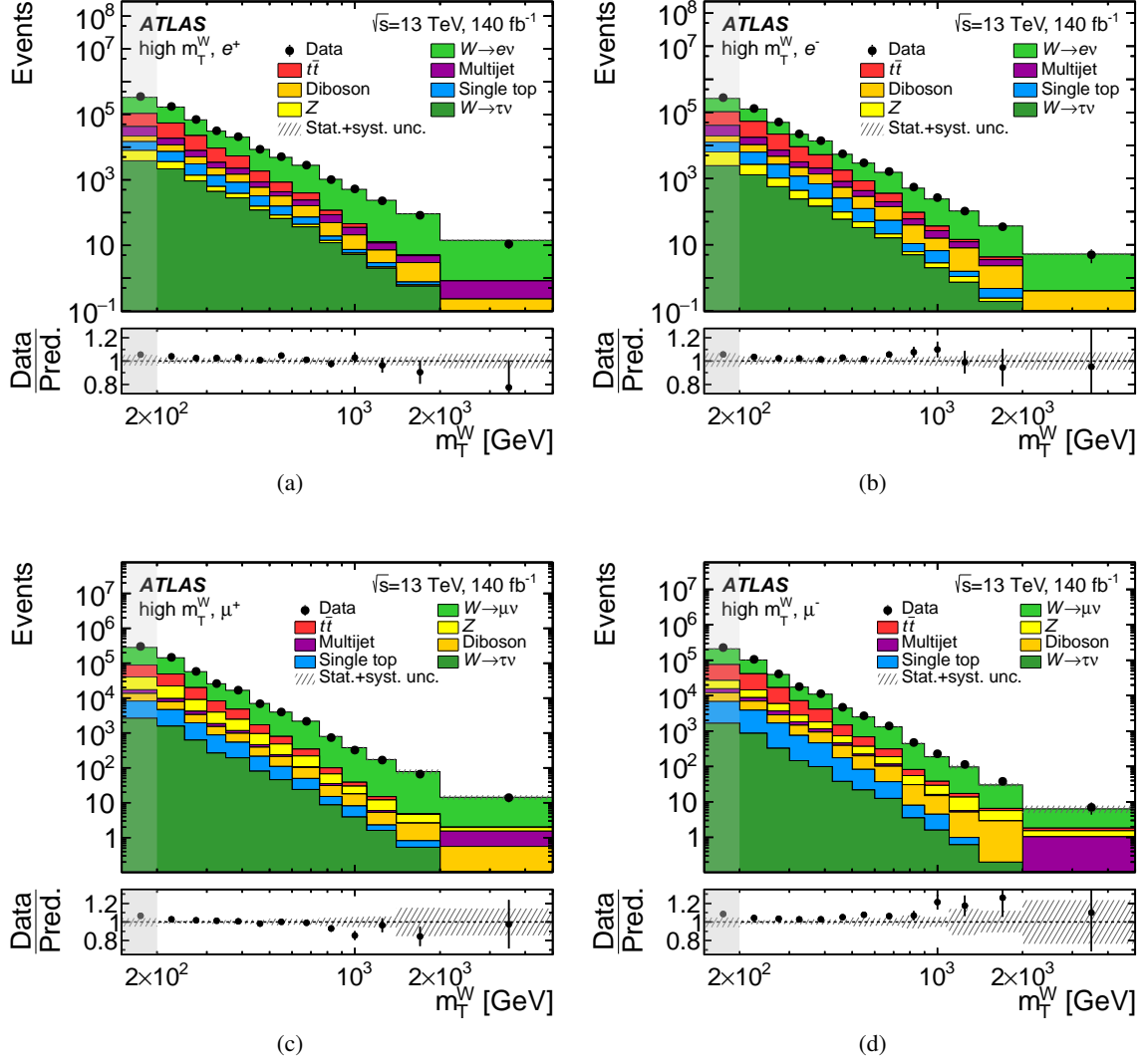


Figure 7: Comparisons of the data and the predictions in the signal region shown in the measurement binning of the transverse mass of the W boson, for the (a) e^+ , (b) e^- , (c) μ^+ and (d) μ^- final states. Statistical and systematic uncertainties of the prediction (except for theoretical uncertainties on the signal) are included in the uncertainty band.

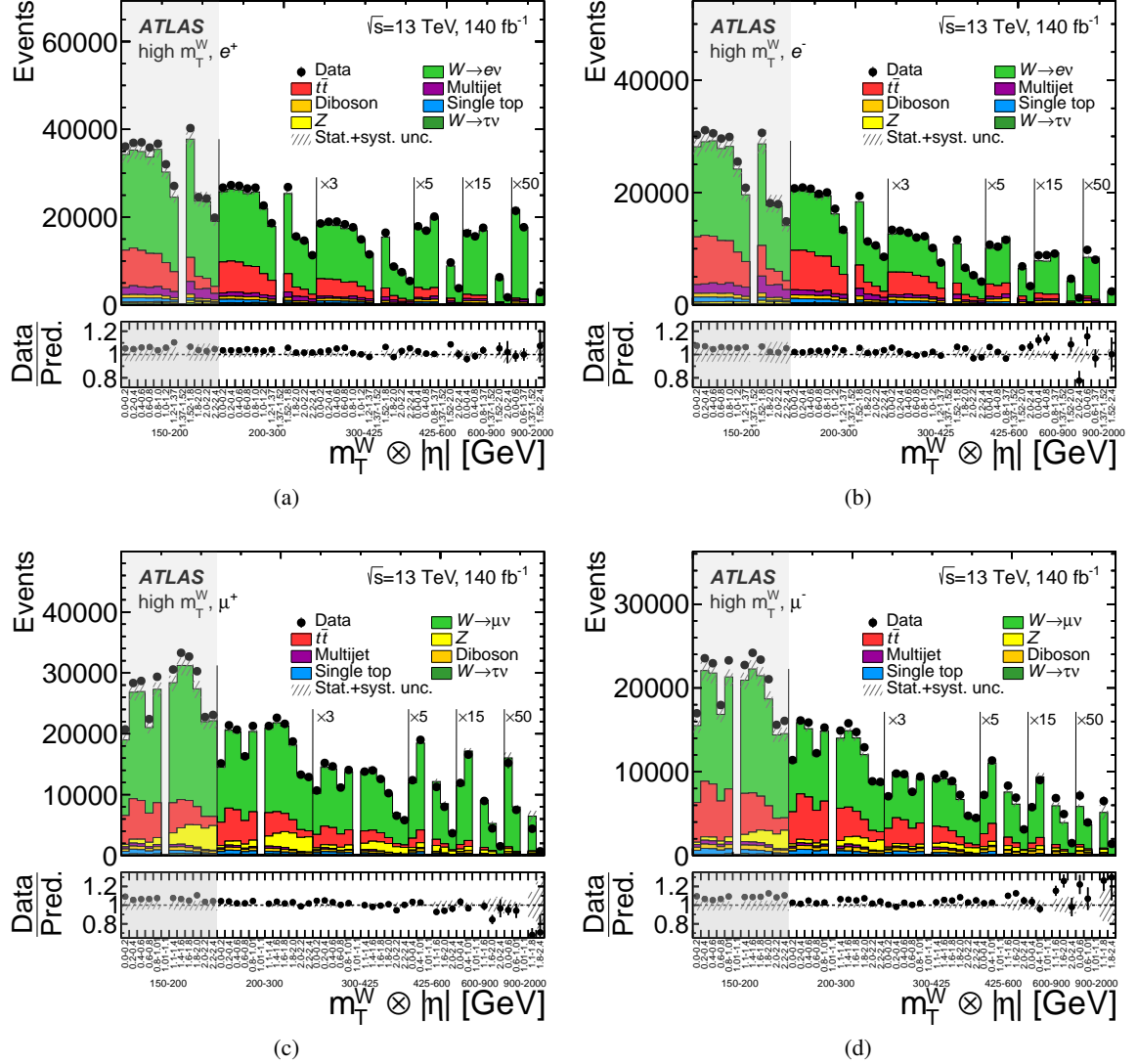


Figure 8: Comparisons of the data and the predictions in the signal region shown in the double-differential measurement binning in the transverse mass of the W boson and the absolute pseudorapidity of the lepton for the (a) e^+ , (b) e^- , (c) μ^+ and (d) μ^- final states. Statistical and systematic uncertainties of the prediction (except for theoretical uncertainties on the signal) are included in the uncertainty band. For better readability, the numbers of predicted and data events are scaled up by factors of 3, 5, 15 and 50, respectively, in the last four m_T^W bins.

7 Systematic uncertainties

The systematic uncertainties on the measurements are discussed separately for those sources which arise only in the electron channel, those which arise only in the muon channel, and those which are common to both measurements. Each source is classified as being correlated or uncorrelated between measurement bins in a single channel. All bin-to-bin correlated sources are also correlated between measurements of the same lepton flavour but opposite lepton charge. In addition, all common bin-to-bin correlated sources are considered to be correlated between the two lepton flavour channel measurements.

The correlated uncertainty contributions are propagated by the offset method in which the values from each source are coherently shifted upwards and downwards by one standard deviation and the magnitude of the change in the measurement is computed. Only the systematic uncertainties with an impact of at least 0.5% in at least one bin of any of the measurement distributions are propagated. By default the computed systematic uncertainties are symmetrised unless they are one-sided or strongly asymmetric.

A summary of the statistical and systematic uncertainties in the single- and double-differential cross-sections are shown in Figure 9 for the electron channel and Figure 10 for the muon channel. The systematic uncertainties in the cross-section in the electron channel are dominated primarily by the uncertainties in the determination of the multijet background described in Section 5.2.1 and by the electron energy scale. In the muon channel the charge-dependent impact in the muon momentum scale calibration (sagitta bias) is the dominant uncertainty at larger values of m_T^W and $|\eta|$, while various sources contribute on a similar level at smaller values of m_T^W .

7.1 Electron channel

Multijet background The uncertainty in the multijet background is driven by the statistical and systematic uncertainties in the fake efficiency estimate, as the real efficiency is taken from the MC simulation directly. The fake efficiency depends on the selections used to define the multijet enriched regions and the modelling of the backgrounds with real electrons in these regions. Biases from the selection are estimated by varying the E_T^{miss} range from $E_T^{\text{miss}} < 65$ GeV to $E_T^{\text{miss}} < 30$ GeV and $30 < E_T^{\text{miss}} < 65$ GeV and by asking for an additional jet well separated from the electron. The modelling of the real electron contributions is varied by scaling the cross-sections of the MC samples by $\pm 10\%$ and by using the alternative SHERPA signal sample normalised to the POWHEG+PYTHIA prediction. Finally, as E_T^{miss} itself depends on the sum of transverse momenta of all reconstructed and calibrated objects in the event an ambiguity can arise depending on which calibration is applied to a certain object. Applying e.g. a jet calibration or an electron calibration to a certain reconstructed object typically results in a factor of two difference in transverse momentum. While not a problem for well identified (“tight”) objects this is different for objects that only satisfy the less stringent (“loose”) requirements utilised in the matrix method, for which the true nature (electron or jet) is unknown. A systematic uncertainty is assigned by attempting to estimate the actual contribution of true electrons and jets as a function of the event kinematics.

While asking for an additional jet leads to negligible differences, all other uncertainties have a 1%-3% impact on the measurement at low m_T^W , which is decreasing for higher values of m_T^W . They constitute the dominant source of uncertainty in the measurement at low m_T^W .

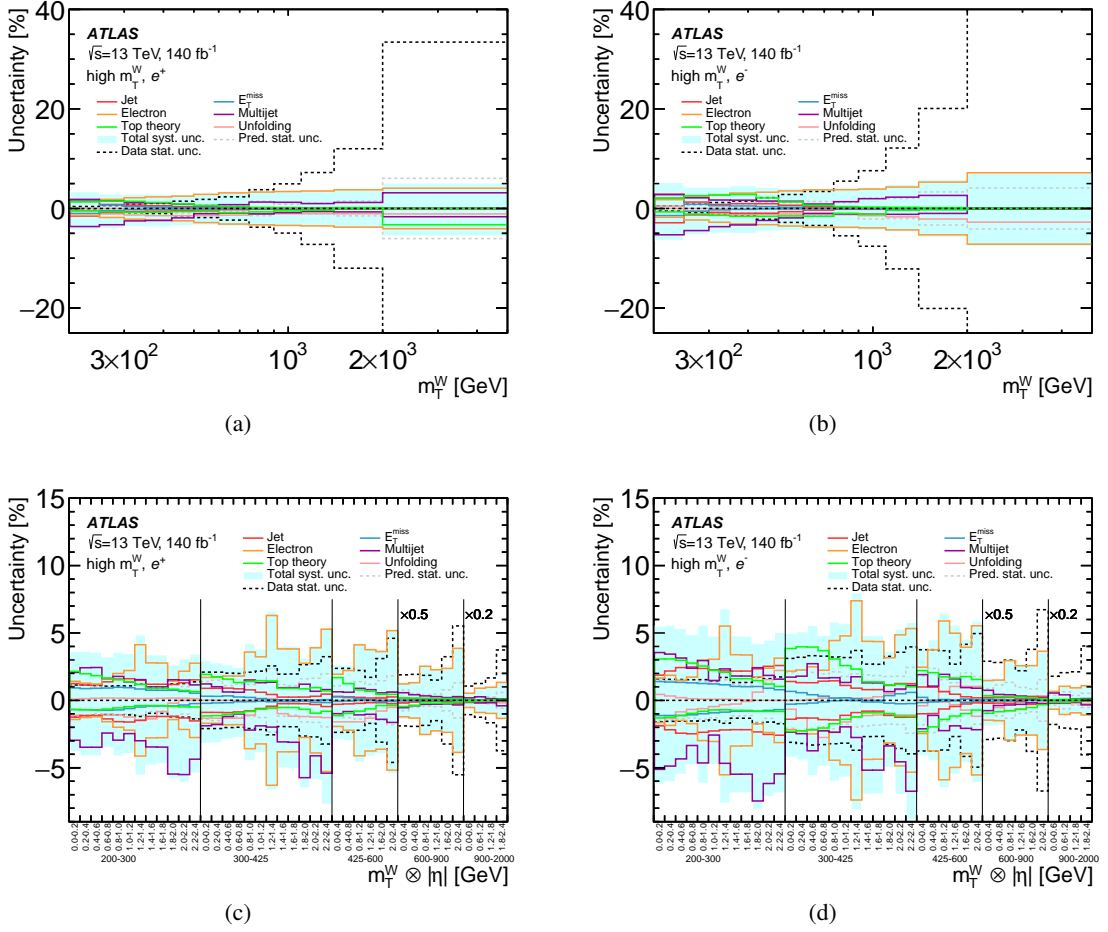


Figure 9: Summary of the uncertainties in the unfolded (a, b) single-differential and (c, d) double-differential cross-sections for the (a, c) e^+ and (b, d) e^- final state. Similar sources of uncertainties are combined via their quadratic sum. The light blue band indicates the total systematic uncertainty. In addition the statistical uncertainties in the prediction and in the data are shown.

Electron trigger, reconstruction, identification and isolation efficiencies The efficiencies of the trigger, electron reconstruction and identification, and of the isolation criteria are estimated with $Z \rightarrow e^+e^-$ data using a tag-and-probe method [66, 71]. The uncertainties are given in a scheme using a single nuisance parameter for each of the isolation, reconstruction and trigger efficiency contributions and two nuisance parameters for the charge misidentification. The remaining identification uncertainties are given by 16 sources correlated between measurement bins. An additional 18 nuisance parameters describe the impact of sources uncorrelated in $|\eta|$ and p_T , but fully correlated between electron charges.

Among those, the largest uncertainties are due to the isolation and identification efficiencies. The former is largest for $m_T^W \sim 1$ TeV where it reaches 2%. The latter is dominated by one bin-to-bin correlated source in particular which reaches 1% in size for m_T^W above 0.5 TeV, while the uncorrelated sources contribute typically at the level of 1% in their respective $|\eta|$ bin.

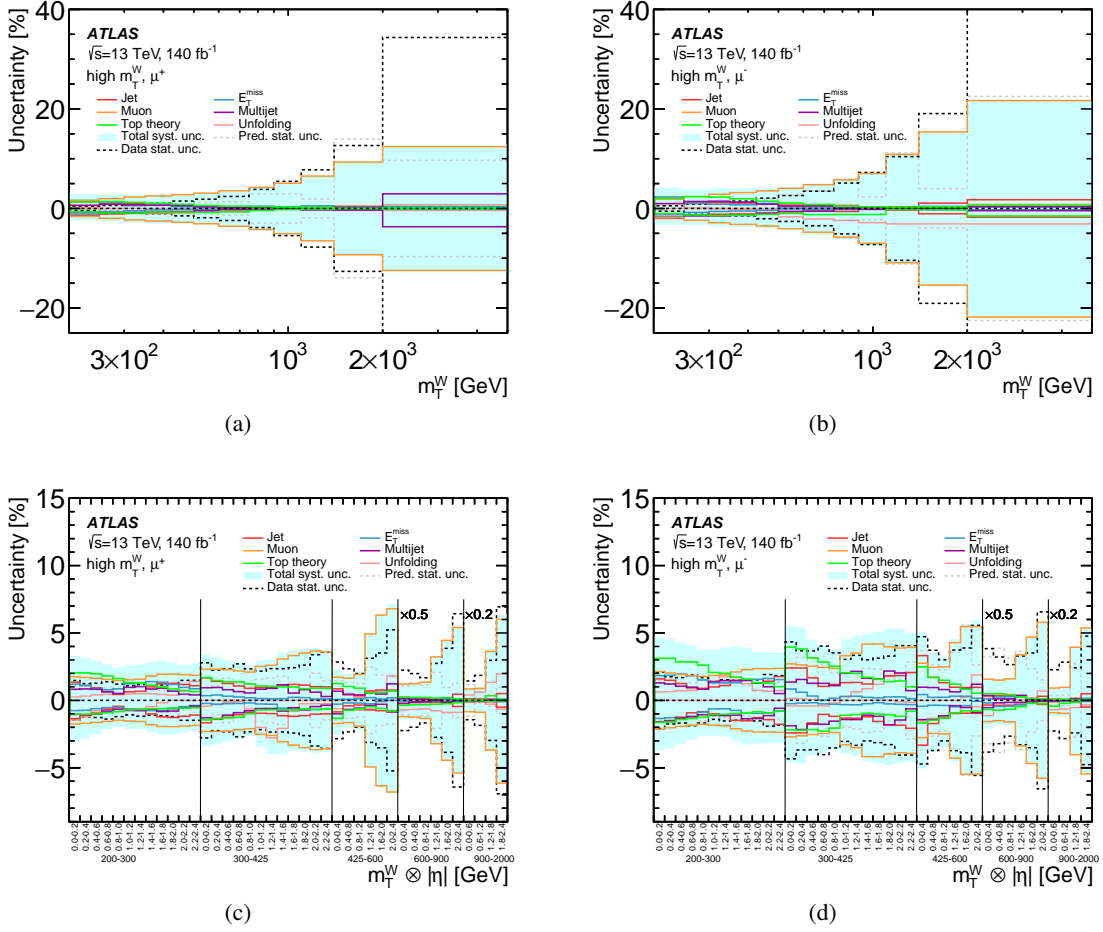


Figure 10: Summary of the uncertainties in the unfolded (a, b) single-differential and (c, d) double-differential cross-sections for the (a, c) μ^+ and (b, d) μ^- final state. Similar sources of uncertainties are combined via their quadratic sum. The light blue band indicates the total systematic uncertainty. In addition the statistical uncertainties in the prediction and in the data are shown.

Electron energy scale and resolution The determination of the electron energy scale and resolution is presented in Ref. [56]. The related uncertainties are described by 25 nuisance parameters for the energy scale and a further nine for the resolution. The energy scale is the larger contribution to the measurement uncertainty rising from 0.5% at low m_T^W to 3% in the highest m_T^W bin.

7.2 Muon channel

Multijet background As for the electron channel, the multijet background estimation in the muon channel depends on the selections used to define the fake enriched region and the modelling of the real electron contribution in this region. Biases from these contributions are estimated by varying the E_T^{miss} range used in the same way as in the electron channel and, additionally, varying the jet multiplicity, the impact parameter selection, or the $\Delta\phi(\mu, E_T^{\text{miss}})$ selection individually. The modelling of the real electron contribution is varied by scaling the cross-sections by $\pm 10\%$ and by using the alternative SHERPA signal

MC sample in the fake enriched region. All of these uncertainty estimates are found to contribute less than 1% to the final cross-section measurement.

Muon trigger, identification, vertex association and isolation efficiency The muon efficiency corrections are obtained for the full Run 2 data using $Z \rightarrow \mu^+ \mu^-$ data and simulation with a tag-and-probe method described in Refs. [58, 67]. The vertex association efficiency corrects for losses arising from the d_0 and z_0 impact parameter selection criteria. Each of these contributions is associated with two nuisance parameters for a correlated and uncorrelated statistical component of the uncertainty. The largest impact on the measurement is from the identification efficiency which rises from 1% at low m_T^W to 5% in the highest bin.

Muon momentum scale and resolution The uncertainties in the determination of the muon momentum and resolution are discussed in Ref. [72], and are determined using similar samples as for the muon efficiency corrections above. In total six nuisance parameters are used to describe the impacts of these uncertainties. They relate to separate resolution effects in the ID and muon spectrometer, biases in the momentum scale, and three contributions related to the sagitta bias, which are anti-correlated between the muon charges. The three contributions are a global residual bias, a specific component for the high- p_T extrapolation of muons with $|\eta| > 1.1$ and $p_T > 450$ GeV, and a contribution from local biases in $|\eta|$ and ϕ of the muon. The first two of these three contributions have the largest impact and dominate the overall uncertainty for $m_T^W > 600$ GeV, reaching up to 10% at the highest values of m_T^W for the former and up to 20% at the highest values of m_T^W and $|\eta|$ for the latter.

7.3 Common uncertainties

Top-quark background The $t\bar{t}$ background uncertainties are divided into a number of contributions. The influence of hadronisation and fragmentation models is determined by re-showering the nominal top-quark generator-level events with HERWIG 7 [73]. The sensitivity to initial (ISR) and final (FSR) state QCD radiation is determined by varying a parameter of the A14 tune [74] corresponding to a variation of α_S for the ISR, and by variations of the renormalisation scale in the FSR part of the PS sample. The POWHEG h_{damp} parameter is a resummation damping factor that effectively regulates the high- p_T radiation against which the $t\bar{t}$ system recoils. It is changed from 1.5 to 3 times the top-quark mass. The p_T -hard parameter controlling the matching of POWHEG matrix elements to the PS is also varied. The PDF uncertainty is evaluated by using the RMS of one hundred replicas of the nominal NNPDF3.0_{NLO} PDF set.

The relative size of the systematic uncertainties discussed above are evaluated before the reweighting of the $t\bar{t}$ MC sample to the NNLO QCD calculations including NLO EW corrections described in Section 3. The sequence (top p_T , $t\bar{t}$ mass) in which the reweighting is performed is another source of uncertainty. Potential differences in the modelling of additional radiation between the NNLO calculation and the PS are also taken into account, separately for the p_T of the top quark and the $t\bar{t}$ mass. The choice of PDF has also been varied in order to assess the impact on the EW corrections. Finally, separate variations of the factorisation and renormalisation scales μ_R and μ_F , in the NNLO calculation are taken into account by varying the scales independently by factors of two.

The interference between the tW and $t\bar{t}$ production processes is accounted for in the simulation through the diagram subtraction scheme [45] as discussed above, and the difference to the dynamic scale diagram

removal scheme [75] is used as uncertainty. The POWHEG h_{damp} parameter is varied for the tW samples in the same way as for the $t\bar{t}$ samples. In addition, a normalization uncertainty of 4% is assigned, arising from the uncertainty in the theoretical prediction at NNLO [76]. This is also assigned to all single-top channels which is 90% dominated by tW production.

The largest uncertainties are due to the hadronisation and fragmentation models, the interference between tW and $t\bar{t}$, and the differences in the modelling of additional radiation between the NNLO calculation and the PS. At small $|\eta|$ and for the negative lepton charges, where the contribution from top background is largest, these uncertainties extend up to 2-3% each.

EW background The remaining EW background processes lead to small contributions in the signal region. A correlated normalisation uncertainty is applied for each process separately, taken to be 5% for $Z \rightarrow \ell\ell$ and $W \rightarrow \tau\nu$ [77], and 6% for diboson processes.

Jet uncertainties The uncertainties in the jet energy scale and resolution directly influence the $E_{\text{T}}^{\text{miss}}$ reconstruction and are described in detail in Ref. [62]. The Jet Energy Scale (JES) uncertainties are described using the 29 nuisance parameter scheme, which considers uncertainties arising from the pile-up correction to jets, calibration biases, the jet flavour response, the modelling of jets and of the detector, as well as punch through and the response of high p_{T} jets. The Jet Energy Resolution (JER) uncertainties use an eight-parameter scheme. They are larger than the JES contributions but still remain below 1.5% throughout the measurement range.

Uncertainties in the $E_{\text{T}}^{\text{miss}}$ soft term The $E_{\text{T}}^{\text{miss}}$ soft term uncertainties arise from the momentum scale of this contribution to the $E_{\text{T}}^{\text{miss}}$, and from the separate parallel and perpendicular resolution modelling of the tracks comprising the soft term with respect to the mean p_{T} of the tracks [65]. These contributions are largest at low m_{T}^{W} , and dominate the uncertainty in the lowest m_{T}^{W} bin reaching 1.5%. In the shadow bin this rises to 4%.

Pile-up modelling To account for differences between simulation and data in the pile-up distribution, the pile-up profile in the simulation is corrected to match the one in data. The uncertainty in the correction factor is $\pm 4\%$ and is applied in the measurement as a variation of the event weight.

MC statistics The size of the MC samples used in the analysis leads to uncertainties that are considered uncorrelated between measurements bins, charges and flavours.

Luminosity The uncertainty of the ATLAS luminosity measurement is 0.83% and is discussed in detail in Ref. [78].

Unfolding uncertainties The uncertainty in the unfolding procedure is estimated for two sources. The first contribution assesses the bias arising from differences between data and MC simulation in the measured observables m_T^W and $|\eta|$. This is estimated by reweighting the MC simulation at the particle level such that its resulting distribution at reconstruction level matches the distributions observed in the data. The uncertainty is derived by unfolding the resulting distribution on reconstruction level with the nominal unfolding procedure and comparing the result to the reweighted particle level MC spectra. The uncertainty is found to be below 1% throughout the range of the measurement.

A second contribution to the unfolding uncertainty quantifies the impact of poor modelling in unmeasured observables for example (but not only) the transverse momentum of the W boson which is modelled differently by the POWHEG+PYTHIA and SHERPA signal MC samples. The uncertainty is estimated by reweighting the alternative SHERPA signal MC sample to the POWHEG+PYTHIA spectra at the particle level in m_T^W and $|\eta|$ and then unfolding the resulting distribution on reconstruction level with the nominal unfolding procedure. The difference between the unfolded distribution and the reweighted one at particle level is taken as the uncertainty, and has an impact on the measurement of typically 1%.

8 Results

8.1 Separate differential cross-sections in the electron and muon channels

The unfolded Born-level cross-section measurements $d\sigma/dm_T^W$ including their statistical, systematic and total uncertainties are presented in Figure 11 separately for each lepton charge and flavour. Note that here and in the following the luminosity uncertainty of 0.83% is not shown and not included in the overall systematic and total uncertainty bands. Detailed tables for all results including the systematic uncertainties separately for each source can be found in HEPDATA [79, 80].

The data are compared to predictions from SHERPA, using the CT18NNLO PDF set, and POWHEG+PYTHIA using the CT14NNLO PDF set. The lower panels in each of the figures show the ratio of the two predictions to the data measurement and the uncertainty contributions.

The cross-sections are observed to fall over seven orders of magnitude as the m_T^W increases from 200 – 5000 GeV. The e^+ and μ^+ cross-sections are everywhere larger than the corresponding e^- and μ^- cross-sections as expected from the difference between the u - and d -quark PDFs in the proton. The predictions describe the data well within the measurement uncertainties.

The measurements have a data statistical uncertainty ranging from about 0.5% at low m_T^W to about 33% in the e^+ and μ^+ channels and about 50% in the e^- and μ^- channels at the highest values of m_T^W .

In the e^+ channel the total systematic uncertainty varies from 3% – 5% over the m_T^W range, compared to 5% – 8% for the e^- measurement. At low m_T^W , the largest contribution to the systematic uncertainty in both cases are from the E_T^{miss} , JER, and multijet background estimations. At higher m_T^W the largest contributions to the experimental uncertainty are from the multijet estimation, the electron calibration, and the top-quark background, specifically the choice of the single-top tW subtraction scheme.

In comparison, the muon channel measurements achieve a better systematic uncertainty at low m_T^W , 3% and 4% for μ^+ and μ^- respectively, due to a variety of smaller contributions. However, the systematic uncertainty is worse at large values of m_T^W , reaching 13% for μ^+ and 22% for μ^- , driven by two muon sagitta uncertainty sources.

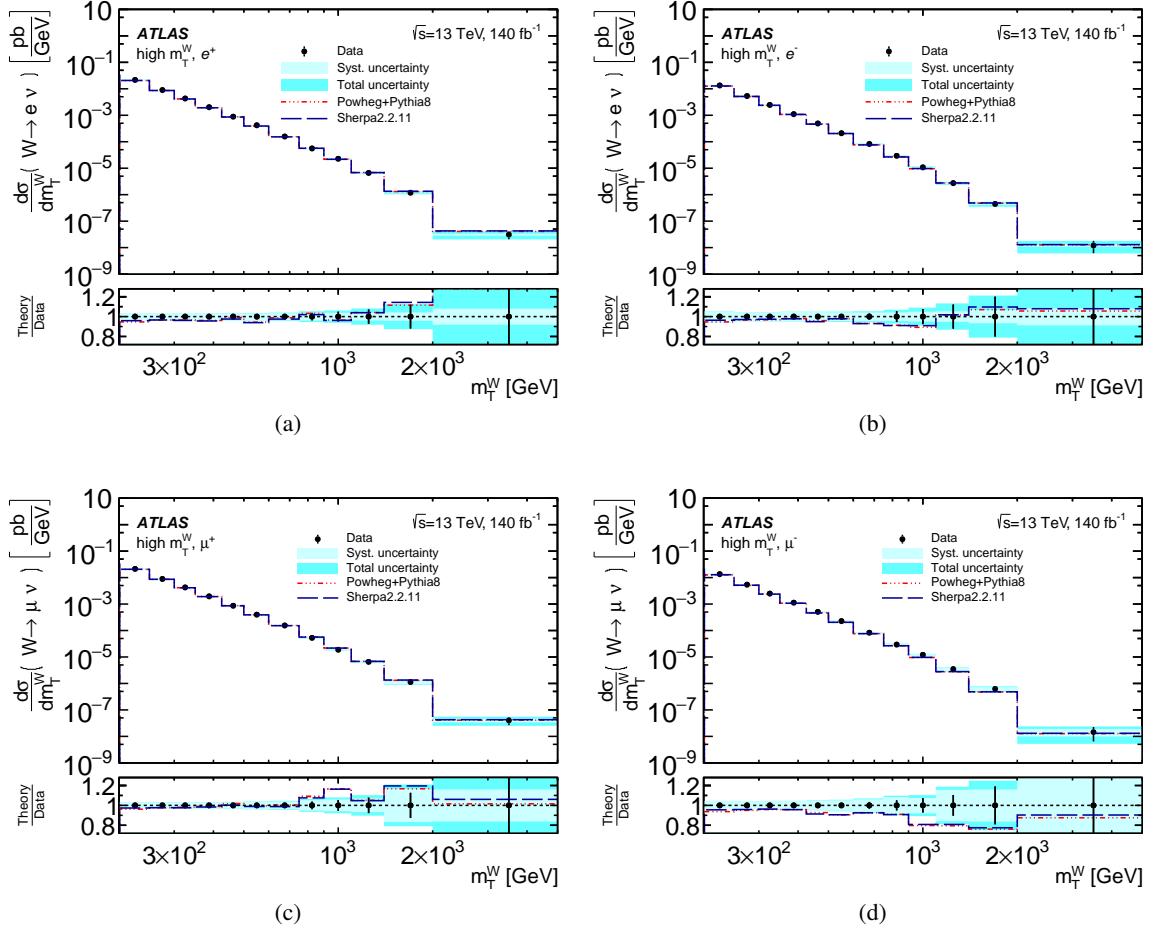


Figure 11: Unfolded differential cross-section binned in m_T^W region for the (a) e^+ , (b) e^- , (c) μ^+ and (d) μ^- final states. The error bars represent the statistical uncertainty. The inner shaded band represents the systematic uncertainty in the combined cross-sections, and the outer shaded band represents the total measurement uncertainty (excluding the luminosity uncertainty). The data are compared to predictions from SHERPA and POWHEG+PYTHIA.

The Born-level two-dimensional cross-sections $d^2\sigma/dm_T^W d|\eta|$ are shown in Figure 12 separately for each lepton charge and flavour. The data are presented in each m_T^W bin separated by the vertical lines, and the measurements for $m_T^W \geq 300$ GeV are scaled by the factors shown for presentation purposes only. The measurements are compared to the SHERPA and POWHEG+PYTHIA predictions which describe the data well.

The cross-sections at low m_T^W show a plateau-like behavior for $|\eta|$ up to 1.4, and then decrease at larger pseudorapidity. With increasing m_T^W the plateau region narrows.

8.2 Electron-muon ratios of charge-integrated cross-sections

Charge-integrated single- and double-differential cross-sections have also been extracted separately for the electron (e^\pm) and muon (μ^\pm) channel and can be found in HEPDATA.

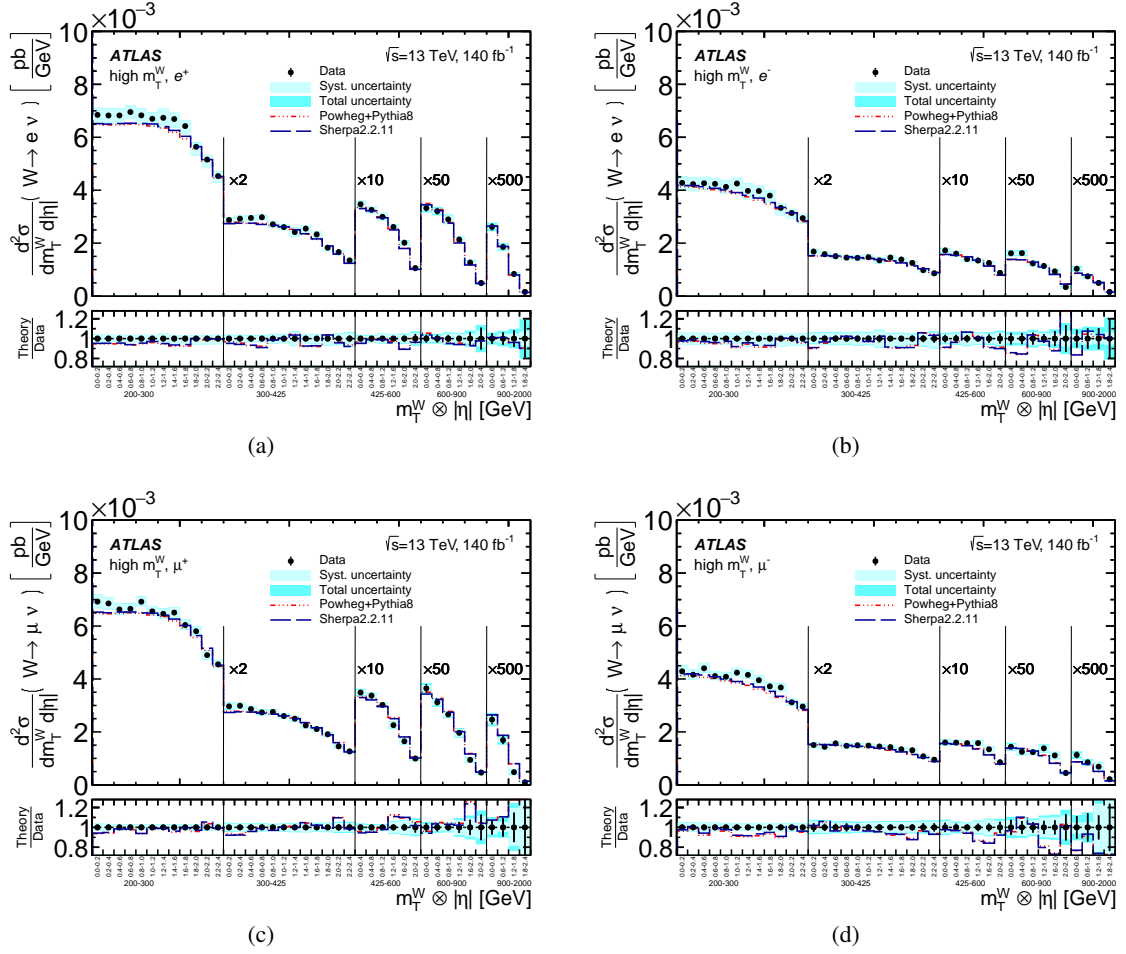


Figure 12: Two-dimensional unfolded cross-section binned in $|\eta|$ and m_T^W for the (a) e^+ , (b) e^- , (c) μ^+ and (d) μ^- final states. The error bars represent the statistical uncertainty. The inner shaded band represents the systematic uncertainty in the combined cross-sections, and the outer shaded band represents the total measurement uncertainty (excluding the luminosity uncertainty). The data are compared to predictions from SHERPA and POWHEG+PYTHIA. For better readability, the cross-sections in the last four m_T^W bins are scaled up by factors of 2, 10, 50 and 500, respectively.

Ratios of the charge-integrated cross-sections for the e^\pm to the μ^\pm final state are shown in Figure 13. Here all asymmetric uncertainties are symmetrized and the one-sided uncertainties are mirrored. This ratio provides a test of lepton flavour universality and is consistent with unity within the uncertainties.

8.3 Combination of electron and muon channels

The measurements in the e^\pm and μ^\pm final states are combined using a χ^2 minimisation procedure [81–83] under the assumption that the unfolded measurements for the same charge should agree. The technique improves the statistical precision of the data as well as the systematic uncertainty in case of uncertainties that are not (fully) correlated between the lepton flavours. The bin-to-bin correlated systematic uncertainties are taken into account by introducing a nuisance parameter for each source of uncertainty modelled as a unit Gaussian probability density contributing to the χ^2 definition. The systematic sources and their correlations

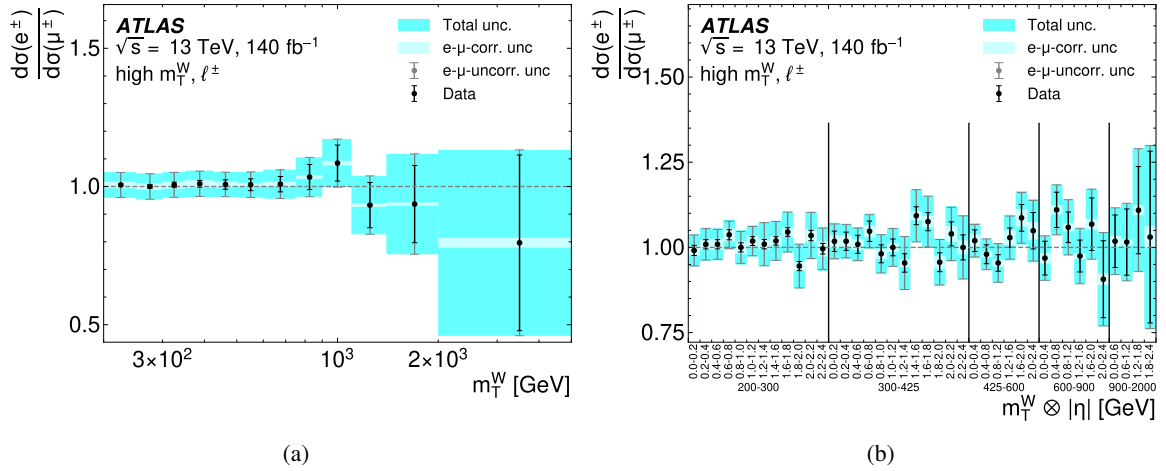


Figure 13: Ratio of the unfolded (a) single- and (b) double-differential electron- and muon-channel cross-sections in the combined ℓ^\pm -channel. The error bars represent the uncorrelated (systematic and statistical) uncertainties between the electron and muon channels, while the inner uncertainty band corresponds to the correlated uncertainties. The total uncertainty in the ratio is presented with the outer uncertainty band.

between channels are discussed in Section 7. The nuisance parameter values are optimised in the fit which minimises the χ^2 difference between the combined cross-section and the separate flavour channels, summed over the measurement bins. The combination provides new orthogonal systematic uncertainty sources which are linear combinations of the original sources, and therefore lose their association to specific experimental causes. In order to aid interpretation, the covariance matrix is rotated back to the (approximately) original physical source decomposition. Both versions are available in HEPDATA. The combination is first performed for the double-differential cross-sections, and simultaneously for both lepton charges, which allows optimal systematic constraints from the separate charge combinations and from the additional information encoded in the $|\eta|$ variable. The resulting shifts and constraints on the nuisance parameters are then transferred to the combination of the single-differential cross-sections.

The combined cross-sections $d^2\sigma/dm_T^W d|\eta|$ for the ℓ^+ and ℓ^- final states are shown in Figure 14. The double-differential cross-section combination shows good agreement between the lepton flavours. The fit has 80 degrees of freedom, and the total χ^2 is found to be 74 yielding $\chi^2/\text{dof} = 0.92$. In each figure the upper panels show the measured Born-level cross-sections for the electron channel, muon channel and the combination. The ratio of the pre-fit individual channels to the combined measurement is shown in the middle panel. The lower panel displays the pulls of the two channels, defined as the difference between the post-fit single-channel measurement and the combined result in units of the bin-to-bin uncorrelated uncertainty. No coherent trends between the measurements are observed and the pulls are found to be below two standard deviations everywhere.

The post-fit nuisance parameters shown in Figure 15 fluctuate around a mean of zero with shifts typically below one standard deviation. The exception to this is the high- p_T sagitta bias parameter with a shift of 1.8 standard deviations indicating a small residual undercalibration. This systematic source only affects the region $|\eta| > 1.1$. The parameter is also highly constrained by the combination indicating the calibration potential of this measurement. In addition, two of the twelve η binned electron identification systematics have pulls greater than one standard deviation. These sources arise from the limited sample sizes of the $Z \rightarrow e^+e^-$ data and are therefore statistical in nature.

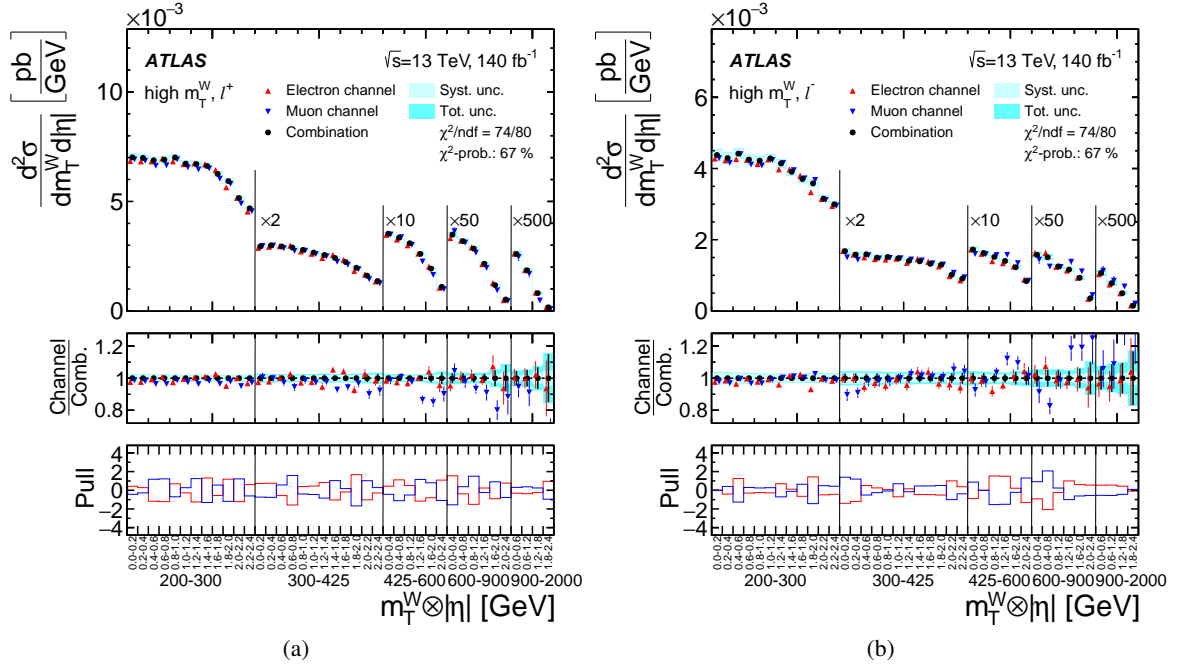


Figure 14: Electron, muon and combined fiducial Born-level cross-sections binned in m_T^W and $|\eta|$, for the (a) positive and (b) negative lepton charge. The error bars represent the statistical uncertainty. The inner shaded band represents the systematic uncertainty in the combined cross-sections, and the outer shaded band represents the total measurement uncertainty (excluding the luminosity uncertainty). For better readability, the cross-sections in the last four m_T^W bins are scaled up by factors of 2, 10, 50 and 500, respectively. The central panel shows the ratio of each measurement channel to the combined data, and the lower panel shows the pull of the post-fit electron and muon channel measurements with respect to the combined data.

8.4 Charge asymmetry of combined cross-sections

An asymmetry in the production of W bosons arises from the purely weak coupling to the quarks, the relative sizes of the production helicity amplitudes, and the PDFs. As the rapidity of the W boson is not directly accessible, measurements of the lepton charge asymmetry, A_ℓ , have been performed at the LHC [9, 84, 85] at 7, 8 and 13 TeV centre-of-mass energies in the resonant production region of the W boson.

The measurements presented here extend the experimental determination of the asymmetry to large m_T^W for the first time. The single- and double-differential lepton charge asymmetries are defined as

$$A_\ell = \frac{d\sigma_+ - d\sigma_-}{d\sigma_+ + d\sigma_-},$$

where $d\sigma_\pm$ represents the cross-section for the ℓ^+ or the ℓ^- final state respectively. The charge asymmetry uses the Born-level flavour-combined measurements with orthogonal uncertainty sources provided by the post-fit combination. They include correlations between the cross-sections for both charges as the flavour combination is performed over both charges simultaneously as described in Section 8.3.

The single- and double-differential determinations of A_ℓ are shown in Figure 16. The asymmetry is found to be large and positive, increasing with m_T^W , as expected from the increasing contribution of the u -valence PDF at larger Bjorken x . The $|\eta|$ dependence of A_ℓ is observed to be approximately constant for $|\eta| \lesssim 1.2$

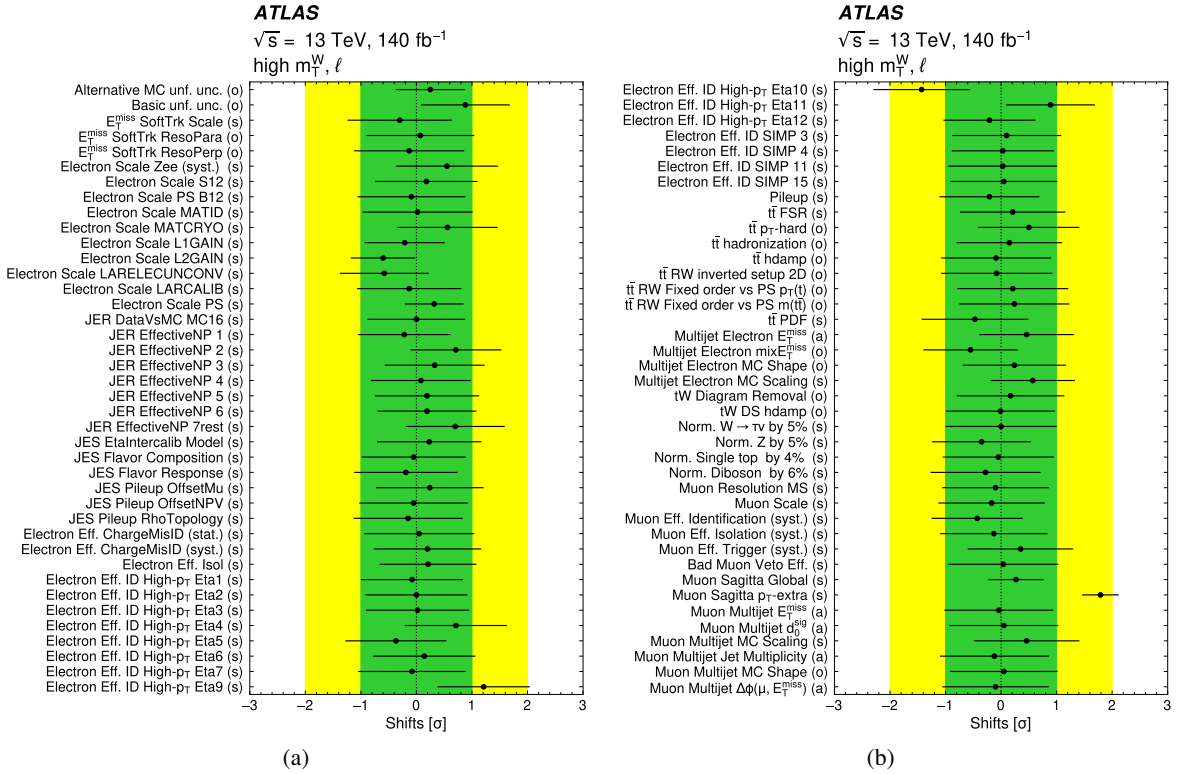


Figure 15: Shifts of the systematic uncertainty nuisance parameters after the combination of the double-differential electron and muon cross-sections. The systematic uncertainties are related to the unfolding procedure (“unf.”), the jet energy scale/resolution (“JER/JES”), the E_T^{miss} scale and resolution, the electron and muon scale, resolution and efficiency (“Eff.”), the multijet and $t\bar{t}$ (where RW refers to a reweighting to NNLO) background estimates and normalization of small background processes (“Norm.”). The uncertainties are marked whether they are symmetric (“s”), asymmetric (“a”) or one-sided (“o”). The systematic uncertainties labeled with “Electron” or “Muon” are not correlated between the lepton flavours.

and to fall rapidly at higher values of $|\eta|$ for larger values of m_T^W . The POWHEG+PYTHIA predictions are here updated to the CT18_{NNLO} PDF set, which is already used for SHERPA. Both predictions provide a good overall description of the measurements. In the highest m_T^W and $|\eta|$ bins the predicted asymmetry from SHERPA and POWHEG+PYTHIA becomes slightly negative. However the measurements do not have the statistical precision to confirm this behaviour.

9 Interpretation and discussion

9.1 Comparison to QCD predictions

The measured cross-sections are compared to a selection of QCD predictions. In particular the MC predictions from POWHEG+PYTHIA and SHERPA are presented together with a fixed-order calculation performed at NNLO with DYTURBO [86, 87]. The NLO EW corrections applied to POWHEG+PYTHIA (see Section 3) are also added to DYTURBO, whereas SHERPA includes these contributions natively. The

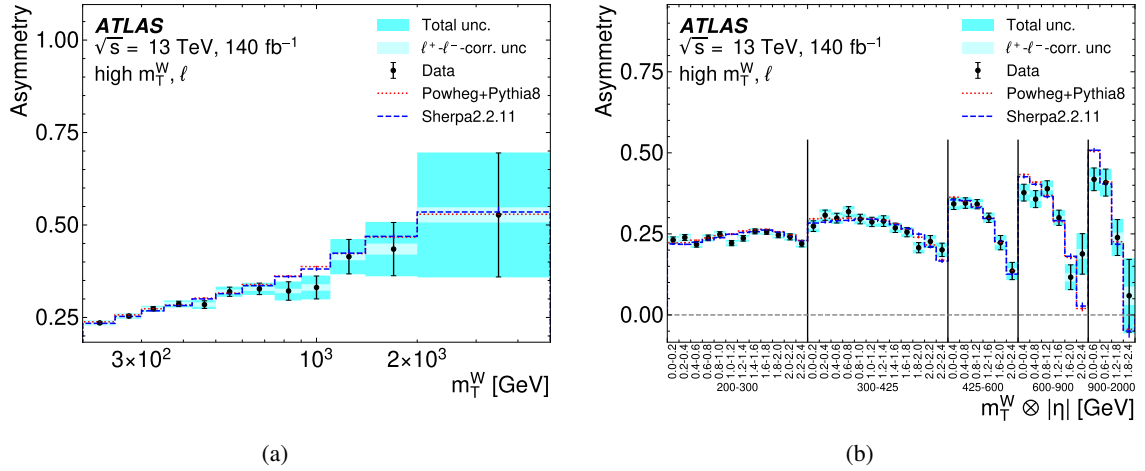


Figure 16: Charge asymmetry of the (a) single- and (b) double-differential electron/muon combined cross-section. The error bars represent the statistical uncertainties. The inner shaded band represents the systematic uncertainties that are correlated between the charges, and the outer shaded band represents the total measurement uncertainty. The data are compared to predictions from SHERPA and POWHEG+PYTHIA, both using the the CT18_{NNLO} PDF set.

predictions from POWHEG+PYTHIA, SHERPA and DYTURBO are shown for the CT18_{NNLO} PDF set. In addition the DYTURBO prediction is shown for four alternative PDF sets - MSHT20_{NNLO} [88], NNPDF4.0_{NNLO} [89], ATLASPDF21_{NNLO} ($T = 3$) [90], and CT18_{QED} [91].

The flavour-combined single- and double-differential cross-sections for the ℓ^+ and ℓ^- final states are compared to the predictions in Figures 17, 18, and 19. The middle panels of Figure 17 and the left panels of Figures 18 and 19 show that the POWHEG+PYTHIA, SHERPA and DYTURBO predictions using the CT18_{NNLO} PDF set agree very well for both lepton charges. They are consistent with the measurements, although a moderate undershoot of the predictions is observed for low m_T^W . The panels also display the DYTURBO calculation using the CT18_{QED} PDF which exhibits a consistently lower cross-section than from the CT18_{NNLO} PDFs. This difference is however small and increases with increasing m_T^W and increasing $|\eta|$ to up to 3%.

The middle panels of Figure 17 and the left panels of Figures 18 and 19 show DYTURBO predictions using different PDF sets as well as the 90% confidence level PDF uncertainty bands from the CT18_{NNLO} PDF. The prediction using MSHT20_{NNLO} is typically rather similar to the one from the CT18_{NNLO} PDF set, while the one using NNPDF4.0_{NNLO} is above the CT18_{NNLO} uncertainty band in the ℓ^+ channel in the region $m_T^W < 900$ GeV. The calculations with the ATLASPDF21_{NNLO} are typically above the CT18_{NNLO} uncertainty band. The DYTURBO predictions using different PDF sets are also compared to the measured single- and double-differential charge asymmetry A_ℓ in Figure 20. For the asymmetries the predictions agree well with the measurements and also for the separate ℓ^+ and ℓ^- final states the predictions are consistent with the measurements taking into account the sizeable uncertainties due to the PDFs. These uncertainties are found to be larger than the experimental uncertainties for $m_T^W \lesssim 1$ TeV, indicating the potential of these measurements to improve PDF determinations.

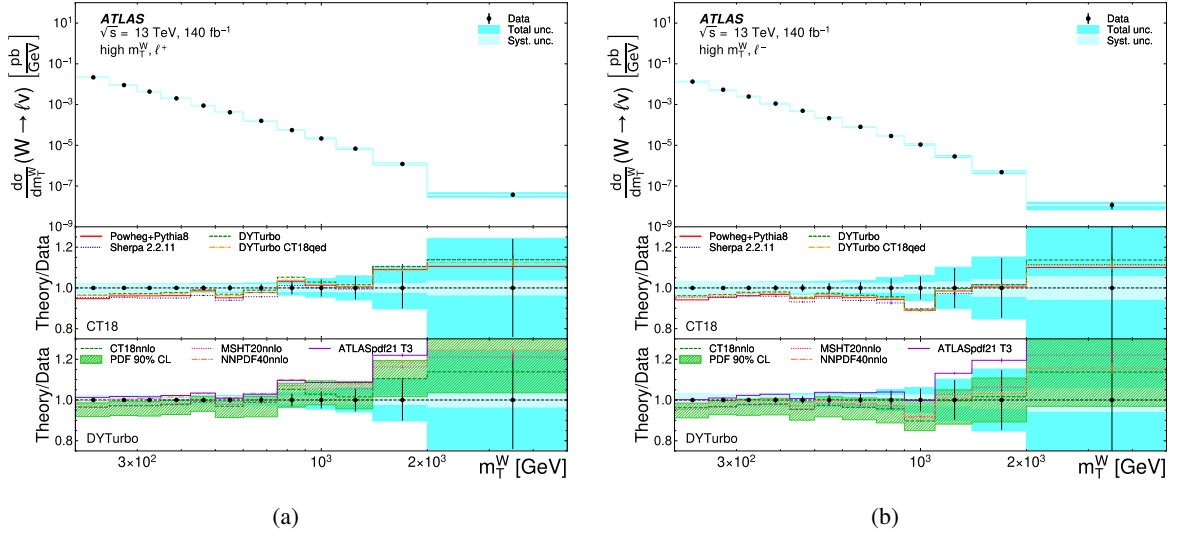


Figure 17: The combined Born-level cross-sections for the single-differential distributions are shown for the (a) ℓ^+ and (b) ℓ^- final state. The middle panels show a comparison to the predictions from SHERPA, POWHEG+PYTHIA and the fixed-order calculation from DYTURBO, each using the CT18NNLO PDF. In addition, a fixed-order calculation using DYTURBO and the CT18QED proton PDF is shown. A comparison to predictions with different PDFs using DYTURBO is displayed in the lower panel. The 90% CL PDF uncertainty is shown for CT18NNLO prediction. The statistical uncertainty of the combination is displayed with the error bars. The inner uncertainty band indicates the systematic uncertainty while the outer band corresponds to the total measurement uncertainty (excluding the luminosity uncertainty).

9.2 Effective Field Theory constraints

The measurements presented here may be sensitive to potential new physics beyond the direct energy reach of the LHC. EFTs are a useful tool for describing the physics below a defined energy cutoff scale Λ . The SMEFT is a generalised extension of the Standard Model, offering a broad and largely model-independent approach to search for new physics [92]. This approach is adopted here to interpret the cross-section measurements in terms of indirect contributions from physics beyond the Standard Model.

The SMEFT Lagrangian includes all possible operators constructed out of the SM field content:

$$\mathcal{L}_{\text{SMEFT}} = \mathcal{L}_{\text{SM}} + \sum_{d>4} \mathcal{L}^{(d)} = \mathcal{L}_{\text{SM}} + \sum_i \frac{c_i^{(d)}}{\Lambda^{d-4}} \mathcal{O}_i^{(d)},$$

where \mathcal{L}_{SM} is the SM Lagrangian, and $\mathcal{O}_i^{(d)}$ are SMEFT operators of dimension $d > 4$. Each operator is weighted by a dimensionless parameter, the Wilson coefficient $c_i^{(d)}$, and is additionally suppressed by powers of the energy cutoff scale Λ .

It is conventional in SMEFT analyses to set Λ to 1 TeV, with higher dimensional operators having increasingly suppressed Wilson coefficients. For this reason, it is common to truncate the SMEFT to dimension $d \leq 6$, as operators with $d > 6$ will likely have reduced impact on physical observables. Additionally, all odd mass-dimension operators in the SMEFT violate at least one of baryon or lepton number conservation, which are believed to be strong symmetries. All odd-dimension operators can therefore also be neglected, which justifies only considering the dimension-6 operators of the SMEFT.

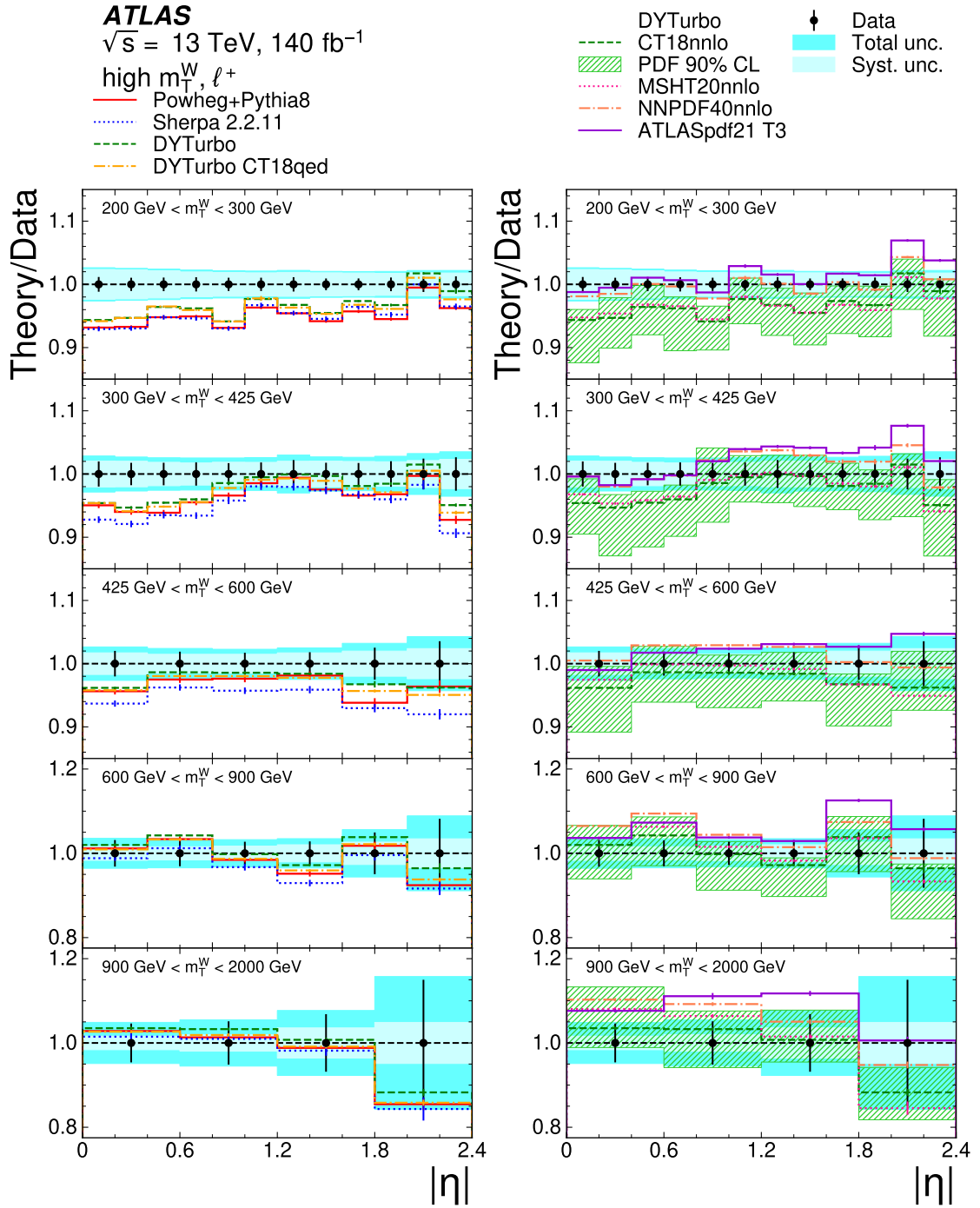


Figure 18: The combined Born-level cross-sections for the double-differential distributions are shown for the ℓ^+ final state. The left panel shows a comparison to the predictions from SHERPA, POWHEG+PYTHIA and the fixed-order calculation from DYTURBO, each using the CT18_{NNLO} PDF. In addition, a fixed-order calculation using DYTURBO and the CT18_{QED} proton PDF is shown. A comparison to predictions with different PDFs using DYTURBO is displayed in the right panel. The CT18_{NNLO} 90% CL PDF uncertainty is shown for the prediction. The statistical uncertainty of the combination is displayed with the error bars. The inner uncertainty band indicates the systematic uncertainty while the outer band corresponds to the total measurement uncertainty (excluding the luminosity uncertainty).

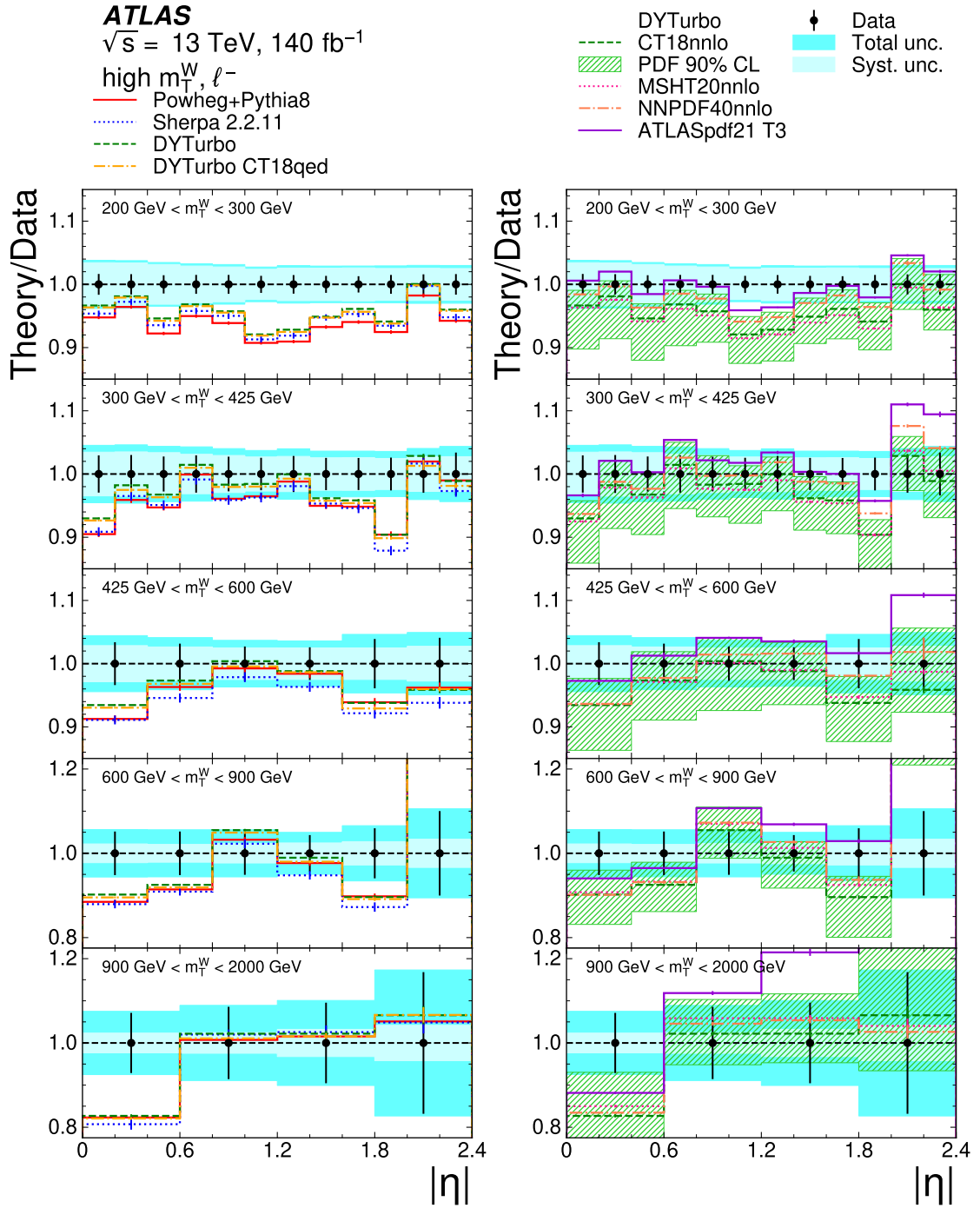


Figure 19: The combined Born-level cross-sections for the double-differential distributions are shown for the ℓ^- final state. The left panel shows a comparison to the predictions from SHERPA, POWHEG+PYTHIA and the fixed-order calculation from DYTURBO, each using the CT18_{NNLO} PDF. In addition, a fixed-order calculation using DYTURBO and the CT18_{QED} proton PDF is shown. A comparison to predictions with different PDFs using DYTURBO is displayed in the right panel. The CT18_{NNLO} 90% CL PDF uncertainty is shown for the prediction. The statistical uncertainty of the combination is displayed with the error bars. The inner uncertainty band indicates the systematic uncertainty while the outer band corresponds to the total measurement uncertainty (excluding the luminosity uncertainty).

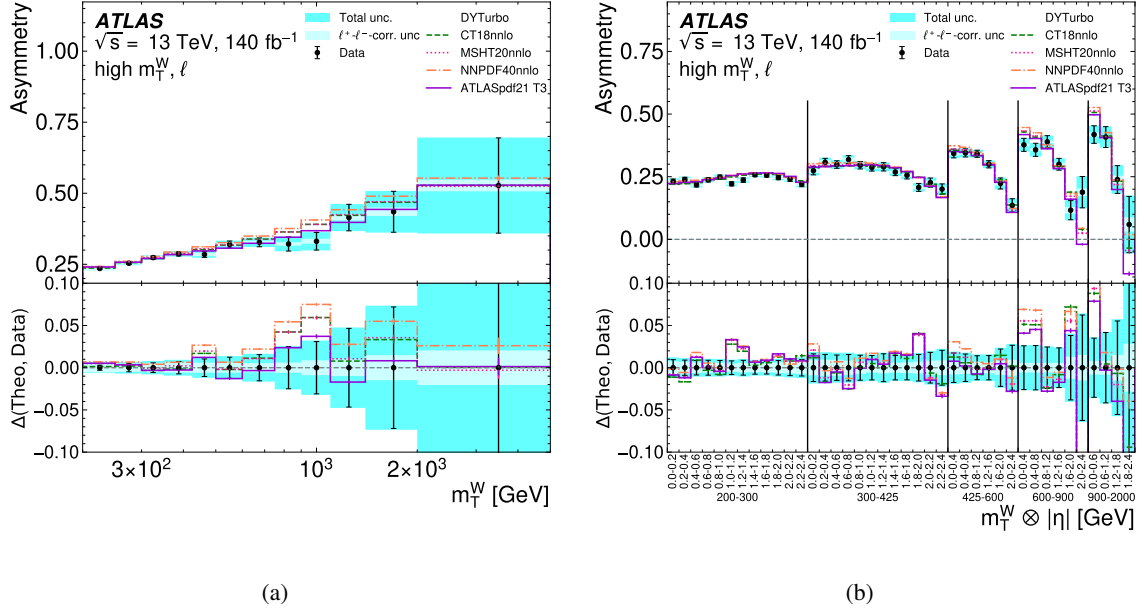


Figure 20: The Born-level lepton charge asymmetry of the combined cross-sections are shown for the (a) single- and (b) double-differential measurements. The error bars represent the statistical and uncorrelated systematic uncertainties between the ℓ^+ - and ℓ^- - channels, while the inner uncertainty band corresponds to the correlated uncertainties. The total uncertainty in the asymmetry is represented with the outer band. In addition, theoretical predictions using DYTURBO for different PDFs are displayed. The lower panels show the absolute difference between each theory calculation and the measured asymmetry.

A complete set of dimension-6 operators of the SMEFT is given by the Warsaw basis [93]. The Warsaw basis provides a minimal basis with all redundant operators removed, containing 2499 dimension-6 operators, each associated with a Wilson coefficient. The Wilson coefficients are unknown free parameters, whose values must be determined experimentally. The number of free parameters can be reduced by imposing symmetries amongst the flavour structure of the fermion generations. The most restrictive flavour symmetry is known as the $U(3)^5$ symmetry, and reduces the number of operators to 59, considering only those that conserve baryon and lepton number [92].

Physical observables receive corrections from the presence of dimension-6 SMEFT operators. The amplitude-squared for a general physics process is given by

$$|\mathcal{A}^2| = |\mathcal{A}_{\text{SM}}|^2 + \sum_i \frac{c_i}{\Lambda^2} \mathcal{A}_{\text{SM}}^\dagger \mathcal{A}_i + \sum_i \frac{|c_i|^2}{\Lambda^4} |\mathcal{A}_i|^2 + \sum_{i,j,i \neq j} \frac{c_i c_j}{\Lambda^4} \mathcal{A}_i^\dagger \mathcal{A}_j,$$

where \mathcal{A}_{SM} is the SM amplitude and \mathcal{A}_i is the contribution from operator \mathcal{O}_i to the amplitude \mathcal{A} . The modifications to physical observables can be separated into three terms:

- Linear interference between the SM and EFT amplitudes.
- Pure quadratic EFT contribution.
- Interference cross terms between EFT amplitudes.

The charged-current Drell–Yan process receives corrections from four different dimension-6 operators, within the $U(3)^5$ symmetry scheme of the Warsaw basis. Those operators and their Wilson coefficients are shown in Table 2.

The sensitivity of the charged-current Drell–Yan process to each operator is studied by generating MC predictions within the SMEFT and comparing against SM predictions. Both SMEFT and SM predictions at LO in QCD are produced using MADGRAPH5_AMC@NLO 2.9.9 [94] and the SMEFTSIM 3.0 package [95]. The m_W, m_Z, G_F electroweak input parameter scheme is used. Events are interfaced with PYTHIA 8.3 [96] for parton showering and hadronisation. The cutoff scale is set to $\Lambda = 1$ TeV.

The effects of each operator on the single-differential cross-section are studied by setting the Wilson coefficient of each of the four operators to unity and setting all others to zero in turn. It is observed that the quark-lepton contact operator $O_{lq}^{(3)}$ gives significant enhancements to the cross section at high m_T^W , whilst the other three operators introduce a constant scaling in the cross-section with no mass dependence. A similar analysis of the double-differential cross-sections shows there is no additional SMEFT operator sensitivity associated with the $|\eta|$ dependence of the cross-sections. Similarly, the charge-separated results do not yield additional sensitivity. Therefore the SMEFT analysis is performed on the single-differential charge-integrated cross sections for the electron, muon and combined channels only.

The statistical model employed is a likelihood function with multivariate Gaussian probability density functions representing the measurement uncertainties. The likelihood is written as

$$L = \frac{1}{\sqrt{(2\pi)^{N_{\text{bins}}|\Sigma|}}} \exp \left\{ -\frac{1}{2} \left[\vec{x} - \vec{\mu}(\vec{\theta}) \right]^T \Sigma^{-1} \left[\vec{x} - \vec{\mu}(\vec{\theta}) \right] \right\} \times \prod_i \theta_i.$$

Here, Σ is the covariance matrix, which includes statistical uncertainties only and is therefore diagonal. The vectors \vec{x} and $\vec{\mu}$ represent the measured distribution and predicted distributions, respectively. Both the experimental and theoretical systematic uncertainties are included as nuisance parameters $\vec{\theta}$, where a shift of $\vec{\theta}_i = 1$ corresponds to a shift of the source i by one standard deviation.

The EFT dependence of the cross-section is parametrised as a quadratic function. In particular, the cross-section in bin i is given by a quadratic function of the Wilson coefficient c :

$$\sigma_i = \sigma_{SM,i} + c \sigma_{\text{lin},i} + c^2 \sigma_{\text{quad},i},$$

where σ_i is the SM prediction, and $\sigma_{\text{lin},i}$ and $\sigma_{\text{quad},i}$ are constants describing the dependence of the cross-section on c and c^2 respectively. These two coefficients, $\sigma_{\text{lin},i}$ and $\sigma_{\text{quad},i}$, as well as b_i must be determined from MC simulation in order to infer information about the Wilson coefficients.

Table 2: Dimension-6 SMEFT operators and their corresponding Wilson coefficients affecting the charged current Drell–Yan, in the $U(3)^5$ symmetry of the Warsaw basis. Here, H is the Higgs doublet, and q, l represent the left-handed quark and lepton doublets respectively. The matrices $\tau^I, I = 1, 2, 3$ represent Pauli matrices, and D_μ^I is the usual Standard Model covariant derivative.

Wilson Coefficient	Operator
$c_{lq}^{(3)}$	$O_{lq}^{(3)} = (\bar{l}\tau^I\gamma_\mu l)(\bar{q}\tau^I\gamma^\mu q)$
$c_{ll}^{(1)}$	$O_{ll}^{(1)} = (\bar{l}\gamma_\mu l)(\bar{l}\gamma^\mu l)$
$c_{Hl}^{(3)}$	$O_{Hl}^{(3)} = (H^\dagger i \overleftrightarrow{D}_\mu^I H)(\bar{l}\tau^I\gamma^\mu l)$
$c_{Hq}^{(3)}$	$O_{Hq}^{(3)} = (H^\dagger i \overleftrightarrow{D}_\mu^I H)(\bar{q}\tau^I\gamma^\mu q)$

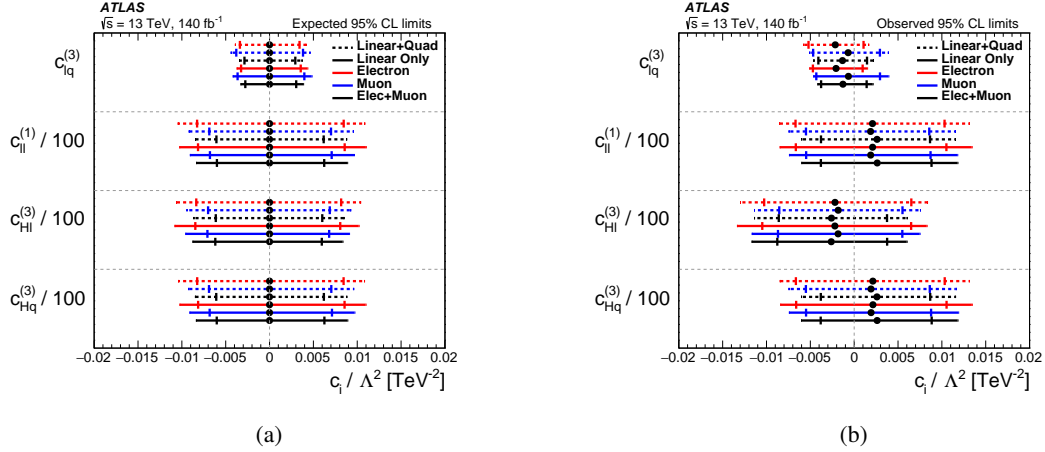


Figure 21: The (a) expected and (b) observed limits on Wilson coefficients at 95% CL. The results are shown for linear-only and linear+quadratic fits, for both the electron and muon channels, as well as their combination. The inner (outer) error bars indicate the limits when using the 68% (90%) CL for the PDF uncertainty.

As the SMEFT and SM predictions are only computed at LO in QCD, the predictions are modified to account for higher-order QCD and EW corrections via

$$\sigma_i = \sigma_i^{\text{best}} \left(1 + c \frac{\sigma_{\text{lin},i}}{\sigma_i^{\text{LO}}} + c^2 \frac{\sigma_{\text{quad},i}}{\sigma_i^{\text{LO}}} \right),$$

where σ_i^{best} represents a higher-order SM prediction, and σ_i^{LO} represents the LO SM prediction. It is assumed that the relative effect of higher-order predictions does not change in the presence of dimension-six operators. The higher-order SM prediction is generated using DYTURBO, as introduced Section 9.1. The prediction uses the CT18_{NNLO} PDF set, with $\alpha_s = 0.118$ and additive EW corrections.

Theoretical uncertainties arising from variations of α_s , PDFs, EW corrections, and the renormalisation (μ_R) and factorisation scale (μ_F) variations are implemented as follows: the value of $\alpha_s(M_Z)$ at the Z pole is varied by ± 0.001 ; μ_R and μ_F are varied independently by factors of 2 avoiding extreme variations; the EW corrections are included as multiplicative factors on the predictions, rather than additive; and the PDF eigenvector variations for the CT18_{NNLO} set are used at the 90% CL.

Expected limits on the Wilson coefficients are derived by using the DYTURBO prediction as the measurement pseudo-data instead of using the actual measurement as for the observed limits. The fits are performed first by using only the linear SM and EFT interference terms, then by including the quadratic pure EFT contributions as well. They are obtained by allowing only one coefficient to be non-zero at a time.

The expected and observed limits on the Wilson coefficients are given in Figure 21 and are also shown in Table 3. All observed limits are compatible with the $c_i = 0$ assumption at 95% CL, indicating no significant deviations from the SM are observed. The strongest limits are derived by using the data from the combined channel due to the reduced statistical and systematic uncertainties after the electron-muon combination. Differences between the constraints obtained using linear+quadratic and linear-only terms are negligible, indicating the constraints are driven mostly by the linear-interference terms. This suggests that the measurement is largely insensitive to the $1/\Lambda^4$ contributions arising from interference between

Table 3: The expected and observed EFT limits at 95% CL, shown for the linear-only and linear+quadratic electron, muon, and combined fits.

	Expected (Linear + Quadratic) [TeV ⁻²]			Observed (Linear + Quadratic) [TeV ⁻²]		
	Electron	Muon	Combined	Electron	Muon	Combined
$c_{lq}^{(3)}/\Lambda^2$	[-0.0039, 0.0041]	[-0.0044, 0.0046]	[-0.0035, 0.0037]	[-0.0058, 0.0016]	[-0.0051, 0.0038]	[-0.0047, 0.0021]
$c_{ll}^{(1)}/\Lambda^2$	[-1.05, 1.08]	[-0.92, 0.95]	[-0.85, 0.87]	[-0.86, 1.31]	[-0.75, 1.15]	[-0.60, 1.15]
$c_{Hl}^{(3)}/\Lambda^2$	[-1.07, 1.03]	[-0.95, 0.92]	[-0.87, 0.84]	[-1.30, 0.83]	[-1.14, 0.75]	[-1.14, 0.60]
$c_{Hq}^{(3)}/\Lambda^2$	[-1.04, 1.08]	[-0.93, 0.95]	[-0.85, 0.88]	[-0.85, 1.31]	[-0.75, 1.16]	[-0.61, 1.15]

	Expected (Linear) [TeV ⁻²]			Observed (Linear) [TeV ⁻²]		
	Electron	Muon	Combined	Electron	Muon	Combined
$c_{lq}^{(3)}/\Lambda^2$	[-0.0038, 0.0043]	[-0.0042, 0.0048]	[-0.0033, 0.0038]	[-0.0051, 0.0015]	[-0.0047, 0.0039]	[-0.0042, 0.0021]
$c_{ll}^{(1)}/\Lambda^2$	[-1.03, 1.10]	[-0.91, 0.96]	[-0.84, 0.89]	[-0.85, 1.34]	[-0.74, 1.18]	[-0.60, 1.18]
$c_{Hl}^{(3)}/\Lambda^2$	[-1.08, 1.02]	[-0.96, 0.91]	[-0.88, 0.83]	[-1.34, 0.83]	[-1.17, 0.75]	[-1.17, 0.60]
$c_{Hq}^{(3)}/\Lambda^2$	[-1.03, 1.10]	[-0.91, 0.97]	[-0.84, 0.89]	[-0.84, 1.34]	[-0.74, 1.19]	[-0.61, 1.18]

SM and dimension-8 operators, implying the constraints are robust despite truncating the SMEFT to dimension-6.

The limits on the EFT Wilson coefficients improve by a factor 1.4 to 2.6 when the fits are performed using only experimental uncertainties. This indicates the importance of increasing the precision of the theoretical predictions, in particular for the PDFs, in future measurements. Figure 21 shows that using the 68% CL PDF uncertainty instead of the 90% CL uncertainty improves the limits on the Wilson coefficients by a factor of 1.1-1.4. The limit on the Wilson coefficient $c_{lq}^{(3)}$ exceeds previous four-fermion limits using ATLAS data [97] as well as limits from low-energy data [98] and global analyses [99, 100].

10 Conclusions

This paper present a first measurement of the W^\pm production cross-section above the resonant production region. The single-differential cross-sections, $d\sigma/dm_T^W$, are measured in the region $200 \leq m_T^W \leq 5000$ GeV. The measurements are also presented as double-differential cross-sections, $d^2\sigma/dm_T^W d|\eta|$, in the region $200 \leq m_T^W \leq 2000$ GeV and $0 \leq |\eta| \leq 2.4$. These fiducial measurements use 140 fb^{-1} of LHC pp collision data collected by ATLAS at a centre-of-mass energy of 13 TeV, and are performed separately for both charges and for the electron and muon final states. They are unfolded for detector effects to the Born level. Corrections to the dressed particle level are also provided.

Combinations of the charge-separated cross-sections for the electron and muon final states are performed to improve the statistical and systematic uncertainties in the measurements. These combined data compare well to state-of-the-art theoretical predictions at NNLO in QCD including NLO EW effects. The uncertainties in the predictions arising from the PDFs are found to be typically larger than the experimental uncertainties, indicating the potential of these measurements to improve PDF determinations. The single- and double-differential lepton charge asymmetry, A_ℓ , is presented and shown to be well described by the predictions.

A test of lepton flavour universality in the range $200 \text{ GeV} < m_T^W < 5000 \text{ GeV}$ is performed by determining the ratio of the charge-combined cross-sections for the electron to the muon final state. No deviations from the Standard Model are observed.

Finally, the single-differential cross-sections are used to search for signals of new physics in an effective field theory approach within the SMEFT $U(3)^5$ symmetry model. The data constrain the Wilson coefficients of four operators in the Warsaw basis. In particular the measurements provide the world-leading constraints on the Wilson coefficient $c_{lq}^{(3)}$.

Acknowledgements

We thank CERN for the very successful operation of the LHC and its injectors, as well as the support staff at CERN and at our institutions worldwide without whom ATLAS could not be operated efficiently.

The crucial computing support from all WLCG partners is acknowledged gratefully, in particular from CERN, the ATLAS Tier-1 facilities at TRIUMF/SFU (Canada), NDGF (Denmark, Norway, Sweden), CC-IN2P3 (France), KIT/GridKA (Germany), INFN-CNAF (Italy), NL-T1 (Netherlands), PIC (Spain), RAL (UK) and BNL (USA), the Tier-2 facilities worldwide and large non-WLCG resource providers. Major contributors of computing resources are listed in Ref. [101].

We gratefully acknowledge the support of ANPCyT, Argentina; YerPhI, Armenia; ARC, Australia; BMWFW and FWF, Austria; ANAS, Azerbaijan; CNPq and FAPESP, Brazil; NSERC, NRC and CFI, Canada; CERN; ANID, Chile; CAS, MOST and NSFC, China; Minciencias, Colombia; MEYS CR, Czech Republic; DNRF and DNSRC, Denmark; IN2P3-CNRS and CEA-DRF/IRFU, France; SRNSFG, Georgia; BMBF, HGF and MPG, Germany; GSRI, Greece; RGC and Hong Kong SAR, China; ICHEP and Academy of Sciences and Humanities, Israel; INFN, Italy; MEXT and JSPS, Japan; CNRST, Morocco; NWO, Netherlands; RCN, Norway; MNiSW, Poland; FCT, Portugal; MNE/IFA, Romania; MSTDI, Serbia; MSSR, Slovakia; ARIS and MVZI, Slovenia; DSI/NRF, South Africa; MICIU/AEI, Spain; SRC and Wallenberg Foundation, Sweden; SERI, SNSF and Cantons of Bern and Geneva, Switzerland; NSTC, Taipei; TENMAK, Türkiye; STFC/UKRI, United Kingdom; DOE and NSF, United States of America.

Individual groups and members have received support from BCKDF, CANARIE, CRC and DRAC, Canada; CERN-CZ, FORTE and PRIMUS, Czech Republic; COST, ERC, ERDF, Horizon 2020, ICSC-NextGenerationEU and Marie Skłodowska-Curie Actions, European Union; Investissements d’Avenir Labex, Investissements d’Avenir Idex and ANR, France; DFG and AvH Foundation, Germany; Herakleitos, Thales and Aristeia programmes co-financed by EU-ESF and the Greek NSRF, Greece; BSF-NSF and MINERVA, Israel; NCN and NAWA, Poland; La Caixa Banking Foundation, CERCA Programme Generalitat de Catalunya and PROMETEO and GenT Programmes Generalitat Valenciana, Spain; Göran Gustafssons Stiftelse, Sweden; The Royal Society and Leverhulme Trust, United Kingdom.

In addition, individual members wish to acknowledge support from Armenia: Yerevan Physics Institute (FAPERJ); CERN: European Organization for Nuclear Research (CERN DOCT); Chile: Agencia Nacional de Investigación y Desarrollo (FONDECYT 1230812, FONDECYT 1230987, FONDECYT 1240864); China: Chinese Ministry of Science and Technology (MOST-2023YFA1605700, MOST-2023YFA1609300), National Natural Science Foundation of China (NSFC - 12175119, NSFC 12275265); Czech Republic: Czech Science Foundation (GACR - 24-11373S), Ministry of Education Youth and Sports (FORTE CZ.02.01.01/00/22_008/0004632), PRIMUS Research Programme (PRIMUS/21/SCI/017); EU: H2020 European Research Council (ERC - 101002463); European Union: European Research Council

(ERC - 948254, ERC 101089007, ERC, BARD, 101116429), Horizon 2020 Framework Programme (MUCCA - CHIST-ERA-19-XAI-00), European Union, Future Artificial Intelligence Research (FAIR-NextGenerationEU PE00000013), Horizon 2020 (EuroHPC - EHPC-DEV-2024D11-051), Italian Center for High Performance Computing, Big Data and Quantum Computing (ICSC, NextGenerationEU); France: Agence Nationale de la Recherche (ANR-21-CE31-0013, ANR-21-CE31-0022, ANR-22-EDIR-0002); Germany: Baden-Württemberg Stiftung (BW Stiftung-Postdoc Eliteprogramme), Deutsche Forschungsgemeinschaft (DFG - 469666862, DFG - CR 312/5-2); China: Research Grants Council (GRF); Italy: Istituto Nazionale di Fisica Nucleare (ICSC, NextGenerationEU), Ministero dell'Università e della Ricerca (PRIN - 20223N7F8K - PNRR M4.C2.1.1); Japan: Japan Society for the Promotion of Science (JSPS KAKENHI JP22H01227, JSPS KAKENHI JP22H04944, JSPS KAKENHI JP22KK0227, JSPS KAKENHI JP23KK0245); Norway: Research Council of Norway (RCN-314472); Poland: Ministry of Science and Higher Education (IDUB AGH, POB8, D4 no 9722), Polish National Science Centre (NCN 2021/42/E/ST2/00350, NCN OPUS 2023/51/B/ST2/02507, NCN OPUS nr 2022/47/B/ST2/03059, NCN UMO-2019/34/E/ST2/00393, UMO-2020/37/B/ST2/01043, UMO-2022/47/O/ST2/00148, UMO-2023/49/B/ST2/04085, UMO-2023/51/B/ST2/00920, UMO-2024/53/N/ST2/00869); Spain: Generalitat Valenciana (Artemisa, FEDER, IDIFEDER/2018/048), Ministry of Science and Innovation (MCIN & NextGenEU PCI2022-135018-2, MICIN & FEDER PID2021-125273NB, RYC2019-028510-I, RYC2020-030254-I, RYC2021-031273-I, RYC2022-038164-I); Sweden: Carl Trygger Foundation (Carl Trygger Foundation CTS 22:2312), Swedish Research Council (Swedish Research Council 2023-04654, VR 2021-03651, VR 2022-03845, VR 2022-04683, VR 2023-03403, VR 2024-05451), Knut and Alice Wallenberg Foundation (KAW 2018.0458, KAW 2022.0358, KAW 2023.0366); Switzerland: Swiss National Science Foundation (SNSF - PCEFP2_194658); United Kingdom: Leverhulme Trust (Leverhulme Trust RPG-2020-004), Royal Society (NIF-R1-231091); United States of America: U.S. Department of Energy (ECA DE-AC02-76SF00515), Neubauer Family Foundation.

References

- [1] S. D. Drell and T.-M. Yan, *Massive Lepton-Pair Production in Hadron-Hadron Collisions at High Energies*, *Phys. Rev. Lett.* **25** (1970) 316.
- [2] C. Duhr, F. Dulat and B. Mistlberger, *Charged current Drell-Yan production at N³LO*, *JHEP* **11** (2020) 143, arXiv: [2007.13313](#) [[hep-ph](#)].
- [3] C. Duhr and B. Mistlberger, *Lepton-pair production at hadron colliders at N³LO in QCD*, *JHEP* **03** (2022) 116, arXiv: [2111.10379](#) [[hep-ph](#)].
- [4] X. Chen et al., *Transverse mass distribution and charge asymmetry in W boson production to third order in QCD*, *Phys. Lett. B* **840** (2023) 137876, arXiv: [2205.11426](#) [[hep-ph](#)].
- [5] J. Campbell and T. Neumann, *Third order QCD predictions for fiducial W-boson production*, *JHEP* **11** (2023) 127, arXiv: [2308.15382](#) [[hep-ph](#)].
- [6] ATLAS Collaboration, *Precise measurements of W- and Z-boson transverse momentum spectra with the ATLAS detector using pp collisions at $\sqrt{s} = 5.02$ TeV and 13 TeV*, *Eur. Phys. J. C* **84** (2024) 1126, arXiv: [2404.06204](#) [[hep-ex](#)].

- [7] ATLAS Collaboration, *Measurement of vector boson production cross sections and their ratios using pp collisions at $\sqrt{s} = 13.6$ TeV with the ATLAS detector*, *Phys. Lett. B* **854** (2024) 138725, arXiv: [2403.12902 \[hep-ex\]](#).
- [8] CMS Collaboration, *Measurement of the inclusive cross sections for W and Z boson production in proton-proton collisions at $\sqrt{s} = 5.02$ and 13 TeV*, 2024, arXiv: [2408.03744 \[hep-ex\]](#).
- [9] CMS Collaboration, *Measurements of the W boson rapidity, helicity, double-differential cross sections, and charge asymmetry in pp collisions at $\sqrt{s} = 13$ TeV*, *Phys. Rev. D* **102** (2020) 092012, arXiv: [2008.04174 \[hep-ex\]](#).
- [10] CMS Collaboration, *Measurements of differential Z boson production cross sections in proton-proton collisions at $\sqrt{s} = 13$ TeV*, *JHEP* **12** (2019) 061, arXiv: [1909.04133 \[hep-ex\]](#).
- [11] LHCb collaboration, *Measurement of the forward Z boson production cross-section in pp collisions at $\sqrt{s} = 13$ TeV*, *JHEP* **09** (2016) 136, arXiv: [1607.06495](#).
- [12] ATLAS Collaboration, *Measurement of the low-mass Drell–Yan differential cross section at $\sqrt{s} = 7$ TeV using the ATLAS detector*, *JHEP* **06** (2014) 112, arXiv: [1404.1212 \[hep-ex\]](#).
- [13] ATLAS Collaboration, *Measurement of the high-mass Drell–Yan differential cross-section in pp collisions at $\sqrt{s} = 7$ TeV with the ATLAS detector*, *Phys. Lett. B* **725** (2013) 223, arXiv: [1305.4192 \[hep-ex\]](#).
- [14] ATLAS Collaboration, *Measurement of the double-differential high-mass Drell–Yan cross section in pp collisions at $\sqrt{s} = 8$ TeV with the ATLAS detector*, *JHEP* **08** (2016) 009, arXiv: [1606.01736 \[hep-ex\]](#).
- [15] CMS Collaboration, *Measurement of the Drell–Yan Cross Section in pp Collisions at $\sqrt{s} = 7$ TeV*, *JHEP* **10** (2011) 007, arXiv: [1108.0566 \[hep-ex\]](#).
- [16] CMS Collaboration, *Measurement of the differential and double-differential Drell–Yan cross sections in proton–proton collisions at $\sqrt{s} = 7$ TeV*, *JHEP* **12** (2013) 030, arXiv: [1310.7291 \[hep-ex\]](#).
- [17] CMS Collaboration, *Measurements of differential and double-differential Drell–Yan cross sections in proton–proton collisions at $\sqrt{s} = 8$ TeV*, *Eur. Phys. J. C* **75** (2015) 147, arXiv: [1412.1115 \[hep-ex\]](#).
- [18] CMS Collaboration, *Measurement of the differential Drell–Yan cross section in proton–proton collisions at $\sqrt{s} = 13$ TeV*, *JHEP* **12** (2019) 059, arXiv: [1812.10529 \[hep-ex\]](#).
- [19] ATLAS Collaboration, *Search for a heavy charged boson in events with a charged lepton and missing transverse momentum from pp collisions at $\sqrt{s} = 13$ TeV with the ATLAS detector*, *Phys. Rev. D* **100** (2019) 052013, arXiv: [1906.05609 \[hep-ex\]](#).
- [20] CMS Collaboration, *Search for new physics in the lepton plus missing transverse momentum final state in proton–proton collisions at $\sqrt{s} = 13$ TeV*, *JHEP* **07** (2022) 067, arXiv: [2202.06075 \[hep-ex\]](#).
- [21] M. Farina et al., *Energy helps accuracy: Electroweak precision tests at hadron colliders*, *Phys. Lett. B* **772** (2017) 210, arXiv: [1609.08157 \[hep-ph\]](#).
- [22] ATLAS Collaboration, *The ATLAS Experiment at the CERN Large Hadron Collider*, *JINST* **3** (2008) S08003.

- [23] ATLAS Collaboration, *ATLAS Insertable B-Layer: Technical Design Report*, ATLAS-TDR-19; CERN-LHCC-2010-013, 2010, URL: <https://cds.cern.ch/record/1291633>, Addendum: ATLAS-TDR-19-ADD-1; CERN-LHCC-2012-009, 2012, URL: <https://cds.cern.ch/record/1451888>.
- [24] B. Abbott et al., *Production and integration of the ATLAS Insertable B-Layer*, *JINST* **13** (2018) T05008, arXiv: [1803.00844](https://arxiv.org/abs/1803.00844) [[physics.ins-det](#)].
- [25] G. Avoni et al., *The new LUCID-2 detector for luminosity measurement and monitoring in ATLAS*, *JINST* **13** (2018) P07017.
- [26] ATLAS Collaboration, *Performance of the ATLAS trigger system in 2015*, *Eur. Phys. J. C* **77** (2017) 317, arXiv: [1611.09661](https://arxiv.org/abs/1611.09661) [[hep-ex](#)].
- [27] ATLAS Collaboration, *Software and computing for Run 3 of the ATLAS experiment at the LHC*, (2024), arXiv: [2404.06335](https://arxiv.org/abs/2404.06335) [[hep-ex](#)].
- [28] P. Nason, *A new method for combining NLO QCD with shower Monte Carlo algorithms*, *JHEP* **11** (2004) 040, arXiv: [hep-ph/0409146](https://arxiv.org/abs/hep-ph/0409146).
- [29] S. Frixione, P. Nason and C. Oleari, *Matching NLO QCD computations with parton shower simulations: the POWHEG method*, *JHEP* **11** (2007) 070, arXiv: [0709.2092](https://arxiv.org/abs/0709.2092) [[hep-ph](#)].
- [30] S. Alioli, P. Nason, C. Oleari and E. Re, *NLO vector-boson production matched with shower in POWHEG*, *JHEP* **07** (2008) 060, arXiv: [0805.4802](https://arxiv.org/abs/0805.4802) [[hep-ph](#)].
- [31] S. Alioli, P. Nason, C. Oleari and E. Re, *A general framework for implementing NLO calculations in shower Monte Carlo programs: the POWHEG BOX*, *JHEP* **06** (2010) 043, arXiv: [1002.2581](https://arxiv.org/abs/1002.2581) [[hep-ph](#)].
- [32] H.-L. Lai et al., *New parton distributions for collider physics*, *Phys. Rev. D* **82** (2010) 074024, arXiv: [1007.2241](https://arxiv.org/abs/1007.2241) [[hep-ph](#)].
- [33] T. Sjöstrand, S. Mrenna and P. Skands, *A Brief Introduction to PYTHIA 8.1*, *Comput. Phys. Commun.* **178** (2008) 852, arXiv: [0710.3820](https://arxiv.org/abs/0710.3820) [[hep-ph](#)].
- [34] P. Golonka and Z. Was, *PHOTOS Monte Carlo: a precision tool for QED corrections in Z and W decays*, *Eur. Phys. J. C* **45** (2006) 97, arXiv: [hep-ph/0506026](https://arxiv.org/abs/hep-ph/0506026).
- [35] N. Davidson, T. Przedzinski and Z. Was, *PHOTOS interface in C++: Technical and physics documentation*, *Comput. Phys. Commun.* **199** (2016) 86, arXiv: [1011.0937](https://arxiv.org/abs/1011.0937) [[hep-ph](#)].
- [36] D. J. Lange, *The EvtGen particle decay simulation package*, *Nucl. Instrum. Meth. A* **462** (2001) 152.
- [37] J. Butterworth, G. Dissertori, S. Dittmaier, D. de Florian, N. Glover et al., *Les Houches 2013: Physics at TeV Colliders: Standard Model Working Group Report*, (2014), arXiv: [1405.1067](https://arxiv.org/abs/1405.1067) [[hep-ph](#)].
- [38] C. Anastasiou, L. J. Dixon, K. Melnikov and F. Petriello, *High precision QCD at hadron colliders: Electroweak gauge boson rapidity distributions at NNLO*, *Phys. Rev. D* **69** (2004) 094008, arXiv: [hep-ph/0312266](https://arxiv.org/abs/hep-ph/0312266).

- [39] S. Dulat et al., *New parton distribution functions from a global analysis of quantum chromodynamics*, *Phys. Rev. D* **93** (2016) 033006, arXiv: [1506.07443 \[hep-ph\]](#).
- [40] A. Arbuzov et al., *Update of the MCSANC Monte Carlo integrator, v. 1.20*, *JETP Lett.* **103** (2016) 131, arXiv: [1509.03052 \[hep-ph\]](#).
- [41] E. Bothmann et al., *Event Generation with Sherpa 2.2*, *SciPost Phys.* **7** (2019) 034, arXiv: [1905.09127 \[hep-ph\]](#).
- [42] NNPDF Collaboration, R. D. Ball et al., *Parton distributions for the LHC run II*, *JHEP* **04** (2015) 040, arXiv: [1410.8849 \[hep-ph\]](#).
- [43] T.-J. Hou et al., *New CTEQ global analysis of quantum chromodynamics with high-precision data from the LHC*, *Phys. Rev. D* **103** (2021) 014013, arXiv: [1912.10053 \[hep-ph\]](#).
- [44] M. Grazzini, S. Kallweit and M. Wiesemann, *Fully differential NNLO computations with MATRIX*, *Eur. Phys. J. C* **78** (2018) 537, arXiv: [1711.06631 \[hep-ph\]](#).
- [45] ATLAS Collaboration, *Inclusive W^\pm and Z^0 cross sections at next-to-next-to leading order QCD for the ATLAS experiment*, ATL-PHYS-PUB-2023-026, 2023, URL: <https://cds.cern.ch/record/2871755>.
- [46] S. Frixione, G. Ridolfi and P. Nason, *A positive-weight next-to-leading-order Monte Carlo for heavy flavour hadroproduction*, *JHEP* **09** (2007) 126, arXiv: [0707.3088 \[hep-ph\]](#).
- [47] T. Sjöstrand et al., *An introduction to PYTHIA 8.2*, *Comput. Phys. Commun.* **191** (2015) 159, arXiv: [1410.3012 \[hep-ph\]](#).
- [48] M. Czakon et al., *Top-pair production at the LHC through NNLO QCD and NLO EW*, *JHEP* **10** (2017) 186, arXiv: [1705.04105 \[hep-ph\]](#).
- [49] E. Re, *Single-top Wt -channel production matched with parton showers using the POWHEG method*, *Eur. Phys. J. C* **71** (2011) 1547, arXiv: [1009.2450 \[hep-ph\]](#).
- [50] P. Golonka and Z. Was, *PHOTOS Monte Carlo: A Precision tool for QED corrections in Z and W decays*, *Eur. Phys. J. C* **45** (2006) 97, arXiv: [hep-ph/0506026 \[hep-ph\]](#).
- [51] NNPDF Collaboration, R. D. Ball et al., *Parton distributions with LHC data*, *Nucl. Phys. B* **867** (2013) 244, arXiv: [1207.1303 \[hep-ph\]](#).
- [52] ATLAS Collaboration, *The Pythia 8 A3 tune description of ATLAS minimum bias and inelastic measurements incorporating the Donnachie–Landshoff diffractive model*, ATL-PHYS-PUB-2016-017, 2016, URL: <https://cds.cern.ch/record/2206965>.
- [53] ATLAS Collaboration, *The ATLAS Simulation Infrastructure*, *Eur. Phys. J. C* **70** (2010) 823, arXiv: [1005.4568 \[physics.ins-det\]](#).
- [54] S. Agostinelli et al., *GEANT4 – a simulation toolkit*, *Nucl. Instrum. Meth. A* **506** (2003) 250.
- [55] ATLAS Collaboration, *ATLAS data quality operations and performance for 2015–2018 data-taking*, *JINST* **15** (2020) P04003, arXiv: [1911.04632 \[physics.ins-det\]](#).

- [56] ATLAS Collaboration, *Electron and photon performance measurements with the ATLAS detector using the 2015–2017 LHC proton–proton collision data*, *JINST* **14** (2019) P12006, arXiv: [1908.00005 \[hep-ex\]](#).
- [57] ATLAS Collaboration, *Vertex Reconstruction Performance of the ATLAS Detector at $\sqrt{s} = 13$ TeV*, ATL-PHYS-PUB-2015-026, 2015, URL: <https://cds.cern.ch/record/2037717>.
- [58] ATLAS Collaboration, *Muon reconstruction and identification efficiency in ATLAS using the full Run 2 pp collision data set at $\sqrt{s} = 13$ TeV*, *Eur. Phys. J. C* **81** (2021) 578, arXiv: [2012.00578 \[hep-ex\]](#).
- [59] ATLAS Collaboration, *Jet reconstruction and performance using particle flow with the ATLAS Detector*, *Eur. Phys. J. C* **77** (2017) 466, arXiv: [1703.10485 \[hep-ex\]](#).
- [60] M. Cacciari, G. P. Salam and G. Soyez, *The anti- k_t jet clustering algorithm*, *JHEP* **04** (2008) 063, arXiv: [0802.1189 \[hep-ph\]](#).
- [61] M. Cacciari, G. P. Salam and G. Soyez, *FastJet user manual*, *Eur. Phys. J. C* **72** (2012) 1896, arXiv: [1111.6097 \[hep-ph\]](#).
- [62] ATLAS Collaboration, *Jet energy scale and resolution measured in proton–proton collisions at $\sqrt{s} = 13$ TeV with the ATLAS detector*, *Eur. Phys. J. C* **81** (2021) 689, arXiv: [2007.02645 \[hep-ex\]](#).
- [63] ATLAS Collaboration, *Performance of pile-up mitigation techniques for jets in pp collisions at $\sqrt{s} = 8$ TeV using the ATLAS detector*, *Eur. Phys. J. C* **76** (2016) 581, arXiv: [1510.03823 \[hep-ex\]](#).
- [64] ATLAS Collaboration, *ATLAS flavour-tagging algorithms for the LHC Run 2 pp collision dataset*, *Eur. Phys. J. C* **83** (2023) 681, arXiv: [2211.16345 \[physics.data-an\]](#).
- [65] ATLAS Collaboration, *The performance of missing transverse momentum reconstruction and its significance with the ATLAS detector using 140fb^{-1} of $\sqrt{s} = 13$ TeV pp collisions*, (2024), arXiv: [2402.05858 \[hep-ex\]](#).
- [66] ATLAS Collaboration, *Performance of electron and photon triggers in ATLAS during LHC Run 2*, *Eur. Phys. J. C* **80** (2020) 47, arXiv: [1909.00761 \[hep-ex\]](#).
- [67] ATLAS Collaboration, *Performance of the ATLAS muon triggers in Run 2*, *JINST* **15** (2020) P09015, arXiv: [2004.13447 \[physics.ins-det\]](#).
- [68] T. Adye, ‘Unfolding algorithms and tests using RooUnfold’, *Proceedings, 2011 Workshop on Statistical Issues Related to Discovery Claims in Search Experiments and Unfolding (PHYSTAT 2011)* (CERN, Geneva, Switzerland, 17th–20th Jan. 2011) 313, arXiv: [1105.1160 \[physics.data-an\]](#).
- [69] G. D’Agostini, *A multidimensional unfolding method based on Bayes’ theorem*, *Nucl. Instrum. Meth. A* **362** (1995) 487.
- [70] S. Schmitt, *Data Unfolding Methods in High Energy Physics*, *EPJ Web Conf.* **137** (2017) 11008, ed. by Y. Foka, N. Brambilla and V. Kovalenko, arXiv: [1611.01927 \[physics.data-an\]](#).
- [71] ATLAS Collaboration, *Electron and photon efficiencies in LHC Run 2 with the ATLAS experiment*, *JHEP* **05** (2024) 162, arXiv: [2308.13362 \[hep-ex\]](#).

- [72] ATLAS Collaboration, *Studies of the muon momentum calibration and performance of the ATLAS detector with pp collisions at $\sqrt{s} = 13$ TeV*, *Eur. Phys. J. C* **83** (2023) 686, arXiv: [2212.07338 \[hep-ex\]](#).
- [73] J. Bellm et al., *Herwig 7.0/Herwig++ 3.0 release note*, *Eur. Phys. J. C* **76** (2016) 196, arXiv: [1512.01178 \[hep-ph\]](#).
- [74] ATLAS Collaboration, *ATLAS Pythia 8 tunes to 7 TeV data*, ATL-PHYS-PUB-2014-021, 2014, URL: <https://cds.cern.ch/record/1966419>.
- [75] S. Frixione, E. Laenen, P. Motylinski, B. R. Webber and C. D. White, *Single-top hadroproduction in association with a W boson*, *JHEP* **07** (2008) 029, arXiv: [0805.3067 \[hep-ph\]](#).
- [76] N. Kidonakis and N. Yamanaka, *Higher-order corrections for tW production at high-energy hadron colliders*, *JHEP* **05** (2021) 278, arXiv: [2102.11300 \[hep-ph\]](#).
- [77] ATLAS Collaboration, *Measurement of W^\pm and Z-boson production cross sections in pp collisions at $\sqrt{s} = 13$ TeV with the ATLAS detector*, *Phys. Lett. B* **759** (2016) 601, arXiv: [1603.09222 \[hep-ex\]](#).
- [78] ATLAS Collaboration, *Luminosity determination in pp collisions at $\sqrt{s} = 13$ TeV using the ATLAS detector at the LHC*, *Eur. Phys. J. C* **83** (2023) 982, arXiv: [2212.09379 \[hep-ex\]](#).
- [79] *The Durham High Energy Physics Database*, URL: <https://www.hepdata.net>.
- [80] E. Maguire, L. Heinrich and G. Watt, *HEPData: a repository for high energy physics data*, *J. Phys. Conf. Ser.* **898** (2017) 102006, arXiv: [1704.05473 \[hep-ex\]](#).
- [81] A. Glazov, *Averaging of DIS cross section data*, *AIP Conf. Proc.* **792** (2005) 237, ed. by W. H. Smith and S. R. Dasu.
- [82] F. D. Aaron et al., *Measurement of the inclusive ep scattering cross section at low Q^2 and x at HERA*, *Eur. Phys. J. C* **63** (2009) 625, arXiv: [0904.0929 \[hep-ex\]](#).
- [83] H1 Collaboration, *Combined measurement and QCD analysis of the inclusive $e^\pm p$ scattering cross sections at HERA*, *JHEP* **01** (2010) 109, arXiv: [0911.0884 \[hep-ex\]](#).
- [84] ATLAS Collaboration, *Precision measurement and interpretation of inclusive W^+ , W^- and Z/γ^* production cross sections with the ATLAS detector*, *Eur. Phys. J. C* **77** (2017) 367, arXiv: [1612.03016 \[hep-ex\]](#).
- [85] ATLAS Collaboration, *Measurement of the cross-section and charge asymmetry of W bosons produced in proton–proton collisions at $\sqrt{s} = 8$ TeV with the ATLAS detector*, *Eur. Phys. J. C* **79** (2019) 760, arXiv: [1904.05631 \[hep-ex\]](#).
- [86] S. Camarda et al., *DYTurbo: fast predictions for Drell-Yan processes*, *Eur. Phys. J. C* **80** (2020) 251, arXiv: [1910.07049 \[hep-ph\]](#), Erratum: *Eur. Phys. J. C* **80** (2020) 440.
- [87] S. Camarda, L. Cieri and G. Ferrera, *Fiducial perturbative power corrections within the q_T subtraction formalism*, *Eur. Phys. J. C* **82** (2022) 575, arXiv: [2111.14509 \[hep-ph\]](#).

- [88] R. S. Thorne, S. Bailey, T. Cridge, L. Harland-Lang and A. D. Martin, *The MSHT20 Parton Distribution Functions*, *SciPost Phys. Proc.* **8** (2022) 018.
- [89] NNPDF Collaboration, R. D. Ball et al., *The path to proton structure at 1% accuracy*, *Eur. Phys. J. C* **82** (2022) 428, arXiv: [2109.02653 \[hep-ph\]](#).
- [90] ATLAS Collaboration, *Determination of the parton distribution functions of the proton using diverse ATLAS data from pp collisions at $\sqrt{s} = 7, 8$ and 13 TeV*, *Eur. Phys. J. C* **82** (2022) 438, arXiv: [2112.11266 \[hep-ex\]](#).
- [91] K. Xie et al., *The photon content of the proton in the CT18 global analysis*, *SciPost Phys. Proc.* **8** (2022) 074, arXiv: [2107.13580 \[hep-ph\]](#).
- [92] I. Brivio and M. Trott, *The standard model as an effective field theory*, *Phys. Rept.* **793** (2019) 1, arXiv: [1706.08945 \[hep-ph\]](#).
- [93] B. Grzadkowski, M. Iskrzynski, M. Misiak and J. Rosiek, *Dimension-six terms in the Standard Model Lagrangian*, *JHEP* **10** (2010) 085, arXiv: [1008.4884 \[hep-ph\]](#).
- [94] J. Alwall, M. Herquet, F. Maltoni, O. Mattelaer and T. Stelzer, *MadGraph 5 : Going Beyond*, *JHEP* **06** (2011) 128, arXiv: [1106.0522 \[hep-ph\]](#).
- [95] I. Brivio, *SMEFTsim 3.0 — a practical guide*, *JHEP* **04** (2021) 073, arXiv: [2012.11343 \[hep-ph\]](#).
- [96] C. Bierlich et al., *A comprehensive guide to the physics and usage of PYTHIA 8.3*, *SciPost Phys. Codeb.* **2022** (2022) 8, arXiv: [2203.11601 \[hep-ph\]](#).
- [97] A. Greljo and D. Marzocca, *High- p_T dilepton tails and flavor physics*, *Eur. Phys. J. C* **77** (2017) 548, arXiv: [1704.09015 \[hep-ph\]](#).
- [98] A. Falkowski, M. González-Alonso and K. Mimouni, *Compilation of low-energy constraints on 4-fermion operators in the SMEFT*, *JHEP* **08** (2017) 123, arXiv: [1706.03783 \[hep-ph\]](#).
- [99] L. Allwicher, C. Cornella, G. Isidori and B. A. Stefanek, *New physics in the third generation. A comprehensive SMEFT analysis and future prospects*, *JHEP* **03** (2024) 049, arXiv: [2311.00020 \[hep-ph\]](#).
- [100] R. Bartocci, A. Biekötter and T. Hurth, *A global analysis of the SMEFT under the minimal MFV assumption*, *JHEP* **05** (2024) 074, arXiv: [2311.04963 \[hep-ph\]](#).
- [101] ATLAS Collaboration, *ATLAS Computing Acknowledgements*, ATL-SOFT-PUB-2025-001, 2025, URL: <https://cds.cern.ch/record/2922210>.

The ATLAS Collaboration

G. Aad ¹⁰⁴, E. Aakvaag ¹⁷, B. Abbott ¹²³, S. Abdelhameed ^{119a}, K. Abeling ⁵⁵, N.J. Abicht ⁴⁹, S.H. Abidi ³⁰, M. Aboeela ⁴⁵, A. Aboulhorma ^{36e}, H. Abramowicz ¹⁵⁷, Y. Abulaiti ¹²⁰, B.S. Acharya ^{69a,69b,n}, A. Ackermann ^{63a}, C. Adam Bourdarios ⁴, L. Adamczyk ^{86a}, S.V. Addepalli ¹⁴⁹, M.J. Addison ¹⁰³, J. Adelman ¹¹⁸, A. Adiguzel ^{22c}, T. Adye ¹³⁷, A.A. Affolder ¹³⁹, Y. Afik ⁴⁰, M.N. Agaras ¹³, A. Aggarwal ¹⁰², C. Agheorghiesei ^{28c}, F. Ahmadov ^{39,ae}, S. Ahuja ⁹⁷, X. Ai ^{143b}, G. Aielli ^{76a,76b}, A. Aikot ¹⁶⁹, M. Ait Tamlihat ^{36e}, B. Aitbenkikh ^{36a}, M. Akbiyik ¹⁰², T.P.A. Åkesson ¹⁰⁰, A.V. Akimov ¹⁵¹, D. Akiyama ¹⁷⁴, N.N. Akolkar ²⁵, S. Aktas ^{22a}, G.L. Alberghi ^{24b}, J. Albert ¹⁷¹, P. Albicocco ⁵³, G.L. Albouy ⁶⁰, S. Alderweireldt ⁵², Z.L. Alegria ¹²⁴, M. Aleksa ³⁷, I.N. Aleksandrov ³⁹, C. Alexa ^{28b}, T. Alexopoulos ¹⁰, F. Alfonsi ^{24b}, M. Algren ⁵⁶, M. Alhroob ¹⁷³, B. Ali ¹³⁵, H.M.J. Ali ^{93,x}, S. Ali ³², S.W. Alibocus ⁹⁴, M. Aliev ^{34c}, G. Alimonti ^{71a}, W. Alkahi ⁵⁵, C. Allaire ⁶⁶, B.M.M. Allbrooke ¹⁵², J.S. Allen ¹⁰³, J.F. Allen ⁵², P.P. Allport ²¹, A. Aloisio ^{72a,72b}, F. Alonso ⁹², C. Alpigiani ¹⁴², Z.M.K. Alsolami ⁹³, A. Alvarez Fernandez ¹⁰², M. Alves Cardoso ⁵⁶, M.G. Alviggi ^{72a,72b}, M. Aly ¹⁰³, Y. Amaral Coutinho ^{83b}, A. Ambler ¹⁰⁶, C. Amelung ³⁷, M. Amerl ¹⁰³, C.G. Ames ¹¹¹, T. Amezza ¹³⁰, D. Amidei ¹⁰⁸, B. Amini ⁵⁴, K. Amirie ¹⁶¹, A. Amirkhanov ³⁹, S.P. Amor Dos Santos ^{133a}, K.R. Amos ¹⁶⁹, D. Amperiadou ¹⁵⁸, S. An ⁸⁴, C. Anastopoulos ¹⁴⁵, T. Andeen ¹¹, J.K. Anders ⁹⁴, A.C. Anderson ⁵⁹, A. Andreatta ^{71a,71b}, S. Angelidakis ⁹, A. Angerami ⁴², A.V. Anisenkov ³⁹, A. Annovi ^{74a}, C. Antel ⁵⁶, E. Antipov ¹⁵¹, M. Antonelli ⁵³, F. Anulli ^{75a}, M. Aoki ⁸⁴, T. Aoki ¹⁵⁹, M.A. Aparo ¹⁵², L. Aperio Bella ⁴⁸, M. Apicella ³¹, C. Appelt ¹⁵⁷, A. Apyan ²⁷, S.J. Arbiol Val ⁸⁷, C. Arcangeletti ⁵³, A.T.H. Arce ⁵¹, J-F. Arguin ¹¹⁰, S. Argyropoulos ¹⁵⁸, J.-H. Arling ⁴⁸, O. Arnaez ⁴, H. Arnold ¹⁵¹, G. Artoni ^{75a,75b}, H. Asada ¹¹³, K. Asai ¹²¹, S. Asai ¹⁵⁹, S. Asatryan ¹⁷⁹, N.A. Asbah ³⁷, R.A. Ashby Pickering ¹⁷³, A.M. Aslam ⁹⁷, K. Assamagan ³⁰, R. Astalos ^{29a}, K.S.V. Astrand ¹⁰⁰, S. Atashi ¹⁶⁵, R.J. Atkin ^{34a}, H. Atmani ^{36f}, P.A. Atmasiddha ¹³¹, K. Augsten ¹³⁵, A.D. Auriol ⁴¹, V.A. Austrup ¹⁰³, G. Avolio ³⁷, K. Axiotis ⁵⁶, G. Azuelos ^{110,ah}, D. Babal ^{29b}, H. Bachacou ¹³⁸, K. Bachas ^{158,r}, A. Bachiu ³⁵, E. Bachmann ⁵⁰, M.J. Backes ^{63a}, A. Badea ⁴⁰, T.M. Baer ¹⁰⁸, P. Bagnaia ^{75a,75b}, M. Bahmani ¹⁹, D. Bahner ⁵⁴, K. Bai ¹²⁶, J.T. Baines ¹³⁷, L. Baines ⁹⁶, O.K. Baker ¹⁷⁸, E. Bakos ¹⁶, D. Bakshi Gupta ⁸, L.E. Balabram Filho ^{83b}, V. Balakrishnan ¹²³, R. Balasubramanian ⁴, E.M. Baldin ³⁸, P. Balek ^{86a}, E. Ballabene ^{24b,24a}, F. Balli ¹³⁸, L.M. Baltes ^{63a}, W.K. Balunas ³³, J. Balz ¹⁰², I. Bamwidhi ^{119b}, E. Banas ⁸⁷, M. Bandieramonte ¹³², A. Bandyopadhyay ²⁵, S. Bansal ²⁵, L. Barak ¹⁵⁷, M. Barakat ⁴⁸, E.L. Barberio ¹⁰⁷, D. Barberis ^{18b}, M. Barbero ¹⁰⁴, M.Z. Barel ¹¹⁷, T. Barillari ¹¹², M-S. Barisits ³⁷, T. Barklow ¹⁴⁹, P. Baron ¹²⁵, D.A. Baron Moreno ¹⁰³, A. Baroncelli ⁶², A.J. Barr ¹²⁹, J.D. Barr ⁹⁸, F. Barreiro ¹⁰¹, J. Barreiro Guimarães da Costa ¹⁴, M.G. Barros Teixeira ^{133a}, S. Barsov ³⁸, F. Bartels ^{63a}, R. Bartoldus ¹⁴⁹, A.E. Barton ⁹³, P. Bartos ^{29a}, A. Basan ¹⁰², M. Baselga ⁴⁹, S. Bashiri ⁸⁷, A. Bassalat ^{66,b}, M.J. Basso ^{162a}, S. Bataju ⁴⁵, R. Bate ¹⁷⁰, R.L. Bates ⁵⁹, S. Batlamous ¹⁰¹, M. Battaglia ¹³⁹, D. Battulga ¹⁹, M. Bauge ^{75a,75b}, M. Bauer ⁷⁹, P. Bauer ²⁵, L.T. Bayer ⁴⁸, L.T. Bazzano Hurrell ³¹, J.B. Beacham ¹¹², T. Beau ¹³⁰, J.Y. Beaucamp ⁹², P.H. Beauchemin ¹⁶⁴, P. Bechtel ²⁵, H.P. Beck ^{20,q}, K. Becker ¹⁷³, A.J. Beddall ⁸², V.A. Bednyakov ³⁹, C.P. Bee ¹⁵¹, L.J. Beemster ¹⁶, M. Begalli ^{83d}, M. Begel ³⁰, J.K. Behr ⁴⁸, J.F. Beirer ³⁷, F. Beisiegel ²⁵, M. Belfkir ^{119b}, G. Bella ¹⁵⁷, L. Bellagamba ^{24b}, A. Bellerive ³⁵, P. Bellos ²¹, K. Beloborodov ³⁸, D. Benchekroun ^{36a}, F. Bendebba ^{36a}, Y. Benhammou ¹⁵⁷,

K.C. Benkendorfer ⁶¹, L. Beresford ⁴⁸, M. Beretta ⁵³, E. Bergeaas Kuutmann ¹⁶⁷, N. Berger ⁴,
 B. Bergmann ¹³⁵, J. Beringer ^{18a}, G. Bernardi ⁵, C. Bernius ¹⁴⁹, F.U. Bernlochner ²⁵,
 F. Bernon ³⁷, A. Berrocal Guardia ¹³, T. Berry ⁹⁷, P. Berta ¹³⁶, A. Berthold ⁵⁰, A. Berti ^{133a},
 R. Bertrand ¹⁰⁴, S. Bethke ¹¹², A. Betti ^{75a,75b}, T.F. Beumker ¹⁷⁷, A.J. Bevan ⁹⁶, L. Bezio ⁵⁶,
 N.K. Bhalla ⁵⁴, S. Bharthuar ¹¹², S. Bhatta ¹⁵¹, P. Bhattarai ¹⁴⁹, Z.M. Bhatti ¹²⁰, K.D. Bhide ⁵⁴,
 V.S. Bhopatkar ¹²⁴, R.M. Bianchi ¹³², G. Bianco ^{24b,24a}, O. Biebel ¹¹¹, M. Biglietti ^{77a},
 C.S. Billingsley ⁴⁵, Y. Bimgdi ^{36f}, M. Bindi ⁵⁵, A. Bingham ¹⁷⁷, A. Bingul ^{22b}, C. Bini ^{75a,75b},
 G.A. Bird ³³, M. Birman ¹⁷⁵, M. Biros ¹³⁶, S. Biryukov ¹⁵², T. Bisanz ⁴⁹, E. Bisceglie ^{24b,24a},
 J.P. Biswal ¹³⁷, D. Biswas ¹⁴⁷, I. Bloch ⁴⁸, A. Blue ⁵⁹, U. Blumenschein ⁹⁶, J. Blumenthal ¹⁰²,
 V.S. Bobrovnikov ³⁹, M. Boehler ⁵⁴, B. Boehm ¹⁷², D. Bogavac ¹³, A.G. Bogdanchikov ³⁸,
 L.S. Boggia ¹³⁰, V. Boisvert ⁹⁷, P. Bokan ³⁷, T. Bold ^{86a}, M. Bomben ⁵, M. Bona ⁹⁶,
 M. Boonekamp ¹³⁸, A.G. Borbély ⁵⁹, I.S. Bordulev ³⁸, G. Borissov ⁹³, D. Bortoletto ¹²⁹,
 D. Boscherini ^{24b}, M. Bosman ¹³, K. Bouaouda ^{36a}, N. Bouchhar ¹⁶⁹, L. Boudet ⁴,
 J. Boudreau ¹³², E.V. Bouhova-Thacker ⁹³, D. Boumediene ⁴¹, R. Bouquet ^{57b,57a}, A. Boveia ¹²²,
 J. Boyd ³⁷, D. Boye ³⁰, I.R. Boyko ³⁹, L. Bozianu ⁵⁶, J. Bracinek ²¹, N. Brahimi ⁴,
 G. Brandt ¹⁷⁷, O. Brandt ³³, B. Brau ¹⁰⁵, J.E. Brau ¹²⁶, R. Brenner ¹⁷⁵, L. Brenner ¹¹⁷,
 R. Brenner ¹⁶⁷, S. Bressler ¹⁷⁵, G. Brianti ^{78a,78b}, D. Britton ⁵⁹, D. Britzger ¹¹², I. Brock ²⁵,
 R. Brock ¹⁰⁹, G. Brooijmans ⁴², A.J. Brooks ⁶⁸, E.M. Brooks ^{162b}, E. Brost ³⁰,
 L.M. Brown ^{171,162a}, L.E. Bruce ⁶¹, T.L. Bruckler ¹²⁹, P.A. Bruckman de Renstrom ⁸⁷,
 B. Brüers ⁴⁸, A. Bruni ^{24b}, G. Bruni ^{24b}, D. Brunner ^{47a,47b}, M. Bruschi ^{24b}, N. Bruscinò ^{75a,75b},
 T. Buanes ¹⁷, Q. Buat ¹⁴², D. Buchin ¹¹², A.G. Buckley ⁵⁹, O. Bulekov ⁸², B.A. Bullard ¹⁴⁹,
 S. Burdin ⁹⁴, C.D. Burgard ⁴⁹, A.M. Burger ⁹¹, B. Burghgrave ⁸, O. Burlayenko ⁵⁴,
 J. Burleson ¹⁶⁸, J.T.P. Burr ³³, J.C. Burzynski ¹⁴⁸, E.L. Busch ⁴², V. Büscher ¹⁰², P.J. Bussey ⁵⁹,
 J.M. Butler ²⁶, C.M. Buttar ⁵⁹, J.M. Butterworth ⁹⁸, W. Buttinger ¹³⁷, C.J. Buxo Vazquez ¹⁰⁹,
 A.R. Buzykaev ³⁹, S. Cabrera Urbán ¹⁶⁹, L. Cadamuro ⁶⁶, D. Caforio ⁵⁸, H. Cai ¹³²,
 Y. Cai ^{24b,114c,24a}, Y. Cai ^{114a}, V.M.M. Cairo ³⁷, O. Cakir ^{3a}, N. Calace ³⁷, P. Calafiura ^{18a},
 G. Calderini ¹³⁰, P. Calfayan ³⁵, G. Callea ⁵⁹, L.P. Caloba ^{83b}, D. Calvet ⁴¹, S. Calvet ⁴¹,
 R. Camacho Toro ¹³⁰, S. Camarda ³⁷, D. Camarero Munoz ²⁷, P. Camarri ^{76a,76b},
 C. Camincher ¹⁷¹, M. Campanelli ⁹⁸, A. Camplani ⁴³, V. Canale ^{72a,72b}, A.C. Canbay ^{3a},
 E. Canonero ⁹⁷, J. Cantero ¹⁶⁹, Y. Cao ¹⁶⁸, F. Capocasa ²⁷, M. Capua ^{44b,44a}, A. Carbone ^{71a,71b},
 R. Cardarelli ^{76a}, J.C.J. Cardenas ⁸, M.P. Cardiff ²⁷, G. Carducci ^{44b,44a}, T. Carli ³⁷,
 G. Carlino ^{72a}, J.I. Carlotto ¹³, B.T. Carlson ^{132,s}, E.M. Carlson ¹⁷¹, J. Carmignani ⁹⁴,
 L. Carminati ^{71a,71b}, A. Carnelli ⁴, M. Carnesale ³⁷, S. Caron ¹¹⁶, E. Carquin ^{140f}, I.B. Carr ¹⁰⁷,
 S. Carrá ^{71a}, G. Carratta ^{24b,24a}, A.M. Carroll ¹²⁶, M.P. Casado ^{13,i}, M. Caspar ⁴⁸,
 F.L. Castillo ⁴, L. Castillo Garcia ¹³, V. Castillo Gimenez ¹⁶⁹, N.F. Castro ^{133a,133e},
 A. Catinaccio ³⁷, J.R. Catmore ¹²⁸, T. Cavaliere ⁴, V. Cavaliere ³⁰, L.J. Caviedes Betancourt ^{23b},
 Y.C. Cekmecelioglu ⁴⁸, E. Celebi ⁸², S. Cella ³⁷, V. Cepaitis ⁵⁶, K. Cerny ¹²⁵,
 A.S. Cerqueira ^{83a}, A. Cerri ^{74a,74b,ak}, L. Cerrito ^{76a,76b}, F. Cerutti ^{18a}, B. Cervato ^{71a,71b},
 A. Cervelli ^{24b}, G. Cesarini ⁵³, S.A. Cetin ⁸², P.M. Chabrilat ¹³⁰, J. Chan ^{18a}, W.Y. Chan ¹⁵⁹,
 J.D. Chapman ³³, E. Chapon ¹³⁸, B. Chargeishvili ^{155b}, D.G. Charlton ²¹, C. Chauhan ¹³⁶,
 Y. Che ^{114a}, S. Chekanov ⁶, S.V. Chekulaev ^{162a}, G.A. Chelkov ^{39,a}, B. Chen ¹⁵⁷, B. Chen ¹⁷¹,
 H. Chen ^{114a}, H. Chen ³⁰, J. Chen ^{144a}, J. Chen ¹⁴⁸, M. Chen ¹²⁹, S. Chen ⁸⁹, S.J. Chen ^{114a},
 X. Chen ^{144a}, X. Chen ^{15,ag}, Z. Chen ⁶², C.L. Cheng ¹⁷⁶, H.C. Cheng ^{64a}, S. Cheong ¹⁴⁹,
 A. Cheplakov ³⁹, E. Cheremushkina ⁴⁸, E. Cherepanova ¹¹⁷, R. Cherkaoui El Moursli ^{36e},
 E. Cheu ⁷, K. Cheung ⁶⁵, L. Chevalier ¹³⁸, V. Chiarella ⁵³, G. Chiarelli ^{74a}, G. Chiodini ^{70a},
 A.S. Chisholm ²¹, A. Chitan ^{28b}, M. Chitishvili ¹⁶⁹, M.V. Chizhov ^{39,t}, K. Choi ¹¹, Y. Chou ¹⁴²,
 E.Y.S. Chow ¹¹⁶, K.L. Chu ¹⁷⁵, M.C. Chu ^{64a}, X. Chu ^{14,114c}, Z. Chubinidze ⁵³, J. Chudoba ¹³⁴,

J.J. Chwastowski ⁸⁷, D. Cieri ¹¹², K.M. Ciesla ^{86a}, V. Cindro ⁹⁵, A. Ciocio ^{18a}, F. Cirotto ^{72a,72b}, Z.H. Citron ¹⁷⁵, M. Citterio ^{71a}, D.A. Ciubotaru ^{28b}, A. Clark ⁵⁶, P.J. Clark ⁵², N. Clarke Hall ⁹⁸, C. Clarry ¹⁶¹, S.E. Clawson ⁴⁸, C. Clement ^{47a,47b}, Y. Coadou ¹⁰⁴, M. Cobal ^{69a,69c}, A. Coccaro ^{57b}, R.F. Coelho Barrue ^{133a}, R. Coelho Lopes De Sa ¹⁰⁵, S. Coelli ^{71a}, L.S. Colangeli ¹⁶¹, B. Cole ⁴², P. Collado Soto ¹⁰¹, J. Collot ⁶⁰, P. Conde Muiño ^{133a,133g}, M.P. Connell ^{34c}, S.H. Connell ^{34c}, E.I. Conroy ¹²⁹, F. Conventi ^{72a,ai}, H.G. Cooke ²¹, A.M. Cooper-Sarkar ¹²⁹, L. Corazzina ^{75a,75b}, F.A. Corchia ^{24b,24a}, A. Cordeiro Oudot Choi ¹⁴², L.D. Corpe ⁴¹, M. Corradi ^{75a,75b}, F. Corriveau ^{106,ac}, A. Cortes-Gonzalez ¹⁹, M.J. Costa ¹⁶⁹, F. Costanza ⁴, D. Costanzo ¹⁴⁵, B.M. Cote ¹²², J. Couthures ⁴, G. Cowan ⁹⁷, K. Cranmer ¹⁷⁶, L. Cremer ⁴⁹, D. Cremonini ^{24b,24a}, S. Crépe-Renaudin ⁶⁰, F. Crescioli ¹³⁰, T. Cresta ^{73a,73b}, M. Cristinziani ¹⁴⁷, M. Cristoforetti ^{78a,78b}, V. Croft ¹¹⁷, J.E. Crosby ¹²⁴, G. Crosetti ^{44b,44a}, A. Cueto ¹⁰¹, H. Cui ⁹⁸, Z. Cui ⁷, W.R. Cunningham ⁵⁹, F. Curcio ¹⁶⁹, J.R. Curran ⁵², M.J. Da Cunha Sargedas De Sousa ^{57b,57a}, J.V. Da Fonseca Pinto ^{83b}, C. Da Via ¹⁰³, W. Dabrowski ^{86a}, T. Dado ³⁷, S. Dahbi ¹⁵⁴, T. Dai ¹⁰⁸, D. Dal Santo ²⁰, C. Dallapiccola ¹⁰⁵, M. Dam ⁴³, G. D'amen ³⁰, V. D'Amico ¹¹¹, J. Damp ¹⁰², J.R. Dandoy ³⁵, D. Dannheim ³⁷, G. D'anniballe ^{74a,74b}, M. Danninger ¹⁴⁸, V. Dao ¹⁵¹, G. Darbo ^{57b}, S.J. Das ³⁰, F. Dattola ⁴⁸, S. D'Auria ^{71a,71b}, A. D'Avanzo ^{72a,72b}, T. Davidek ¹³⁶, J. Davidson ¹⁷³, I. Dawson ⁹⁶, K. De ⁸, C. De Almeida Rossi ¹⁶¹, R. De Asmundis ^{72a}, N. De Biase ⁴⁸, S. De Castro ^{24b,24a}, N. De Groot ¹¹⁶, P. de Jong ¹¹⁷, H. De la Torre ¹¹⁸, A. De Maria ^{114a}, A. De Salvo ^{75a}, U. De Sanctis ^{76a,76b}, F. De Santis ^{70a,70b}, A. De Santo ¹⁵², J.B. De Vivie De Regie ⁶⁰, J. Debevc ⁹⁵, D.V. Dedovich ³⁹, J. Degens ⁹⁴, A.M. Deiana ⁴⁵, J. Del Peso ¹⁰¹, L. Delagrangé ¹³⁰, F. Deliot ¹³⁸, C.M. Delitzsch ⁴⁹, M. Della Pietra ^{72a,72b}, D. Della Volpe ⁵⁶, A. Dell'Acqua ³⁷, L. Dell'Asta ^{71a,71b}, M. Delmastro ⁴, C.C. Delogu ¹⁰², P.A. Delsart ⁶⁰, S. Demers ¹⁷⁸, M. Demichev ³⁹, S.P. Denisov ³⁸, H. Denizli ^{22a,m}, L. D'Eramo ⁴¹, D. Derendarz ⁸⁷, F. Derue ¹³⁰, P. Dervan ⁹⁴, K. Desch ²⁵, F.A. Di Bello ^{57b,57a}, A. Di Ciaccio ^{76a,76b}, L. Di Ciaccio ⁴, A. Di Domenico ^{75a,75b}, C. Di Donato ^{72a,72b}, A. Di Girolamo ³⁷, G. Di Gregorio ³⁷, A. Di Luca ^{78a,78b}, B. Di Micco ^{77a,77b}, R. Di Nardo ^{77a,77b}, K.F. Di Petrillo ⁴⁰, M. Diamantopoulou ³⁵, F.A. Dias ¹¹⁷, M.A. Diaz ^{140a,140b}, A.R. Didenko ³⁹, M. Didenko ¹⁶⁹, S.D. Diefenbacher ^{18a}, E.B. Diehl ¹⁰⁸, S. Díez Cornell ⁴⁸, C. Diez Pardos ¹⁴⁷, C. Dimitriadi ¹⁵⁰, A. Dimitrievska ²¹, A. Dimri ¹⁵¹, J. Dingfelder ²⁵, T. Dingley ¹²⁹, I-M. Dinu ^{28b}, S.J. Dittmeier ^{63b}, F. Dittus ³⁷, M. Divisek ¹³⁶, B. Dixit ⁹⁴, F. Djama ¹⁰⁴, T. Djobava ^{155b}, C. Doglioni ^{103,100}, A. Dohnalova ^{29a}, Z. Dolezal ¹³⁶, K. Domijan ^{86a}, K.M. Dona ⁴⁰, M. Donadelli ^{83d}, B. Dong ¹⁰⁹, J. Donini ⁴¹, A. D'Onofrio ^{72a,72b}, M. D'Onofrio ⁹⁴, J. Dopke ¹³⁷, A. Doria ^{72a}, N. Dos Santos Fernandes ^{133a}, P. Dougan ¹⁰³, M.T. Dova ⁹², A.T. Doyle ⁵⁹, M.A. Dragnet ¹²⁹, M.P. Drescher ⁵⁵, E. Dreyer ¹⁷⁵, I. Drivas-koulouris ¹⁰, M. Drnevich ¹²⁰, M. Drozdova ⁵⁶, D. Du ⁶², T.A. du Pree ¹¹⁷, Z. Duan ^{114a}, F. Dubinin ³⁹, M. Dubovsky ^{29a}, E. Duchovni ¹⁷⁵, G. Duckeck ¹¹¹, P.K. Duckett ⁹⁸, O.A. Ducu ^{28b}, D. Duda ⁵², A. Dudarev ³⁷, E.R. Duden ²⁷, M. D'uffizi ¹⁰³, L. Duflost ⁶⁶, M. Dührssen ³⁷, I. Duminica ^{28g}, A.E. Dumitriu ^{28b}, M. Dunford ^{63a}, S. Dungs ⁴⁹, K. Dunne ^{47a,47b}, A. Duperrin ¹⁰⁴, H. Duran Yildiz ^{3a}, M. Düren ⁵⁸, A. Durglishvili ^{155b}, D. Duvnjak ³⁵, B.L. Dwyer ¹¹⁸, G.I. Dyckes ^{18a}, M. Dyndal ^{86a}, B.S. Dziedzic ³⁷, Z.O. Earnshaw ¹⁵², G.H. Eberwein ¹²⁹, B. Eckerova ^{29a}, S. Eggebrecht ⁵⁵, E. Egidio Purcino De Souza ^{83e}, G. Eigen ¹⁷, K. Einsweiler ^{18a}, T. Ekelof ¹⁶⁷, P.A. Ekman ¹⁰⁰, S. El Farkh ^{36b}, Y. El Ghazali ⁶², H. El Jarrari ³⁷, A. El Moussaouy ^{36a}, V. Ellajosyula ¹⁶⁷, M. Ellert ¹⁶⁷, F. Ellinghaus ¹⁷⁷, N. Ellis ³⁷, J. Elmsheuser ³⁰, M. Elsayy ^{119a}, M. Elsing ³⁷, D. Emeliyanov ¹³⁷, Y. Enari ⁸⁴, I. Ene ^{18a}, S. Epari ¹¹⁰, D. Ernani Martins Neto ⁸⁷, F. Ernst ³⁷, M. Errenst ¹⁷⁷, M. Escalier ⁶⁶, C. Escobar ¹⁶⁹, E. Etzion ¹⁵⁷, G. Evans ^{133a,133b}, H. Evans ⁶⁸, L.S. Evans ⁹⁷, A. Ezhilov ³⁸, S. Ezzarqtouni ^{36a},

F. Fabbri [ID24b,24a](#), L. Fabbri [ID24b,24a](#), G. Facini [ID98](#), V. Fadeyev [ID139](#), R.M. Fakhrutdinov [ID38](#), D. Fakoudis [ID102](#), S. Falciano [ID75a](#), L.F. Falda Ulhoa Coelho [ID133a](#), F. Fallavollita [ID112](#), G. Falsetti [ID44b,44a](#), J. Faltova [ID136](#), C. Fan [ID168](#), K.Y. Fan [ID64b](#), Y. Fan [ID14](#), Y. Fang [ID14,114c](#), M. Fanti [ID71a,71b](#), M. Faraj [ID69a,69b](#), Z. Farazpay [ID99](#), A. Farbin [ID8](#), A. Farilla [ID77a](#), T. Farooque [ID109](#), J.N. Farr [ID178](#), S.M. Farrington [ID137,52](#), F. Fassi [ID36e](#), D. Fassouliotis [ID9](#), L. Fayard [ID66](#), P. Federic [ID136](#), P. Federicova [ID134](#), O.L. Fedin [ID38,a](#), M. Feickert [ID176](#), L. Feligioni [ID104](#), D.E. Fellers [ID18a](#), C. Feng [ID143a](#), Z. Feng [ID117](#), M.J. Fenton [ID165](#), L. Ferencz [ID48](#), B. Fernandez Barbadillo [ID93](#), P. Fernandez Martinez [ID67](#), M.J.V. Fernoux [ID104](#), J. Ferrando [ID93](#), A. Ferrari [ID167](#), P. Ferrari [ID117,116](#), R. Ferrari [ID73a](#), D. Ferrere [ID56](#), C. Ferretti [ID108](#), M.P. Fewell [ID1](#), D. Fiacco [ID75a,75b](#), F. Fiedler [ID102](#), P. Fiedler [ID135](#), S. Filimonov [ID39](#), M.S. Filip [ID28b,u](#), A. Filipčič [ID95](#), E.K. Filmer [ID162a](#), F. Filthaut [ID116](#), M.C.N. Fiolhais [ID133a,133c,c](#), L. Fiorini [ID169](#), W.C. Fisher [ID109](#), T. Fitschen [ID103](#), P.M. Fitzhugh [ID138](#), I. Fleck [ID147](#), P. Fleischmann [ID108](#), T. Flick [ID177](#), M. Flores [ID34d,af](#), L.R. Flores Castillo [ID64a](#), L. Flores Sanz De Acedo [ID37](#), F.M. Follega [ID78a,78b](#), N. Fomin [ID33](#), J.H. Foo [ID161](#), A. Formica [ID138](#), A.C. Forti [ID103](#), E. Fortin [ID37](#), A.W. Fortman [ID18a](#), L. Foster [ID18a](#), L. Fountas [ID9j](#), D. Fournier [ID66](#), H. Fox [ID93](#), P. Francavilla [ID74a,74b](#), S. Francescato [ID61](#), S. Franchellucci [ID56](#), M. Franchini [ID24b,24a](#), S. Franchino [ID63a](#), D. Francis [ID37](#), L. Franco [ID116](#), V. Franco Lima [ID37](#), L. Franconi [ID48](#), M. Franklin [ID61](#), G. Frattari [ID27](#), Y.Y. Frid [ID157](#), J. Friend [ID59](#), N. Fritzsche [ID37](#), A. Froch [ID56](#), D. Froidevaux [ID37](#), J.A. Frost [ID129](#), Y. Fu [ID109](#), S. Fuenzalida Garrido [ID140f](#), M. Fujimoto [ID104](#), K.Y. Fung [ID64a](#), E. Furtado De Simas Filho [ID83e](#), M. Furukawa [ID159](#), J. Fuster [ID169](#), A. Gaa [ID55](#), A. Gabrielli [ID24b,24a](#), A. Gabrielli [ID161](#), P. Gadow [ID37](#), G. Gagliardi [ID57b,57a](#), L.G. Gagnon [ID18a](#), S. Gaid [ID88b](#), S. Galantzan [ID157](#), J. Gallagher [ID1](#), E.J. Gallas [ID129](#), A.L. Gallen [ID167](#), B.J. Gallop [ID137](#), K.K. Gan [ID122](#), S. Ganguly [ID159](#), Y. Gao [ID52](#), A. Garabaglu [ID142](#), F.M. Garay Walls [ID140a,140b](#), C. García [ID169](#), A. Garcia Alonso [ID117](#), A.G. Garcia Caffaro [ID178](#), J.E. García Navarro [ID169](#), M. Garcia-Sciveres [ID18a](#), G.L. Gardner [ID131](#), R.W. Gardner [ID40](#), N. Garelli [ID164](#), R.B. Garg [ID149](#), J.M. Gargan [ID52](#), C.A. Garner [ID161](#), C.M. Garvey [ID34a](#), V.K. Gassmann [ID164](#), G. Gaudio [ID73a](#), V. Gautam [ID13](#), P. Gauzzi [ID75a,75b](#), J. Gavranovic [ID95](#), I.L. Gavrilenko [ID133a](#), A. Gavrilyuk [ID38](#), C. Gay [ID170](#), G. Gaycken [ID126](#), E.N. Gazis [ID10](#), A. Gekow [ID122](#), C. Gemme [ID57b](#), M.H. Genest [ID60](#), A.D. Gentry [ID115](#), S. George [ID97](#), T. Geralis [ID46](#), A.A. Gerwin [ID123](#), P. Gessinger-Befurt [ID37](#), M.E. Geyik [ID177](#), M. Ghani [ID173](#), K. Ghorbanian [ID96](#), A. Ghosal [ID147](#), A. Ghosh [ID165](#), A. Ghosh [ID7](#), B. Giacobbe [ID24b](#), S. Giagu [ID75a,75b](#), T. Giani [ID117](#), A. Giannini [ID62](#), S.M. Gibson [ID97](#), M. Gignac [ID139](#), D.T. Gil [ID86b](#), A.K. Gilbert [ID86a](#), B.J. Gilbert [ID42](#), D. Gillberg [ID35](#), G. Gilles [ID117](#), D.M. Gingrich [ID2,ah](#), M.P. Giordani [ID69a,69c](#), P.F. Giraud [ID138](#), G. Giugliarelli [ID69a,69c](#), D. Giugni [ID71a](#), F. Giuli [ID76a,76b](#), I. Gkialas [ID9j](#), L.K. Gladilin [ID38](#), C. Glasman [ID101](#), M. Glazewska [ID20](#), G. Glemža [ID48](#), M. Glisic [ID126](#), I. Gnesi [ID44b](#), Y. Go [ID30](#), M. Goblirsch-Kolb [ID37](#), B. Gocke [ID49](#), D. Godin [ID110](#), B. Gokturk [ID22a](#), S. Goldfarb [ID107](#), T. Golling [ID56](#), M.G.D. Gololo [ID34c](#), D. Golubkov [ID38](#), J.P. Gombas [ID109](#), A. Gomes [ID133a,133b](#), G. Gomes Da Silva [ID147](#), A.J. Gomez Delegido [ID169](#), R. Gonçalves [ID133a](#), L. Gonella [ID21](#), A. Gongadze [ID155c](#), F. Gonnella [ID21](#), J.L. Gonski [ID149](#), R.Y. González Andana [ID52](#), S. González de la Hoz [ID169](#), M.V. Gonzalez Rodrigues [ID48](#), R. Gonzalez Suarez [ID167](#), S. Gonzalez-Sevilla [ID56](#), L. Goossens [ID37](#), B. Gorini [ID37](#), E. Gorini [ID70a,70b](#), A. Gorišek [ID95](#), T.C. Gosart [ID131](#), A.T. Goshaw [ID51](#), M.I. Gostkin [ID39](#), S. Goswami [ID124](#), C.A. Gottardo [ID37](#), S.A. Gotz [ID111](#), M. Goughri [ID36b](#), A.G. Goussiou [ID142](#), N. Govender [ID34c](#), R.P. Grabarczyk [ID129](#), I. Grabowska-Bold [ID86a](#), K. Graham [ID35](#), E. Gramstad [ID128](#), S. Grancagnolo [ID70a,70b](#), C.M. Grant [ID1](#), P.M. Gravila [ID28f](#), F.G. Gravili [ID70a,70b](#), H.M. Gray [ID18a](#), M. Greco [ID112](#), M.J. Green [ID1](#), C. Grefe [ID25](#), A.S. Grefsrud [ID17](#), I.M. Gregor [ID48](#), K.T. Greif [ID165](#), P. Grenier [ID149](#), S.G. Grewe [ID112](#), A.A. Grillo [ID139](#), K. Grimm [ID32](#), S. Grinstein [ID13,y](#), J.-F. Grivaz [ID66](#), E. Gross [ID175](#), J. Grosse-Knetter [ID55](#), L. Guan [ID108](#), G. Guerrieri [ID37](#), R. Guevara [ID128](#), R. Gugel [ID102](#), J.A.M. Guhit [ID108](#), A. Guida [ID19](#), E. Guilloton [ID173](#), S. Guindon [ID37](#), F. Guo [ID14,114c](#), J. Guo [ID144a](#), L. Guo [ID48](#), L. Guo [ID114b,w](#), Y. Guo [ID108](#), A. Gupta [ID49](#),

R. Gupta ¹³², S. Gurbuz ²⁵, S.S. Gurdasani ⁴⁸, G. Gustavino ^{75a,75b}, P. Gutierrez ¹²³,
 L.F. Gutierrez Zagazeta ¹³¹, M. Gutsche ⁵⁰, C. Gutschow ⁹⁸, C. Gwenlan ¹²⁹, C.B. Gwilliam ⁹⁴,
 E.S. Haaland ¹²⁸, A. Haas ¹²⁰, M. Habedank ⁵⁹, C. Haber ^{18a}, H.K. Hadavand ⁸, A. Haddad ⁴¹,
 A. Hadeef ⁵⁰, A.I. Hagan ⁹³, J.J. Hahn ¹⁴⁷, E.H. Haines ⁹⁸, M. Haleem ¹⁷², J. Haley ¹²⁴,
 G.D. Hallowell ¹⁰⁴, L. Halser ²⁰, K. Hamano ¹⁷¹, M. Hamer ²⁵, S.E.D. Hammoud ⁶⁶,
 E.J. Hampshire ⁹⁷, J. Han ^{143a}, L. Han ^{114a}, L. Han ⁶², S. Han ^{18a}, K. Hanagaki ⁸⁴,
 M. Hance ¹³⁹, D.A. Hangal ⁴², H. Hanif ¹⁴⁸, M.D. Hank ¹³¹, J.B. Hansen ⁴³, P.H. Hansen ⁴³,
 D. Harada ⁵⁶, T. Harenberg ¹⁷⁷, S. Harkusha ¹⁷⁹, M.L. Harris ¹⁰⁵, Y.T. Harris ²⁵, J. Harrison ¹³,
 N.M. Harrison ¹²², P.F. Harrison ¹⁷³, M.L.E. Hart ⁹⁸, N.M. Hartman ¹¹², N.M. Hartmann ¹¹¹,
 R.Z. Hasan ^{97,137}, Y. Hasegawa ¹⁴⁶, F. Haslbeck ¹²⁹, S. Hassan ¹⁷, R. Hauser ¹⁰⁹,
 M. Haviernik ¹³⁶, C.M. Hawkes ²¹, R.J. Hawkins ³⁷, Y. Hayashi ¹⁵⁹, D. Hayden ¹⁰⁹,
 C. Hayes ¹⁰⁸, R.L. Hayes ¹¹⁷, C.P. Hays ¹²⁹, J.M. Hays ⁹⁶, H.S. Hayward ⁹⁴, M. He ^{14,114c},
 Y. He ⁴⁸, Y. He ⁹⁸, N.B. Heatley ⁹⁶, V. Hedberg ¹⁰⁰, C. Heidegger ⁵⁴, K.K. Heidegger ⁵⁴,
 J. Heilman ³⁵, S. Heim ⁴⁸, T. Heim ^{18a}, J.G. Heinlein ¹³¹, J.J. Heinrich ¹²⁶, L. Heinrich ¹¹²,
 J. Hejbal ¹³⁴, A. Held ¹⁷⁶, S. Hellesund ¹⁷, C.M. Helling ¹⁷⁰, S. Hellman ^{47a,47b},
 L. Henkelmann ³³, A.M. Henriques Correia ³⁷, H. Herde ¹⁰⁰, Y. Hernández Jiménez ¹⁵¹,
 L.M. Herrmann ²⁵, T. Herrmann ⁵⁰, G. Herten ⁵⁴, R. Hertenberger ¹¹¹, L. Hervas ³⁷,
 M.E. Hesping ¹⁰², N.P. Hessey ^{162a}, J. Hessler ¹¹², M. Hidaoui ^{36b}, N. Hidic ¹³⁶, E. Hill ¹⁶¹,
 T.S. Hillersoy ¹⁷, S.J. Hillier ²¹, J.R. Hinds ¹⁰⁹, F. Hinterkeuser ²⁵, M. Hirose ¹²⁷, S. Hirose ¹⁶³,
 D. Hirschbuehl ¹⁷⁷, T.G. Hitchings ¹⁰³, B. Hiti ⁹⁵, J. Hobbs ¹⁵¹, R. Hobincu ^{28e}, N. Hod ¹⁷⁵,
 A.M. Hodges ¹⁶⁸, M.C. Hodgkinson ¹⁴⁵, B.H. Hodgkinson ¹²⁹, A. Hoecker ³⁷, D.D. Hofer ¹⁰⁸,
 J. Hofer ¹⁶⁹, M. Holzbock ³⁷, L.B.A.H. Hommels ³³, V. Homsak ¹²⁹, B.P. Honan ¹⁰³,
 J.J. Hong ⁶⁸, T.M. Hong ¹³², B.H. Hooberman ¹⁶⁸, W.H. Hopkins ⁶, M.C. Hoppesch ¹⁶⁸,
 Y. Horii ¹¹³, M.E. Horstmann ¹¹², S. Hou ¹⁵⁴, M.R. Housenga ¹⁶⁸, A.S. Howard ⁹⁵,
 J. Howarth ⁵⁹, J. Hoya ⁶, M. Hrabovsky ¹²⁵, T. Hryn'ova ⁴, P.J. Hsu ⁶⁵, S.-C. Hsu ¹⁴²,
 T. Hsu ⁶⁶, M. Hu ^{18a}, Q. Hu ⁶², S. Huang ³³, X. Huang ^{14,114c}, Y. Huang ¹³⁶, Y. Huang ^{114b},
 Y. Huang ¹⁰², Y. Huang ¹⁴, Z. Huang ⁶⁶, Z. Hubacek ¹³⁵, M. Huebner ²⁵, F. Huegging ²⁵,
 T.B. Huffman ¹²⁹, M. Hufnagel Maranha De Faria ^{83a}, C.A. Hugli ⁴⁸, M. Huhtinen ³⁷,
 S.K. Huiberts ¹⁷, R. Hulskens ¹⁰⁶, C.E. Hultquist ^{18a}, N. Huseynov ^{12,g}, J. Huston ¹⁰⁹, J. Huth ⁶¹,
 R. Hyneman ⁷, G. Iacobucci ⁵⁶, G. Iakovidis ³⁰, L. Iconomidou-Fayard ⁶⁶, J.P. Iddon ³⁷,
 P. Iengo ^{72a,72b}, R. Iguchi ¹⁵⁹, Y. Iiyama ¹⁵⁹, T. Iizawa ¹⁵⁹, Y. Ikegami ⁸⁴, D. Iliadis ¹⁵⁸,
 N. Ilic ¹⁶¹, H. Imam ^{36a}, G. Inacio Goncalves ^{83d}, S.A. Infante Cabanas ^{140c},
 T. Ingebretsen Carlson ^{47a,47b}, J.M. Inglis ⁹⁶, G. Introzzi ^{73a,73b}, M. Iodice ^{77a}, V. Ippolito ^{75a,75b},
 R.K. Irwin ⁹⁴, M. Ishino ¹⁵⁹, W. Islam ¹⁷⁶, C. Issever ¹⁹, S. Istin ^{22a,am}, K. Itabashi ⁸⁴,
 H. Ito ¹⁷⁴, R. Iuppa ^{78a,78b}, A. Ivina ¹⁷⁵, V. Izzo ^{72a}, P. Jacka ¹³⁴, P. Jackson ¹, P. Jain ⁴⁸,
 K. Jakobs ⁵⁴, T. Jakoubek ¹⁷⁵, J. Jamieson ⁵⁹, W. Jang ¹⁵⁹, S. Jankovych ¹³⁶, M. Javurkova ¹⁰⁵,
 P. Jawahar ¹⁰³, L. Jeanty ¹²⁶, J. Jejelava ^{155a}, P. Jenni ^{54,f}, C.E. Jessiman ³⁵, C. Jia ^{143a},
 H. Jia ¹⁷⁰, J. Jia ¹⁵¹, X. Jia ^{14,114c}, Z. Jia ^{114a}, C. Jiang ⁵², Q. Jiang ^{64b}, S. Jiggins ⁴⁸,
 M. Jimenez Ortega ¹⁶⁹, J. Jimenez Pena ¹³, S. Jin ^{114a}, A. Jinaru ^{28b}, O. Jinnouchi ¹⁴¹,
 P. Johansson ¹⁴⁵, K.A. Johns ⁷, J.W. Johnson ¹³⁹, F.A. Jolly ⁴⁸, D.M. Jones ¹⁵², E. Jones ⁴⁸,
 K.S. Jones ⁸, P. Jones ³³, R.W.L. Jones ⁹³, T.J. Jones ⁹⁴, H.L. Joos ^{55,37}, R. Joshi ¹²²,
 J. Jovicevic ¹⁶, X. Ju ^{18a}, J.J. Junggeburth ³⁷, T. Junkermann ^{63a}, A. Juste Rozas ^{13,y},
 M.K. Juzek ⁸⁷, S. Kabana ^{140e}, A. Kaczmarek ⁸⁷, M. Kado ¹¹², H. Kagan ¹²², M. Kagan ¹⁴⁹,
 A. Kahn ¹³¹, C. Kahra ¹⁰², T. Kaji ¹⁵⁹, E. Kajomovitz ¹⁵⁶, N. Kakati ¹⁷⁵, N. Kakoty ¹³,
 I. Kalaitzidou ⁵⁴, S. Kandel ⁸, N.J. Kang ¹³⁹, D. Kar ^{34g}, K. Karava ¹²⁹, E. Karentzos ²⁵,
 O. Karkout ¹¹⁷, S.N. Karpov ³⁹, Z.M. Karpova ³⁹, V. Kartvelishvili ⁹³, A.N. Karyukhin ³⁸,
 E. Kasimi ¹⁵⁸, J. Katzy ⁴⁸, S. Kaur ³⁵, K. Kawade ¹⁴⁶, M.P. Kawale ¹²³, C. Kawamoto ⁸⁹,

T. Kawamoto [id](#)⁶², E.F. Kay [id](#)³⁷, F.I. Kaya [id](#)¹⁶⁴, S. Kazakos [id](#)¹⁰⁹, V.F. Kazanin [id](#)³⁸, J.M. Keaveney [id](#)^{34a},
 R. Keeler [id](#)¹⁷¹, G.V. Kehris [id](#)⁶¹, J.S. Keller [id](#)³⁵, J.J. Kempster [id](#)¹⁵², O. Kepka [id](#)¹³⁴, J. Kerr [id](#)^{162b},
 B.P. Kerridge [id](#)¹³⁷, B.P. Kerševan [id](#)⁹⁵, L. Keszeghova [id](#)^{29a}, R.A. Khan [id](#)¹³², A. Khanov [id](#)¹²⁴,
 A.G. Kharlamov [id](#)³⁸, T. Kharlamova [id](#)³⁸, E.E. Khoda [id](#)¹⁴², M. Kholodenko [id](#)^{133a}, T.J. Khoo [id](#)¹⁹,
 G. Khorauli [id](#)¹⁷², Y. Khoulaki [id](#)^{36a}, J. Khubua [id](#)^{155b,*}, Y.A.R. Khwaira [id](#)¹³⁰, B. Kibirige [id](#)^{34g}, D. Kim [id](#)⁶,
 D.W. Kim [id](#)^{47a,47b}, Y.K. Kim [id](#)⁴⁰, N. Kimura [id](#)⁹⁸, M.K. Kingston [id](#)⁵⁵, A. Kirchhoff [id](#)⁵⁵, C. Kirfel [id](#)²⁵,
 F. Kirfel [id](#)²⁵, J. Kirk [id](#)¹³⁷, A.E. Kiryunin [id](#)¹¹², S. Kita [id](#)¹⁶³, O. Kivernyk [id](#)²⁵, M. Klassen [id](#)¹⁶⁴,
 C. Klein [id](#)³⁵, L. Klein [id](#)¹⁷², M.H. Klein [id](#)⁴⁵, S.B. Klein [id](#)⁵⁶, U. Klein [id](#)⁹⁴, A. Klimentov [id](#)³⁰,
 T. Klioutchnikova [id](#)³⁷, P. Kluit [id](#)¹¹⁷, S. Kluth [id](#)¹¹², E. Kneringer [id](#)⁷⁹, T.M. Knight [id](#)¹⁶¹, A. Knue [id](#)⁴⁹,
 M. Kobel [id](#)⁵⁰, D. Kobylanskii [id](#)¹⁷⁵, S.F. Koch [id](#)¹²⁹, M. Kocian [id](#)¹⁴⁹, P. Kodyš [id](#)¹³⁶, D.M. Koeck [id](#)¹²⁶,
 T. Koffas [id](#)³⁵, O. Kolay [id](#)⁵⁰, I. Koletsou [id](#)⁴, T. Komarek [id](#)⁸⁷, K. Köneke [id](#)⁵⁵, A.X.Y. Kong [id](#)¹,
 T. Kono [id](#)¹²¹, N. Konstantinidis [id](#)⁹⁸, P. Kontaxakis [id](#)⁵⁶, B. Konya [id](#)¹⁰⁰, R. Kopeliansky [id](#)⁴²,
 S. Koperny [id](#)^{86a}, K. Korcyl [id](#)⁸⁷, K. Kordas [id](#)^{158,d}, A. Korn [id](#)⁹⁸, S. Korn [id](#)⁵⁵, I. Korolov [id](#)¹³,
 N. Korotkova [id](#)³⁸, B. Kortman [id](#)¹¹⁷, O. Kortner [id](#)¹¹², S. Kortner [id](#)¹¹², W.H. Kostecka [id](#)¹¹⁸,
 M. Kostov [id](#)^{29a}, V.V. Kostyukhin [id](#)¹⁴⁷, A. Kotsokechagia [id](#)³⁷, A. Kotwal [id](#)⁵¹, A. Koulouris [id](#)³⁷,
 A. Kourkoumeli-Charalampidi [id](#)^{73a,73b}, C. Kourkoumelis [id](#)⁹, E. Kourlitis [id](#)¹¹², O. Kovanda [id](#)¹²⁶,
 R. Kowalewski [id](#)¹⁷¹, W. Kozanecki [id](#)¹²⁶, A.S. Kozhin [id](#)³⁸, V.A. Kramarenko [id](#)³⁸, G. Kramberger [id](#)⁹⁵,
 P. Kramer [id](#)²⁵, M.W. Krasny [id](#)¹³⁰, A. Krasznahorkay [id](#)¹⁰⁵, A.C. Kraus [id](#)¹¹⁸, J.W. Kraus [id](#)¹⁷⁷,
 J.A. Kremer [id](#)⁴⁸, N.B. Kregel [id](#)¹⁴⁷, T. Kresse [id](#)⁵⁰, L. Kretschmann [id](#)¹⁷⁷, J. Kretschmar [id](#)⁹⁴,
 K. Kreul [id](#)¹⁹, P. Krieger [id](#)¹⁶¹, K. Krizka [id](#)²¹, K. Kroeninger [id](#)⁴⁹, H. Kroha [id](#)¹¹², J. Kroll [id](#)¹³⁴,
 J. Kroll [id](#)¹³¹, K.S. Krowpman [id](#)¹⁰⁹, U. Kruchonak [id](#)³⁹, H. Krüger [id](#)²⁵, N. Krumnack [id](#)⁸¹, M.C. Kruse [id](#)⁵¹,
 O. Kuchinskaia [id](#)³⁹, S. Kuday [id](#)^{3a}, S. Kuehn [id](#)³⁷, R. Kuesters [id](#)⁵⁴, T. Kuhl [id](#)⁴⁸, V. Kukhtin [id](#)³⁹,
 Y. Kulchitsky [id](#)³⁹, S. Kuleshov [id](#)^{140d,140b}, J. Kull [id](#)¹, M. Kumar [id](#)^{34g}, N. Kumari [id](#)⁴⁸, P. Kumari [id](#)^{162b},
 A. Kupco [id](#)¹³⁴, T. Kupfer [id](#)⁴⁹, A. Kupich [id](#)³⁸, O. Kuprash [id](#)⁵⁴, H. Kurashige [id](#)⁸⁵, L.L. Kurchaninov [id](#)^{162a},
 O. Kurdysh [id](#)⁴, Y.A. Kurochkin [id](#)³⁸, A. Kurova [id](#)³⁸, M. Kuze [id](#)¹⁴¹, A.K. Kvam [id](#)¹⁰⁵, J. Kvita [id](#)¹²⁵,
 N.G. Kyriacou [id](#)¹⁰⁸, C. Lacasta [id](#)¹⁶⁹, F. Lacava [id](#)^{75a,75b}, H. Lacker [id](#)¹⁹, D. Lacour [id](#)¹³⁰, N.N. Lad [id](#)⁹⁸,
 E. Ladygin [id](#)³⁹, A. Lafarge [id](#)⁴¹, B. Laforge [id](#)¹³⁰, T. Lagouri [id](#)¹⁷⁸, F.Z. Lahbabi [id](#)^{36a}, S. Lai [id](#)⁵⁵,
 J.E. Lambert [id](#)¹⁷¹, S. Lammers [id](#)⁶⁸, W. Lampl [id](#)⁷, C. Lampoudis [id](#)^{158,d}, G. Lamprinoudis [id](#)¹⁰²,
 A.N. Lancaster [id](#)¹¹⁸, E. Lançon [id](#)³⁰, U. Landgraf [id](#)⁵⁴, M.P.J. Landon [id](#)⁹⁶, V.S. Lang [id](#)⁵⁴,
 O.K.B. Langrekken [id](#)¹²⁸, A.J. Lankford [id](#)¹⁶⁵, F. Lanni [id](#)³⁷, K. Lantzsch [id](#)²⁵, A. Lanza [id](#)^{73a},
 M. Lanzac Berrocal [id](#)¹⁶⁹, J.F. Laporte [id](#)¹³⁸, T. Lari [id](#)^{71a}, D. Larsen [id](#)¹⁷, L. Larson [id](#)¹¹,
 F. Lasagni Manghi [id](#)^{24b}, M. Lassnig [id](#)³⁷, S.D. Lawlor [id](#)¹⁴⁵, R. Lazaridou [id](#)¹⁷³, M. Lazzaroni [id](#)^{71a,71b},
 H.D.M. Le [id](#)¹⁰⁹, E.M. Le Boulicaut [id](#)¹⁷⁸, L.T. Le Pottier [id](#)^{18a}, B. Leban [id](#)^{24b,24a}, F. Ledroit-Guillon [id](#)⁶⁰,
 T.F. Lee [id](#)^{162b}, L.L. Leeuw [id](#)^{34c}, M. Lefebvre [id](#)¹⁷¹, C. Leggett [id](#)^{18a}, G. Lehmann Miotto [id](#)³⁷,
 M. Leigh [id](#)⁵⁶, W.A. Leight [id](#)¹⁰⁵, W. Leinonen [id](#)¹¹⁶, A. Leisos [id](#)^{158,v}, M.A.L. Leite [id](#)^{83c},
 C.E. Leitgeb [id](#)¹⁹, R. Leitner [id](#)¹³⁶, K.J.C. Leney [id](#)⁴⁵, T. Lenz [id](#)²⁵, S. Leone [id](#)^{74a}, C. Leonidopoulos [id](#)⁵²,
 A. Leopold [id](#)¹⁵⁰, J.H. Lepage Bourbonnais [id](#)³⁵, R. Les [id](#)¹⁰⁹, C.G. Lester [id](#)³³, M. Levchenko [id](#)³⁸,
 J. Levêque [id](#)⁴, L.J. Levinson [id](#)¹⁷⁵, G. Levrini [id](#)^{24b,24a}, M.P. Lewicki [id](#)⁸⁷, C. Lewis [id](#)¹⁴², D.J. Lewis [id](#)⁴,
 L. Lewitt [id](#)¹⁴⁵, A. Li [id](#)³⁰, B. Li [id](#)^{143a}, C. Li [id](#)¹⁰⁸, C-Q. Li [id](#)¹¹², H. Li [id](#)^{143a}, H. Li [id](#)¹⁰³, H. Li [id](#)¹⁵, H. Li [id](#)⁶²,
 H. Li [id](#)^{143a}, J. Li [id](#)^{144a}, K. Li [id](#)¹⁴, L. Li [id](#)^{144a}, R. Li [id](#)¹⁷⁸, S. Li [id](#)^{14,114c}, S. Li [id](#)^{144b,144a}, T. Li [id](#)⁵,
 X. Li [id](#)¹⁰⁶, Z. Li [id](#)¹⁵⁹, Z. Li [id](#)^{14,114c}, Z. Li [id](#)⁶², S. Liang [id](#)^{14,114c}, Z. Liang [id](#)¹⁴, M. Liberatore [id](#)¹³⁸,
 B. Liberti [id](#)^{76a}, K. Lie [id](#)^{64c}, J. Lieber Marin [id](#)^{83e}, H. Lien [id](#)⁶⁸, H. Lin [id](#)¹⁰⁸, S.F. Lin [id](#)¹⁵¹,
 L. Linden [id](#)¹¹¹, R.E. Lindley [id](#)⁷, J.H. Lindon [id](#)³⁷, J. Ling [id](#)⁶¹, E. Lipeles [id](#)¹³¹, A. Lipniacka [id](#)¹⁷,
 A. Lister [id](#)¹⁷⁰, J.D. Little [id](#)⁶⁸, B. Liu [id](#)¹⁴, B.X. Liu [id](#)^{114b}, D. Liu [id](#)^{144b,144a}, D. Liu [id](#)¹³⁹, E.H.L. Liu [id](#)²¹,
 J.K.K. Liu [id](#)¹²⁰, K. Liu [id](#)^{144b}, K. Liu [id](#)^{144b,144a}, M. Liu [id](#)⁶², M.Y. Liu [id](#)⁶², P. Liu [id](#)¹⁴,
 Q. Liu [id](#)^{144b,142,144a}, X. Liu [id](#)⁶², X. Liu [id](#)^{143a}, Y. Liu [id](#)^{114b,114c}, Y.L. Liu [id](#)^{143a}, Y.W. Liu [id](#)⁶²,
 Z. Liu [id](#)^{66,1}, S.L. Lloyd [id](#)⁹⁶, E.M. Lobodzinska [id](#)⁴⁸, P. Loch [id](#)⁷, E. Lodhi [id](#)¹⁶¹, T. Lohse [id](#)¹⁹,

K. Lohwasser ¹⁴⁵, E. Loiacono ⁴⁸, J.D. Lomas ²¹, J.D. Long ⁴², I. Longarini ¹⁶⁵, R. Longo ¹⁶⁸,
 A. Lopez Solis ¹³, N.A. Lopez-canelas ⁷, N. Lorenzo Martinez ⁴, A.M. Lory ¹¹¹, M. Losada ^{119a},
 G. Löschcke Centeno ¹⁵², X. Lou ^{47a,47b}, X. Lou ^{14,114c}, A. Lounis ⁶⁶, P.A. Love ⁹³, M. Lu ⁶⁶,
 S. Lu ¹³¹, Y.J. Lu ¹⁵⁴, H.J. Lubatti ¹⁴², C. Luci ^{75a,75b}, F.L. Lucio Alves ^{114a}, F. Luehring ⁶⁸,
 B.S. Lunday ¹³¹, O. Lundberg ¹⁵⁰, J. Lunde ³⁷, N.A. Luongo ⁶, M.S. Lutz ³⁷, A.B. Lux ²⁶,
 D. Lynn ³⁰, R. Lysak ¹³⁴, V. Lysenko ¹³⁵, E. Lytken ¹⁰⁰, V. Lyubushkin ³⁹, T. Lyubushkina ³⁹,
 M.M. Lyukova ¹⁵¹, M.Firdaus M. Soberi ⁵², H. Ma ³⁰, K. Ma ⁶², L.L. Ma ^{143a}, W. Ma ⁶²,
 Y. Ma ¹²⁴, J.C. MacDonald ¹⁰², P.C. Machado De Abreu Farias ^{83e}, R. Madar ⁴¹, T. Madula ⁹⁸,
 J. Maeda ⁸⁵, T. Maeno ³⁰, P.T. Mafa ^{34c,k}, H. Maguire ¹⁴⁵, V. Maiboroda ⁶⁶,
 A. Maio ^{133a,133b,133d}, K. Maj ^{86a}, O. Majersky ⁴⁸, S. Majewski ¹²⁶, R. Makhmanazarov ³⁸,
 N. Makovec ⁶⁶, V. Maksimovic ¹⁶, B. Malaescu ¹³⁰, J. Malamant ¹²⁸, Pa. Malecki ⁸⁷,
 V.P. Maleev ³⁸, F. Malek ^{60,p}, M. Mali ⁹⁵, D. Malito ⁹⁷, U. Mallik ^{80,*}, A. Maloizel ⁵,
 S. Maltezos ¹⁰, A. Malvezzi Lopes ^{83d}, S. Malyukov ³⁹, J. Mamuzic ¹³, G. Mancini ⁵³,
 M.N. Mancini ²⁷, G. Manco ^{73a,73b}, J.P. Mandalia ⁹⁶, S.S. Mandarry ¹⁵², I. Mandić ⁹⁵,
 L. Manhaes de Andrade Filho ^{83a}, I.M. Maniatis ¹⁷⁵, J. Manjarres Ramos ⁹¹, D.C. Mankad ¹⁷⁵,
 A. Mann ¹¹¹, T. Manoussos ³⁷, M.N. Mantinan ⁴⁰, S. Manzoni ³⁷, L. Mao ^{144a},
 X. Mapekula ^{34c}, A. Marantis ¹⁵⁸, R.R. Marcelo Gregorio ⁹⁶, G. Marchiori ⁵,
 M. Marcisovsky ¹³⁴, C. Marcon ^{71a}, E. Maricic ¹⁶, M. Marinescu ⁴⁸, S. Marium ⁴⁸,
 M. Marjanovic ¹²³, A. Markhoos ⁵⁴, M. Markovitch ⁶⁶, M.K. Maroun ¹⁰⁵, E.J. Marshall ⁹³,
 Z. Marshall ^{18a}, S. Marti-Garcia ¹⁶⁹, J. Martin ⁹⁸, T.A. Martin ¹³⁷, V.J. Martin ⁵²,
 B. Martin dit Latour ¹⁷, L. Martinelli ^{75a,75b}, M. Martinez ^{13,y}, P. Martinez Agullo ¹⁶⁹,
 V.I. Martinez Outschoorn ¹⁰⁵, P. Martinez Suarez ¹³, S. Martin-Haugh ¹³⁷, G. Martinovicova ¹³⁶,
 V.S. Martoiu ^{28b}, A.C. Martyniuk ⁹⁸, A. Marzin ³⁷, D. Mascione ^{78a,78b}, L. Masetti ¹⁰²,
 J. Masik ¹⁰³, A.L. Maslennikov ³⁹, S.L. Mason ⁴², P. Massarotti ^{72a,72b}, P. Mastrandrea ^{74a,74b},
 A. Mastroberardino ^{44b,44a}, T. Masubuchi ¹²⁷, T.T. Mathew ¹²⁶, J. Matousek ¹³⁶, D.M. Mattern ⁴⁹,
 J. Maurer ^{28b}, T. Maurin ⁵⁹, A.J. Maury ⁶⁶, B. Maček ⁹⁵, C. Mavungu Tsava ¹⁰⁴,
 D.A. Maximov ³⁸, A.E. May ¹⁰³, E. Mayer ⁴¹, R. Mazini ^{34g}, I. Maznas ¹¹⁸, S.M. Mazza ¹³⁹,
 E. Mazzeo ^{71a,71b}, J.P. Mc Gowan ¹⁷¹, S.P. Mc Kee ¹⁰⁸, C.A. Mc Lean ⁶, C.C. McCracken ¹⁷⁰,
 E.F. McDonald ¹⁰⁷, A.E. McDougall ¹¹⁷, L.F. Mcelhinney ⁹³, J.A. Mcfayden ¹⁵²,
 R.P. McGovern ¹³¹, R.P. Mckenzie ^{34g}, T.C. Mclachlan ⁴⁸, D.J. Mclaughlin ⁹⁸, S.J. McMahon ¹³⁷,
 C.M. Mcpartland ⁹⁴, R.A. McPherson ^{171,ac}, S. Mehlhase ¹¹¹, A. Mehta ⁹⁴, D. Melini ¹⁶⁹,
 B.R. Mellado Garcia ^{34g}, A.H. Melo ⁵⁵, F. Meloni ⁴⁸, A.M. Mendes Jacques Da Costa ¹⁰³,
 L. Meng ⁹³, S. Menke ¹¹², M. Mentink ³⁷, E. Meoni ^{44b,44a}, G. Mercado ¹¹⁸, S. Merianos ¹⁵⁸,
 C. Merlassino ^{69a,69c}, C. Meroni ^{71a,71b}, J. Metcalfe ⁶, A.S. Mete ⁶, E. Meuser ¹⁰², C. Meyer ⁶⁸,
 J-P. Meyer ¹³⁸, Y. Miao ^{114a}, R.P. Middleton ¹³⁷, M. Mihovilovic ⁶⁶, L. Mijović ⁵²,
 G. Mikenberg ¹⁷⁵, M. Mikesikova ¹³⁴, M. Mikuž ⁹⁵, H. Mildner ¹⁰², A. Milic ³⁷,
 D.W. Miller ⁴⁰, E.H. Miller ¹⁴⁹, L.S. Miller ³⁵, A. Milov ¹⁷⁵, D.A. Milstead ^{47a,47b}, T. Min ^{114a},
 A.A. Minaenko ³⁸, I.A. Minashvili ^{155b}, A.I. Mincer ¹²⁰, B. Mindur ^{86a}, M. Mineev ³⁹,
 Y. Mino ⁸⁹, L.M. Mir ¹³, M. Miralles Lopez ⁵⁹, M. Mironova ^{18a}, M.C. Missio ¹¹⁶, A. Mitra ¹⁷³,
 V.A. Mitsou ¹⁶⁹, Y. Mitsumori ¹¹³, O. Miu ¹⁶¹, P.S. Miyagawa ⁹⁶, T. Mkrtychyan ^{63a},
 M. Mlinarevic ⁹⁸, T. Mlinarevic ⁹⁸, M. Mlynarikova ³⁷, S. Mobius ²⁰, M.H. Mohamed Farook ¹¹⁵,
 A.F. Mohammed ^{14,114c}, S. Mohapatra ⁴², S. Mohiuddin ¹²⁴, G. Mokgatitwane ^{34g}, L. Moleri ¹⁷⁵,
 U. Molinatti ¹²⁹, L.G. Mollier ²⁰, B. Mondal ¹⁴⁷, S. Mondal ¹³⁵, K. Mönig ⁴⁸, E. Monnier ¹⁰⁴,
 L. Monsonis Romero ¹⁶⁹, J. Montejo Berlingen ¹³, A. Montella ^{47a,47b}, M. Montella ¹²²,
 F. Montekali ^{77a,77b}, F. Monticelli ⁹², S. Monzani ^{69a,69c}, A. Morancho Tarda ⁴³, N. Morange ⁶⁶,
 A.L. Moreira De Carvalho ⁴⁸, M. Moreno Llácer ¹⁶⁹, C. Moreno Martinez ⁵⁶, J.M. Moreno Perez ^{23b},
 P. Morettini ^{57b}, S. Morgenstern ³⁷, M. Morii ⁶¹, M. Morinaga ¹⁵⁹, M. Moritsu ⁹⁰,

F. Morodei ^{75a,75b}, P. Moschovakos ³⁷, B. Moser ⁵⁴, M. Mosidze ^{155b}, T. Moskalets ⁴⁵, P. Moskvitina ¹¹⁶, J. Moss ³², P. Moszkowicz ^{86a}, A. Moussa ^{36d}, Y. Moyal ¹⁷⁵, H. Moyano Gomez ¹³, E.J.W. Moyse ¹⁰⁵, O. Mtintsilana ^{34g}, S. Muanza ¹⁰⁴, M. Mucha ²⁵, J. Mueller ¹³², R. Müller ³⁷, G.A. Mullier ¹⁶⁷, A.J. Mullin ³³, J.J. Mullin ⁵¹, A.C. Mullins ⁴⁵, A.E. Mulski ⁶¹, D.P. Mungo ¹⁶¹, D. Munoz Perez ¹⁶⁹, F.J. Munoz Sanchez ¹⁰³, W.J. Murray ^{173,137}, M. Muškinja ⁹⁵, C. Mwewa ⁴⁸, A.G. Myagkov ^{38,a}, A.J. Myers ⁸, G. Myers ¹⁰⁸, M. Myska ¹³⁵, B.P. Nachman ^{18a}, K. Nagai ¹²⁹, K. Nagano ⁸⁴, R. Nagasaka ¹⁵⁹, J.L. Nagle ^{30,aj}, E. Nagy ¹⁰⁴, A.M. Nairz ³⁷, Y. Nakahama ⁸⁴, K. Nakamura ⁸⁴, K. Nakkalil ⁵, A. Nandi ^{63b}, H. Nanjo ¹²⁷, E.A. Narayanan ⁴⁵, Y. Narukawa ¹⁵⁹, I. Naryshkin ³⁸, L. Nasella ^{71a,71b}, S. Nasri ^{119b}, C. Nass ²⁵, G. Navarro ^{23a}, J. Navarro-Gonzalez ¹⁶⁹, A. Nayaz ¹⁹, P.Y. Nechaeva ³⁸, S. Nechaeva ^{24b,24a}, F. Nechansky ¹³⁴, L. Nedic ¹²⁹, T.J. Neep ²¹, A. Negri ^{73a,73b}, M. Negrini ^{24b}, C. Nellist ¹¹⁷, C. Nelson ¹⁰⁶, K. Nelson ¹⁰⁸, S. Nemecek ¹³⁴, M. Nessi ^{37,h}, M.S. Neubauer ¹⁶⁸, J. Newell ⁹⁴, P.R. Newman ²¹, Y.W.Y. Ng ¹⁶⁸, B. Ngair ^{119a}, H.D.N. Nguyen ¹¹⁰, J.D. Nichols ¹²³, R.B. Nickerson ¹²⁹, R. Nicolaidou ¹³⁸, J. Nielsen ¹³⁹, M. Niemeyer ⁵⁵, J. Niermann ³⁷, N. Nikiforou ³⁷, V. Nikolaenko ^{38,a}, I. Nikolic-Audit ¹³⁰, P. Nilsson ³⁰, I. Ninca ⁴⁸, G. Ninio ¹⁵⁷, A. Nisati ^{75a}, N. Nishu ², R. Nisius ¹¹², N. Nitika ^{69a,69c}, J-E. Nitschke ⁵⁰, E.K. Nkadimeng ^{34b}, T. Nobe ¹⁵⁹, T. Nommensen ¹⁵³, M.B. Norfolk ¹⁴⁵, B.J. Norman ³⁵, M. Noury ^{36a}, J. Novak ⁹⁵, T. Novak ⁹⁵, R. Novotny ¹³⁵, L. Nozka ¹²⁵, K. Ntekas ¹⁶⁵, N.M.J. Nunes De Moura Junior ^{83b}, J. Ocariz ¹³⁰, A. Ochi ⁸⁵, I. Ochoa ^{133a}, S. Oerdek ^{48,z}, J.T. Offermann ⁴⁰, A. Ogrodnik ¹³⁶, A. Oh ¹⁰³, C.C. Ohm ¹⁵⁰, H. Oide ⁸⁴, M.L. Ojeda ³⁷, Y. Okumura ¹⁵⁹, L.F. Oleiro Seabra ^{133a}, I. Oleksiyuk ⁵⁶, G. Oliveira Correa ¹³, D. Oliveira Damazio ³⁰, J.L. Oliver ¹⁶⁵, Ö.O. Öncel ⁵⁴, A.P. O'Neill ²⁰, A. Onofre ^{133a,133e,e}, P.U.E. Onyisi ¹¹, M.J. Oreglia ⁴⁰, D. Orestano ^{77a,77b}, R. Orlandini ^{77a,77b}, R.S. Orr ¹⁶¹, L.M. Osojnak ¹³¹, Y. Osumi ¹¹³, G. Otero y Garzon ³¹, H. Otono ⁹⁰, G.J. Ottino ^{18a}, M. Ouchrif ^{36d}, F. Ould-Saada ¹²⁸, T. Ovsiannikova ¹⁴², M. Owen ⁵⁹, R.E. Owen ¹³⁷, V.E. Ozcan ^{22a}, F. Ozturk ⁸⁷, N. Ozturk ⁸, S. Ozturk ⁸², H.A. Pacey ¹²⁹, K. Pachal ^{162a}, A. Pacheco Pages ¹³, C. Padilla Aranda ¹³, G. Padovano ^{75a,75b}, S. Pagan Griso ^{18a}, G. Palacino ⁶⁸, A. Palazzo ^{70a,70b}, J. Pampel ²⁵, J. Pan ¹⁷⁸, T. Pan ^{64a}, D.K. Panchal ¹¹, C.E. Pandini ¹¹⁷, J.G. Panduro Vazquez ¹³⁷, H.D. Pandya ¹, H. Pang ¹³⁸, P. Pani ⁴⁸, G. Panizzo ^{69a,69c}, L. Panwar ¹³⁰, L. Paolozzi ⁵⁶, S. Parajuli ¹⁶⁸, A. Paramonov ⁶, C. Paraskevopoulos ⁵³, D. Paredes Hernandez ^{64b}, A. Pareti ^{73a,73b}, K.R. Park ⁴², T.H. Park ¹¹², F. Parodi ^{57b,57a}, J.A. Parsons ⁴², U. Parzefall ⁵⁴, B. Pascual Dias ⁴¹, L. Pascual Dominguez ¹⁰¹, E. Pasqualucci ^{75a}, S. Passaggio ^{57b}, F. Pastore ⁹⁷, P. Patel ⁸⁷, U.M. Patel ⁵¹, J.R. Pater ¹⁰³, T. Pauly ³⁷, F. Pauwels ¹³⁶, C.I. Pazos ¹⁶⁴, M. Pedersen ¹²⁸, R. Pedro ^{133a}, S.V. Peleganchuk ³⁸, O. Penc ³⁷, E.A. Pender ⁵², S. Peng ¹⁵, G.D. Penn ¹⁷⁸, K.E. Penski ¹¹¹, M. Penzin ³⁸, B.S. Peralva ^{83d}, A.P. Pereira Peixoto ¹⁴², L. Pereira Sanchez ¹⁴⁹, D.V. Perepelitsa ^{30,aj}, G. Perera ¹⁰⁵, E. Perez Codina ^{162a}, M. Perganti ¹⁰, H. Pernegger ³⁷, S. Perrella ^{75a,75b}, O. Perrin ⁴¹, K. Peters ⁴⁸, R.F.Y. Peters ¹⁰³, B.A. Petersen ³⁷, T.C. Petersen ⁴³, E. Petit ¹⁰⁴, V. Petousis ¹³⁵, A.R. Petri ^{71a,71b}, C. Petridou ^{158,d}, T. Petru ¹³⁶, A. Petrukhin ¹⁴⁷, M. Pettee ^{18a}, A. Petukhov ⁸², K. Petukhova ³⁷, R. Pezoa ^{140f}, L. Pezzotti ^{24b,24a}, G. Pezzullo ¹⁷⁸, L. Pfaffenbichler ³⁷, A.J. Pflieger ³⁷, T.M. Pham ¹⁷⁶, T. Pham ¹⁰⁷, P.W. Phillips ¹³⁷, G. Piacquadio ¹⁵¹, E. Pianori ^{18a}, F. Piazza ¹²⁶, R. Piegai ³¹, D. Pietreanu ^{28b}, A.D. Pilkington ¹⁰³, M. Pinamonti ^{69a,69c}, J.L. Pinfeld ², B.C. Pinheiro Pereira ^{133a}, J. Pinol Bel ¹³, A.E. Pinto Pinoargote ¹³⁰, L. Pintucci ^{69a,69c}, K.M. Piper ¹⁵², A. Pirttikoski ⁵⁶, D.A. Pizzi ³⁵, L. Pizzimento ^{64b}, A. Plebani ³³, M.-A. Pleier ³⁰, V. Pleskot ¹³⁶, E. Plotnikova ³⁹, G. Poddar ⁹⁶, R. Poettgen ¹⁰⁰, L. Poggioli ¹³⁰, S. Polacek ¹³⁶, G. Polesello ^{73a}, A. Poley ¹⁴⁸, A. Polini ^{24b}, C.S. Pollard ¹⁷³, Z.B. Pollock ¹²², E. Pompa Pacchi ¹²³, N.I. Pond ⁹⁸,

D. Ponomarenko ⁶⁸, L. Pontecorvo ³⁷, S. Popa ^{28a}, G.A. Popeneciu ^{28d}, A. Poreba ³⁷,
 D.M. Portillo Quintero ^{162a}, S. Pospisil ¹³⁵, M.A. Postill ¹⁴⁵, P. Postolache ^{28c}, K. Potamianos ¹⁷³,
 P.A. Potepa ^{86a}, I.N. Potrap ³⁹, C.J. Potter ³³, H. Potti ¹⁵³, J. Poveda ¹⁶⁹,
 M.E. Pozo Astigarraga ³⁷, R. Pozzi ³⁷, A. Prades Ibanez ^{76a,76b}, J. Pretel ¹⁷¹, D. Price ¹⁰³,
 M. Primavera ^{70a}, L. Primomo ^{69a,69c}, M.A. Principe Martin ¹⁰¹, R. Privara ¹²⁵, T. Procter ^{86b},
 M.L. Proffitt ¹⁴², N. Proklova ¹³¹, K. Prokofiev ^{64c}, G. Proto ¹¹², J. Proudfoot ⁶,
 M. Przybycien ^{86a}, W.W. Przygoda ^{86b}, A. Psallidas ⁴⁶, J.E. Puddefoot ¹⁴⁵, D. Pudzha ⁵³,
 D. Pyatiizbyantseva ¹¹⁶, J. Qian ¹⁰⁸, R. Qian ¹⁰⁹, D. Qichen ¹⁰³, Y. Qin ¹³, T. Qiu ⁵²,
 A. Quadt ⁵⁵, M. Queitsch-Maitland ¹⁰³, G. Quetant ⁵⁶, R.P. Quinn ¹⁷⁰, G. Rabanal Bolanos ⁶¹,
 D. Rafanoharana ⁵⁴, F. Raffaeli ^{76a,76b}, F. Ragusa ^{71a,71b}, J.L. Rainbolt ⁴⁰, J.A. Raine ⁵⁶,
 S. Rajagopalan ³⁰, E. Ramakoti ³⁹, L. Rambelli ^{57b,57a}, I.A. Ramirez-Berend ³⁵, K. Ran ^{48,114c},
 D.S. Rankin ¹³¹, N.P. Rapheeha ^{34g}, H. Rasheed ^{28b}, D.F. Rassloff ^{63a}, A. Rastogi ^{18a},
 S. Rave ¹⁰², S. Ravera ^{57b,57a}, B. Ravina ³⁷, I. Ravinovich ¹⁷⁵, M. Raymond ³⁷, A.L. Read ¹²⁸,
 N.P. Readioff ¹⁴⁵, D.M. Rebuzzi ^{73a,73b}, A.S. Reed ¹¹², K. Reeves ²⁷, J.A. Reidelsturz ¹⁷⁷,
 D. Reikher ¹²⁶, A. Rej ⁴⁹, C. Rembser ³⁷, H. Ren ⁶², M. Renda ^{28b}, F. Renner ⁴⁸,
 A.G. Rennie ⁵⁹, A.L. Rescia ⁴⁸, S. Resconi ^{71a}, M. Ressegotti ^{57b,57a}, S. Rettie ³⁷,
 W.F. Rettie ³⁵, E. Reynolds ^{18a}, O.L. Rezanova ³⁹, P. Reznicek ¹³⁶, H. Riani ^{36d}, N. Ribaric ⁵¹,
 E. Ricci ^{78a,78b}, R. Richter ¹¹², S. Richter ^{47a,47b}, E. Richter-Was ^{86b}, M. Ridel ¹³⁰,
 S. Ridouani ^{36d}, P. Rieck ¹²⁰, P. Riedler ³⁷, E.M. Riefel ^{47a,47b}, J.O. Rieger ¹¹⁷,
 M. Rijssenbeek ¹⁵¹, M. Rimoldi ³⁷, L. Rinaldi ^{24b,24a}, P. Rincke ¹⁶⁷, G. Ripellino ¹⁶⁷, I. Riu ¹³,
 J.C. Rivera Vergara ¹⁷¹, F. Rizatdinova ¹²⁴, E. Rizvi ⁹⁶, B.R. Roberts ^{18a}, S.S. Roberts ¹³⁹,
 D. Robinson ³³, M. Robles Manzano ¹⁰², A. Robson ⁵⁹, A. Rocchi ^{76a,76b}, C. Roda ^{74a,74b},
 S. Rodriguez Bosca ³⁷, Y. Rodriguez Garcia ^{23a}, A.M. Rodríguez Vera ¹¹⁸, S. Roe ³⁷,
 J.T. Roemer ³⁷, O. Røhne ¹²⁸, R.A. Rojas ³⁷, C.P.A. Roland ¹³⁰, A. Romaniouk ⁷⁹,
 E. Romano ^{73a,73b}, M. Romano ^{24b}, A.C. Romero Hernandez ¹⁶⁸, N. Rompotis ⁹⁴, L. Roos ¹³⁰,
 S. Rosati ^{75a}, B.J. Rosser ⁴⁰, E. Rossi ¹²⁹, E. Rossi ^{72a,72b}, L.P. Rossi ⁶¹, L. Rossini ⁵⁴,
 R. Rosten ¹²², M. Rotaru ^{28b}, B. Rottler ⁵⁴, D. Rousseau ⁵⁶, D. Rousso ⁴⁸, S. Roy-Garand ¹⁶¹,
 A. Rozanov ¹⁰⁴, Z.M.A. Rozario ⁵⁹, Y. Rozen ¹⁵⁶, A. Rubio Jimenez ¹⁶⁹, V.H. Ruelas Rivera ¹⁹,
 T.A. Ruggeri ¹, A. Ruggiero ¹²⁹, A. Ruiz-Martinez ¹⁶⁹, A. Rummler ³⁷, Z. Rurikova ⁵⁴,
 N.A. Rusakovich ³⁹, H.L. Russell ¹⁷¹, G. Russo ^{75a,75b}, J.P. Rutherford ⁷,
 S. Rutherford Colmenares ³³, M. Rybar ¹³⁶, P. Rybczynski ^{86a}, A. Ryzhov ⁴⁵,
 J.A. Sabater Iglesias ⁵⁶, H.F.W. Sadrozinski ¹³⁹, F. Safai Tehrani ^{75a}, S. Saha ¹, M. Sahinsky ⁸²,
 B. Sahoo ¹⁷⁵, A. Saibel ¹⁶⁹, B.T. Saifuddin ¹²³, M. Saimpert ¹³⁸, G.T. Saito ^{83c}, M. Saito ¹⁵⁹,
 T. Saito ¹⁵⁹, A. Sala ^{71a,71b}, A. Salnikov ¹⁴⁹, J. Salt ¹⁶⁹, A. Salvador Salas ¹⁵⁷, F. Salvatore ¹⁵²,
 A. Salzburger ³⁷, D. Sammel ⁵⁴, E. Sampson ⁹³, D. Sampsonidis ^{158,d}, D. Sampsonidou ¹²⁶,
 J. Sánchez ¹⁶⁹, V. Sanchez Sebastian ¹⁶⁹, H. Sandaker ¹²⁸, C.O. Sander ⁴⁸, J.A. Sandesara ¹⁷⁶,
 M. Sandhoff ¹⁷⁷, C. Sandoval ^{23b}, L. Sanfilippo ^{63a}, D.P.C. Sankey ¹³⁷, T. Sano ⁸⁹,
 A. Sansoni ⁵³, L. Santi ³⁷, C. Santoni ⁴¹, H. Santos ^{133a,133b}, A. Santra ¹⁷⁵, E. Sanzani ^{24b,24a},
 K.A. Saoucha ^{88b}, J.G. Saraiva ^{133a,133d}, J. Sardain ⁷, O. Sasaki ⁸⁴, K. Sato ¹⁶³, C. Sauer ³⁷,
 E. Sauvan ⁴, P. Savard ^{161,ah}, R. Sawada ¹⁵⁹, C. Sawyer ¹³⁷, L. Sawyer ⁹⁹, C. Sbarra ^{24b},
 A. Sbrizzi ^{24b,24a}, T. Scanlon ⁹⁸, J. Schaarschmidt ¹⁴², U. Schäfer ¹⁰², A.C. Schaffer ^{66,45},
 D. Schaile ¹¹¹, R.D. Schamberger ¹⁵¹, C. Scharf ¹⁹, M.M. Schefer ²⁰, V.A. Schegelsky ³⁸,
 D. Scheirich ¹³⁶, M. Schernau ^{140e}, C. Scheulen ⁵⁶, C. Schiavi ^{57b,57a}, M. Schioppa ^{44b,44a},
 B. Schlag ¹⁴⁹, S. Schlenker ³⁷, J. Schmeing ¹⁷⁷, E. Schmidt ¹¹², M.A. Schmidt ¹⁷⁷,
 K. Schmieden ¹⁰², C. Schmitt ¹⁰², N. Schmitt ¹⁰², S. Schmitt ⁴⁸, L. Schoeffel ¹³⁸,
 A. Schoening ^{63b}, P.G. Scholer ³⁵, E. Schopf ¹⁴⁷, M. Schott ²⁵, S. Schramm ⁵⁶, F. Schroeder ¹⁷⁷,
 T. Schroer ⁵⁶, H-C. Schultz-Coulon ^{63a}, M. Schumacher ⁵⁴, B.A. Schumm ¹³⁹, Ph. Schune ¹³⁸,

H.R. Schwartz [id139](#), A. Schwartzman [id149](#), T.A. Schwarz [id108](#), Ph. Schwemling [id138](#),
 R. Schwienhorst [id109](#), F.G. Sciacca [id20](#), A. Sciandra [id30](#), G. Sciolla [id27](#), F. Scuri [id74a](#),
 C.D. Sebastiani [id37](#), K. Sedlaczek [id118](#), S.C. Seidel [id115](#), A. Seiden [id139](#), B.D. Seidlitz [id42](#), C. Seitz [id48](#),
 J.M. Seixas [id83b](#), G. Sekhniaidze [id72a](#), L. Selem [id60](#), N. Semprini-Cesari [id24b,24a](#), A. Semushin [id179](#),
 D. Sengupta [id56](#), V. Senthilkumar [id169](#), L. Serin [id66](#), M. Sessa [id76a,76b](#), H. Severini [id123](#),
 F. Sforza [id57b,57a](#), A. Sfyrla [id56](#), Q. Sha [id14](#), E. Shabalina [id55](#), H. Shaddix [id118](#), A.H. Shah [id33](#),
 R. Shaheen [id150](#), J.D. Shahinian [id131](#), M. Shamim [id37](#), L.Y. Shan [id14](#), M. Shapiro [id18a](#), A. Sharma [id37](#),
 A.S. Sharma [id170](#), P. Sharma [id30](#), P.B. Shatalov [id38](#), K. Shaw [id152](#), S.M. Shaw [id103](#), Q. Shen [id144a](#),
 D.J. Sheppard [id148](#), P. Sherwood [id98](#), L. Shi [id98](#), X. Shi [id14](#), S. Shimizu [id84](#), C.O. Shimmin [id178](#),
 I.P.J. Shipsey [id129,*](#), S. Shirabe [id90](#), M. Shiyakova [id39,aa](#), M.J. Shochet [id40](#), D.R. Shope [id128](#),
 B. Shrestha [id123](#), S. Shrestha [id122,al](#), I. Shreyber [id39](#), M.J. Shroff [id171](#), P. Sicho [id134](#), A.M. Sickles [id168](#),
 E. Sideras Haddad [id34g,166](#), A.C. Sidley [id117](#), A. Sidoti [id24b](#), F. Siegert [id50](#), Dj. Sijacki [id16](#), F. Sili [id92](#),
 J.M. Silva [id52](#), I. Silva Ferreira [id83b](#), M.V. Silva Oliveira [id30](#), S.B. Silverstein [id47a](#), S. Simion [id66](#),
 R. Simoniello [id37](#), E.L. Simpson [id103](#), H. Simpson [id152](#), L.R. Simpson [id6](#), S. Simsek [id82](#),
 S. Sindhu [id55](#), P. Sinervo [id161](#), S.N. Singh [id27](#), S. Singh [id30](#), S. Sinha [id48](#), S. Sinha [id103](#),
 M. Sioli [id24b,24a](#), K. Sioulas [id9](#), I. Siral [id37](#), E. Sitnikova [id48](#), J. Sjölin [id47a,47b](#), A. Skaf [id55](#),
 E. Skorda [id21](#), P. Skubic [id123](#), M. Slawinska [id87](#), I. Slazyk [id17](#), V. Smakhtin [id175](#), B.H. Smart [id137](#),
 S.Yu. Smirnov [id140b](#), Y. Smirnov [id82](#), L.N. Smirnova [id38,a](#), O. Smirnova [id100](#), A.C. Smith [id42](#),
 D.R. Smith [id165](#), J.L. Smith [id103](#), M.B. Smith [id35](#), R. Smith [id149](#), H. Smitmanns [id102](#), M. Smizanska [id93](#),
 K. Smolek [id135](#), P. Smolyanskiy [id135](#), A.A. Snesarev [id39](#), H.L. Snoek [id117](#), S. Snyder [id30](#),
 R. Sobie [id171,ac](#), A. Soffer [id157](#), C.A. Solans Sanchez [id37](#), E.Yu. Soldatov [id39](#), U. Soldevila [id169](#),
 A.A. Solodkov [id34g](#), S. Solomon [id27](#), A. Soloshenko [id39](#), K. Solovieva [id54](#), O.V. Solovyanov [id41](#),
 P. Sommer [id50](#), A. Sonay [id13](#), A. Sopczak [id135](#), A.L. Soppio [id52](#), F. Sopkova [id29b](#), J.D. Sorenson [id115](#),
 I.R. Sotarriva Alvarez [id141](#), V. Sothilingam [id63a](#), O.J. Soto Sandoval [id140c,140b](#), S. Sottocornola [id68](#),
 R. Soualah [id88a](#), Z. Soumami [id36e](#), D. South [id48](#), N. Soybelman [id175](#), S. Spagnolo [id70a,70b](#),
 M. Spalla [id112](#), D. Sperlich [id54](#), B. Spisso [id72a,72b](#), D.P. Spiteri [id59](#), L. Splendori [id104](#), M. Spousta [id136](#),
 E.J. Staats [id35](#), R. Stamen [id63a](#), E. Stanecka [id87](#), W. Stanek-Maslouska [id48](#), M.V. Stange [id50](#),
 B. Stanislaus [id18a](#), M.M. Stanitzki [id48](#), B. Stapf [id48](#), E.A. Starchenko [id38](#), G.H. Stark [id139](#), J. Stark [id91](#),
 P. Staroba [id134](#), P. Starovoitov [id88b](#), R. Staszewski [id87](#), G. Stavropoulos [id46](#), A. Steff [id37](#),
 P. Steinberg [id30](#), B. Stelzer [id148,162a](#), H.J. Stelzer [id132](#), O. Stelzer-Chilton [id162a](#), H. Stenzel [id58](#),
 T.J. Stevenson [id152](#), G.A. Stewart [id37](#), J.R. Stewart [id124](#), M.C. Stockton [id37](#), G. Stoicea [id28b](#),
 M. Stolarski [id133a](#), S. Stonjek [id112](#), A. Straessner [id50](#), J. Strandberg [id150](#), S. Strandberg [id47a,47b](#),
 M. Stratmann [id177](#), M. Strauss [id123](#), T. Strebler [id104](#), P. Strizenec [id29b](#), R. Ströhmer [id172](#),
 D.M. Strom [id126](#), R. Stroynowski [id45](#), A. Strubig [id47a,47b](#), S.A. Stucci [id30](#), B. Stugu [id17](#), J. Stupak [id123](#),
 N.A. Styles [id48](#), D. Su [id149](#), S. Su [id62](#), X. Su [id62](#), D. Suchy [id29a](#), K. Sugizaki [id131](#), V.V. Sulin [id38](#),
 M.J. Sullivan [id94](#), D.M.S. Sultan [id129](#), L. Sultanaliyeva [id38](#), S. Sultansoy [id3b](#), S. Sun [id176](#), W. Sun [id14](#),
 O. Sunneborn Gudnadottir [id167](#), N. Sur [id100](#), M.R. Sutton [id152](#), H. Suzuki [id163](#), M. Svatos [id134](#),
 P.N. Swallow [id33](#), M. Swiatlowski [id162a](#), T. Swirski [id172](#), I. Sykora [id29a](#), M. Sykora [id136](#),
 T. Sykora [id136](#), D. Ta [id102](#), K. Tackmann [id48,z](#), A. Taffard [id165](#), R. Tafirout [id162a](#), Y. Takubo [id84](#),
 M. Talby [id104](#), A.A. Talyshev [id38](#), K.C. Tam [id64b](#), N.M. Tamir [id157](#), A. Tanaka [id159](#), J. Tanaka [id159](#),
 R. Tanaka [id66](#), M. Tanasini [id151](#), Z. Tao [id170](#), S. Tapia Araya [id140f](#), S. Tapprogge [id102](#),
 A. Tarek Abouelfadl Mohamed [id109](#), S. Tarem [id156](#), K. Tariq [id14](#), G. Tarna [id28b](#), G.F. Tartarelli [id71a](#),
 M.J. Tartarin [id91](#), P. Tas [id136](#), M. Tasevsky [id134](#), E. Tassi [id44b,44a](#), A.C. Tate [id168](#), G. Tateno [id159](#),
 Y. Tayalati [id36e,ab](#), G.N. Taylor [id107](#), W. Taylor [id162b](#), A.S. Tegetmeier [id91](#), P. Teixeira-Dias [id97](#),
 J.J. Teoh [id161](#), K. Terashi [id159](#), J. Terron [id101](#), S. Terzo [id13](#), M. Testa [id53](#), R.J. Teuscher [id161,ac](#),
 A. Thaler [id79](#), O. Theiner [id56](#), T. Thevenaux-Pelzer [id104](#), D.W. Thomas [id97](#), J.P. Thomas [id21](#),
 E.A. Thompson [id18a](#), P.D. Thompson [id21](#), E. Thomson [id131](#), R.E. Thornberry [id45](#), C. Tian [id62](#),

Y. Tian ⁵⁶, V. Tikhomirov ⁸², Yu.A. Tikhonov ³⁹, S. Timoshenko ³⁸, D. Timoshyn ¹³⁶,
 E.X.L. Ting ¹, P. Tipton ¹⁷⁸, A. Tishelman-Charny ³⁰, K. Todome ¹⁴¹, S. Todorova-Nova ¹³⁶,
 S. Todt ⁵⁰, L. Toffolin ^{69a,69c}, M. Togawa ⁸⁴, J. Tojo ⁹⁰, S. Tokár ^{29a}, O. Toldaiev ⁶⁸,
 G. Tolkachev ¹⁰⁴, M. Tomoto ^{84,113}, L. Tompkins ^{149,o}, E. Torrence ¹²⁶, H. Torres ⁹¹,
 E. Torró Pastor ¹⁶⁹, M. Toscani ³¹, C. Tosciri ⁴⁰, M. Tost ¹¹, D.R. Tovey ¹⁴⁵, T. Trefzger ¹⁷²,
 P.M. Tricarico ¹³, A. Tricoli ³⁰, I.M. Trigger ^{162a}, S. Trincaz-Duvoid ¹³⁰, D.A. Trischuk ²⁷,
 A. Tropina ³⁹, L. Truong ^{34c}, M. Trzebinski ⁸⁷, A. Trzupiek ⁸⁷, F. Tsai ¹⁵¹, M. Tsai ¹⁰⁸,
 A. Tsiamis ¹⁵⁸, P.V. Tsiareshka ³⁹, S. Tsigaridas ^{162a}, A. Tsirigotis ^{158,v}, V. Tsiskaridze ¹⁶¹,
 E.G. Tskhadadze ^{155a}, M. Tsopoulou ¹⁵⁸, Y. Tsujikawa ⁸⁹, I.I. Tsukerman ³⁸, V. Tsulaia ^{18a},
 S. Tsuno ⁸⁴, K. Tsuru ¹²¹, D. Tsybychev ¹⁵¹, Y. Tu ^{64b}, A. Tudorache ^{28b}, V. Tudorache ^{28b},
 S. Turchikhin ^{57b,57a}, I. Turk Cakir ^{3a}, R. Turra ^{71a}, T. Turtuvshin ^{39,ad}, P.M. Tuts ⁴²,
 S. Tzamarias ^{158,d}, E. Tzovara ¹⁰², Y. Uematsu ⁸⁴, F. Ukegawa ¹⁶³, P.A. Ulloa Poblete ^{140c,140b},
 E.N. Umaka ³⁰, G. Unal ³⁷, A. Undrus ³⁰, G. Unel ¹⁶⁵, J. Urban ^{29b}, P. Urrejola ^{140a},
 G. Usai ⁸, R. Ushioda ¹⁶⁰, M. Usman ¹¹⁰, F. Ustuner ⁵², Z. Uysal ⁸², V. Vacek ¹³⁵,
 B. Vachon ¹⁰⁶, T. Vafeiadis ³⁷, A. Vaitkus ⁹⁸, C. Valderanis ¹¹¹, E. Valdes Santurio ^{47a,47b},
 M. Valente ^{162a}, S. Valentinetti ^{24b,24a}, A. Valero ¹⁶⁹, E. Valiente Moreno ¹⁶⁹, A. Vallier ⁹¹,
 J.A. Valls Ferrer ¹⁶⁹, D.R. Van Arneman ¹¹⁷, T.R. Van Daalen ¹⁴², A. Van Der Graaf ⁴⁹,
 H.Z. Van Der Schyf ^{34g}, P. Van Gemmeren ⁶, M. Van Rijnbach ³⁷, S. Van Stroud ⁹⁸,
 I. Van Vulpen ¹¹⁷, P. Vana ¹³⁶, M. Vanadia ^{76a,76b}, U.M. Vande Voorde ¹⁵⁰, W. Vandelli ³⁷,
 E.R. Vandewall ¹²⁴, D. Vannicola ¹⁵⁷, L. Vannoli ⁵³, R. Vari ^{75a}, M. Varma ¹⁷⁸, E.W. Varnes ⁷,
 C. Varni ^{18b}, D. Varouchas ⁶⁶, L. Varriale ¹⁶⁹, K.E. Varvell ¹⁵³, M.E. Vasile ^{28b}, L. Vaslin ⁸⁴,
 M.D. Vassilev ¹⁴⁹, A. Vasyukov ³⁹, L.M. Vaughan ¹²⁴, R. Vavricka ¹³⁶, T. Vazquez Schroeder ¹³,
 J. Veatch ³², V. Vecchio ¹⁰³, M.J. Veen ¹⁰⁵, I. Veliscek ³⁰, L.M. Veloce ¹⁶¹, F. Veloso ^{133a,133c},
 S. Veneziano ^{75a}, A. Ventura ^{70a,70b}, S. Ventura Gonzalez ¹³⁸, A. Verbytskyi ¹¹²,
 M. Verducci ^{74a,74b}, C. Vergis ⁹⁶, M. Verissimo De Araujo ^{83b}, W. Verkerke ¹¹⁷,
 J.C. Vermeulen ¹¹⁷, C. Vernieri ¹⁴⁹, M. Vessella ¹⁶⁵, M.C. Vetterli ^{148,ah}, A. Vgenopoulos ¹⁰²,
 N. Viaux Maira ^{140f}, T. Vickey ¹⁴⁵, O.E. Vickey Boeriu ¹⁴⁵, G.H.A. Viehhauser ¹²⁹, L. Vigani ^{63b},
 M. Vigl ¹¹², M. Villa ^{24b,24a}, M. Villaplana Perez ¹⁶⁹, E.M. Villhauer ⁴⁰, E. Vilucchi ⁵³,
 M.G. Vinciter ³⁵, A. Visibile ¹¹⁷, C. Vittori ³⁷, I. Vivarelli ^{24b,24a}, E. Voevodina ¹¹², F. Vogel ¹¹¹,
 J.C. Voigt ⁵⁰, P. Vokac ¹³⁵, Yu. Volkotrub ^{86b}, E. Von Toerne ²⁵, B. Vormwald ³⁷,
 K. Vorobev ⁵¹, M. Vos ¹⁶⁹, K. Voss ¹⁴⁷, M. Vozak ³⁷, L. Vozdecky ¹²³, N. Vranjes ¹⁶,
 M. Vranjes Milosavljevic ¹⁶, M. Vreeswijk ¹¹⁷, N.K. Vu ^{144b,144a}, R. Vuillermet ³⁷,
 O. Vujinovic ¹⁰², I. Vukotic ⁴⁰, I.K. Vyas ³⁵, J.F. Wack ³³, S. Wada ¹⁶³, C. Wagner ¹⁴⁹,
 J.M. Wagner ^{18a}, W. Wagner ¹⁷⁷, S. Wahdan ¹⁷⁷, H. Wahlberg ⁹², C.H. Waits ¹²³, J. Walder ¹³⁷,
 R. Walker ¹¹¹, W. Walkowiak ¹⁴⁷, A. Wall ¹³¹, E.J. Wallin ¹⁰⁰, T. Wamorkar ^{18a}, A.Z. Wang ¹³⁹,
 C. Wang ¹⁰², C. Wang ¹¹, H. Wang ^{18a}, J. Wang ^{64c}, P. Wang ¹⁰³, P. Wang ⁹⁸, R. Wang ⁶¹,
 R. Wang ⁶, S.M. Wang ¹⁵⁴, S. Wang ¹⁴, T. Wang ⁶², T. Wang ⁶², W.T. Wang ⁸⁰, W. Wang ¹⁴,
 X. Wang ¹⁶⁸, X. Wang ^{144a}, X. Wang ⁴⁸, Y. Wang ^{114a}, Y. Wang ⁶², Z. Wang ¹⁰⁸,
 Z. Wang ^{144b}, Z. Wang ¹⁰⁸, C. Wanotayaroj ⁸⁴, A. Warburton ¹⁰⁶, A.L. Warnerbring ¹⁴⁷,
 N. Warrack ⁵⁹, S. Waterhouse ⁹⁷, A.T. Watson ²¹, H. Watson ⁵², M.F. Watson ²¹, E. Watton ⁵⁹,
 G. Watts ¹⁴², B.M. Waugh ⁹⁸, J.M. Webb ⁵⁴, C. Weber ³⁰, H.A. Weber ¹⁹, M.S. Weber ²⁰,
 S.M. Weber ^{63a}, C. Wei ⁶², Y. Wei ⁵⁴, A.R. Weidberg ¹²⁹, E.J. Weik ¹²⁰, J. Weingarten ⁴⁹,
 C. Weiser ⁵⁴, C.J. Wells ⁴⁸, T. Wenaus ³⁰, B. Wendland ⁴⁹, T. Wengler ³⁷, N.S. Wenke ¹¹²,
 N. Wermes ²⁵, M. Wessels ^{63a}, A.M. Wharton ⁹³, A.S. White ⁶¹, A. White ⁸, M.J. White ¹,
 D. Whiteson ¹⁶⁵, L. Wickremasinghe ¹²⁷, W. Wiedenmann ¹⁷⁶, M. Wielers ¹³⁷, R. Wierda ¹⁵⁰,
 C. Wiglesworth ⁴³, H.G. Wilkens ³⁷, J.J.H. Wilkinson ³³, D.M. Williams ⁴², H.H. Williams ¹³¹,
 S. Williams ³³, S. Willocq ¹⁰⁵, B.J. Wilson ¹⁰³, D.J. Wilson ¹⁰³, P.J. Windischhofer ⁴⁰,

F.I. Winkel ¹, F. Winklmeier ¹²⁶, B.T. Winter ⁵⁴, M. Wittgen ¹⁴⁹, M. Wobisch ⁹⁹, T. Wojtkowski ⁶⁰, Z. Wolffs ¹¹⁷, J. Wollrath ³⁷, M.W. Wolter ⁸⁷, H. Wolters ^{133a,133c}, M.C. Wong ¹³⁹, E.L. Woodward ⁴², S.D. Worm ⁴⁸, B.K. Wosiek ⁸⁷, K.W. Woźniak ⁸⁷, S. Wozniowski ⁵⁵, K. Wraight ⁵⁹, C. Wu ¹⁶¹, C. Wu ²¹, J. Wu ¹⁵⁹, M. Wu ^{114b}, M. Wu ¹¹⁶, S.L. Wu ¹⁷⁶, S. Wu ¹⁴, X. Wu ⁶², Y. Wu ⁶², Z. Wu ⁴, J. Wuerzinger ¹¹², T.R. Wyatt ¹⁰³, B.M. Wynne ⁵², S. Xella ⁴³, L. Xia ^{114a}, M. Xia ¹⁵, M. Xie ⁶², A. Xiong ¹²⁶, J. Xiong ^{18a}, D. Xu ¹⁴, H. Xu ⁶², L. Xu ⁶², R. Xu ¹³¹, T. Xu ¹⁰⁸, Y. Xu ¹⁴², Z. Xu ⁵², Z. Xu ^{114a}, B. Yabsley ¹⁵³, S. Yacoob ^{34a}, Y. Yamaguchi ⁸⁴, E. Yamashita ¹⁵⁹, H. Yamauchi ¹⁶³, T. Yamazaki ^{18a}, Y. Yamazaki ⁸⁵, S. Yan ⁵⁹, Z. Yan ¹⁰⁵, H.J. Yang ^{144a,144b}, H.T. Yang ⁶², S. Yang ⁶², T. Yang ^{64c}, X. Yang ³⁷, X. Yang ¹⁴, Y. Yang ¹⁵⁹, Y. Yang ⁶², W-M. Yao ^{18a}, C.L. Yardley ¹⁵², J. Ye ¹⁴, S. Ye ³⁰, X. Ye ⁶², Y. Yeh ⁹⁸, I. Yeletsikh ³⁹, B. Yeo ^{18b}, M.R. Yexley ⁹⁸, T.P. Yildirim ¹²⁹, P. Yin ⁴², K. Yorita ¹⁷⁴, C.J.S. Young ³⁷, C. Young ¹⁴⁹, N.D. Young ¹²⁶, Y. Yu ⁶², J. Yuan ^{14,114c}, M. Yuan ¹⁰⁸, R. Yuan ^{144b,144a}, L. Yue ⁹⁸, M. Zaazoua ⁶², B. Zabinski ⁸⁷, I. Zahir ^{36a}, A. Zaid ^{57b,57a}, Z.K. Zak ⁸⁷, T. Zakareishvili ¹⁶⁹, S. Zambito ⁵⁶, J.A. Zamora Saa ^{140d}, J. Zang ¹⁵⁹, D. Zanzi ⁵⁴, R. Zanzottera ^{71a,71b}, O. Zaplatilek ¹³⁵, C. Zeitnitz ¹⁷⁷, H. Zeng ¹⁴, J.C. Zeng ¹⁶⁸, D.T. Zenger Jr ²⁷, O. Zenin ³⁸, T. Ženiš ^{29a}, S. Zenz ⁹⁶, D. Zerwas ⁶⁶, M. Zhai ^{14,114c}, D.F. Zhang ¹⁴⁵, G. Zhang ¹⁴, J. Zhang ^{143a}, J. Zhang ⁶, K. Zhang ^{14,114c}, L. Zhang ⁶², L. Zhang ^{114a}, P. Zhang ^{14,114c}, R. Zhang ¹⁷⁶, S. Zhang ⁹¹, T. Zhang ¹⁵⁹, X. Zhang ^{144a}, Y. Zhang ¹⁴², Y. Zhang ⁹⁸, Y. Zhang ⁶², Y. Zhang ^{114a}, Z. Zhang ^{18a}, Z. Zhang ^{143a}, Z. Zhang ⁶⁶, H. Zhao ¹⁴², T. Zhao ^{143a}, Y. Zhao ³⁵, Z. Zhao ⁶², Z. Zhao ⁶², A. Zhemchugov ³⁹, J. Zheng ^{114a}, K. Zheng ¹⁶⁸, X. Zheng ⁶², Z. Zheng ¹⁴⁹, D. Zhong ¹⁶⁸, B. Zhou ¹⁰⁸, H. Zhou ⁷, N. Zhou ^{144a}, Y. Zhou ¹⁵, Y. Zhou ^{114a}, Y. Zhou ⁷, C.G. Zhu ^{143a}, J. Zhu ¹⁰⁸, X. Zhu ^{144b}, Y. Zhu ^{144a}, Y. Zhu ⁶², X. Zhuang ¹⁴, K. Zhukov ⁶⁸, N.I. Zimine ³⁹, J. Zinsser ^{63b}, M. Ziolkowski ¹⁴⁷, L. Živković ¹⁶, A. Zoccoli ^{24b,24a}, K. Zoch ⁶¹, T.G. Zorbas ¹⁴⁵, O. Zormpa ⁴⁶, L. Zwalinski ³⁷.

¹Department of Physics, University of Adelaide, Adelaide; Australia.

²Department of Physics, University of Alberta, Edmonton AB; Canada.

³(^a)Department of Physics, Ankara University, Ankara; (^b)Division of Physics, TOBB University of Economics and Technology, Ankara; Türkiye.

⁴LAPP, Université Savoie Mont Blanc, CNRS/IN2P3, Annecy; France.

⁵APC, Université Paris Cité, CNRS/IN2P3, Paris; France.

⁶High Energy Physics Division, Argonne National Laboratory, Argonne IL; United States of America.

⁷Department of Physics, University of Arizona, Tucson AZ; United States of America.

⁸Department of Physics, University of Texas at Arlington, Arlington TX; United States of America.

⁹Physics Department, National and Kapodistrian University of Athens, Athens; Greece.

¹⁰Physics Department, National Technical University of Athens, Zografou; Greece.

¹¹Department of Physics, University of Texas at Austin, Austin TX; United States of America.

¹²Institute of Physics, Azerbaijan Academy of Sciences, Baku; Azerbaijan.

¹³Institut de Física d'Altes Energies (IFAE), Barcelona Institute of Science and Technology, Barcelona; Spain.

¹⁴Institute of High Energy Physics, Chinese Academy of Sciences, Beijing; China.

¹⁵Physics Department, Tsinghua University, Beijing; China.

¹⁶Institute of Physics, University of Belgrade, Belgrade; Serbia.

¹⁷Department for Physics and Technology, University of Bergen, Bergen; Norway.

¹⁸(^a)Physics Division, Lawrence Berkeley National Laboratory, Berkeley CA; (^b)University of California, Berkeley CA; United States of America.

- ¹⁹Institut für Physik, Humboldt Universität zu Berlin, Berlin; Germany.
- ²⁰Albert Einstein Center for Fundamental Physics and Laboratory for High Energy Physics, University of Bern, Bern; Switzerland.
- ²¹School of Physics and Astronomy, University of Birmingham, Birmingham; United Kingdom.
- ²²(^a) Department of Physics, Bogazici University, Istanbul; (^b) Department of Physics Engineering, Gaziantep University, Gaziantep; (^c) Department of Physics, Istanbul University, Istanbul; Türkiye.
- ²³(^a) Facultad de Ciencias y Centro de Investigaciones, Universidad Antonio Nariño, Bogotá; (^b) Departamento de Física, Universidad Nacional de Colombia, Bogotá; Colombia.
- ²⁴(^a) Dipartimento di Fisica e Astronomia A. Righi, Università di Bologna, Bologna; (^b) INFN Sezione di Bologna; Italy.
- ²⁵Physikalisches Institut, Universität Bonn, Bonn; Germany.
- ²⁶Department of Physics, Boston University, Boston MA; United States of America.
- ²⁷Department of Physics, Brandeis University, Waltham MA; United States of America.
- ²⁸(^a) Transilvania University of Brasov, Brasov; (^b) Horia Hulubei National Institute of Physics and Nuclear Engineering, Bucharest; (^c) Department of Physics, Alexandru Ioan Cuza University of Iasi, Iasi; (^d) National Institute for Research and Development of Isotopic and Molecular Technologies, Physics Department, Cluj-Napoca; (^e) National University of Science and Technology Politehnica, Bucharest; (^f) West University in Timisoara, Timisoara; (^g) Faculty of Physics, University of Bucharest, Bucharest; Romania.
- ²⁹(^a) Faculty of Mathematics, Physics and Informatics, Comenius University, Bratislava; (^b) Department of Subnuclear Physics, Institute of Experimental Physics of the Slovak Academy of Sciences, Kosice; Slovak Republic.
- ³⁰Physics Department, Brookhaven National Laboratory, Upton NY; United States of America.
- ³¹Universidad de Buenos Aires, Facultad de Ciencias Exactas y Naturales, Departamento de Física, y CONICET, Instituto de Física de Buenos Aires (IFIBA), Buenos Aires; Argentina.
- ³²California State University, CA; United States of America.
- ³³Cavendish Laboratory, University of Cambridge, Cambridge; United Kingdom.
- ³⁴(^a) Department of Physics, University of Cape Town, Cape Town; (^b) iThemba Labs, Western Cape; (^c) Department of Mechanical Engineering Science, University of Johannesburg, Johannesburg; (^d) National Institute of Physics, University of the Philippines Diliman (Philippines); (^e) University of South Africa, Department of Physics, Pretoria; (^f) University of Zululand, KwaDlangezwa; (^g) School of Physics, University of the Witwatersrand, Johannesburg; South Africa.
- ³⁵Department of Physics, Carleton University, Ottawa ON; Canada.
- ³⁶(^a) Faculté des Sciences Ain Chock, Université Hassan II de Casablanca; (^b) Faculté des Sciences, Université Ibn-Tofail, Kénitra; (^c) Faculté des Sciences Semlalia, Université Cadi Ayyad, LPHEA-Marrakech; (^d) LPMR, Faculté des Sciences, Université Mohamed Premier, Oujda; (^e) Faculté des sciences, Université Mohammed V, Rabat; (^f) Institute of Applied Physics, Mohammed VI Polytechnic University, Ben Guerir; Morocco.
- ³⁷CERN, Geneva; Switzerland.
- ³⁸Affiliated with an institute formerly covered by a cooperation agreement with CERN.
- ³⁹Affiliated with an international laboratory covered by a cooperation agreement with CERN.
- ⁴⁰Enrico Fermi Institute, University of Chicago, Chicago IL; United States of America.
- ⁴¹LPC, Université Clermont Auvergne, CNRS/IN2P3, Clermont-Ferrand; France.
- ⁴²Nevis Laboratory, Columbia University, Irvington NY; United States of America.
- ⁴³Niels Bohr Institute, University of Copenhagen, Copenhagen; Denmark.
- ⁴⁴(^a) Dipartimento di Fisica, Università della Calabria, Rende; (^b) INFN Gruppo Collegato di Cosenza, Laboratori Nazionali di Frascati; Italy.
- ⁴⁵Physics Department, Southern Methodist University, Dallas TX; United States of America.

- ⁴⁶National Centre for Scientific Research "Demokritos", Agia Paraskevi; Greece.
- ⁴⁷(^a)Department of Physics, Stockholm University;(^b)Oskar Klein Centre, Stockholm; Sweden.
- ⁴⁸Deutsches Elektronen-Synchrotron DESY, Hamburg and Zeuthen; Germany.
- ⁴⁹Fakultät Physik , Technische Universität Dortmund, Dortmund; Germany.
- ⁵⁰Institut für Kern- und Teilchenphysik, Technische Universität Dresden, Dresden; Germany.
- ⁵¹Department of Physics, Duke University, Durham NC; United States of America.
- ⁵²SUPA - School of Physics and Astronomy, University of Edinburgh, Edinburgh; United Kingdom.
- ⁵³INFN e Laboratori Nazionali di Frascati, Frascati; Italy.
- ⁵⁴Physikalisches Institut, Albert-Ludwigs-Universität Freiburg, Freiburg; Germany.
- ⁵⁵II. Physikalisches Institut, Georg-August-Universität Göttingen, Göttingen; Germany.
- ⁵⁶Département de Physique Nucléaire et Corpusculaire, Université de Genève, Genève; Switzerland.
- ⁵⁷(^a)Dipartimento di Fisica, Università di Genova, Genova;(^b)INFN Sezione di Genova; Italy.
- ⁵⁸II. Physikalisches Institut, Justus-Liebig-Universität Giessen, Giessen; Germany.
- ⁵⁹SUPA - School of Physics and Astronomy, University of Glasgow, Glasgow; United Kingdom.
- ⁶⁰LPSC, Université Grenoble Alpes, CNRS/IN2P3, Grenoble INP, Grenoble; France.
- ⁶¹Laboratory for Particle Physics and Cosmology, Harvard University, Cambridge MA; United States of America.
- ⁶²Department of Modern Physics and State Key Laboratory of Particle Detection and Electronics, University of Science and Technology of China, Hefei; China.
- ⁶³(^a)Kirchhoff-Institut für Physik, Ruprecht-Karls-Universität Heidelberg, Heidelberg;(^b)Physikalisches Institut, Ruprecht-Karls-Universität Heidelberg, Heidelberg; Germany.
- ⁶⁴(^a)Department of Physics, Chinese University of Hong Kong, Shatin, N.T., Hong Kong;(^b)Department of Physics, University of Hong Kong, Hong Kong;(^c)Department of Physics and Institute for Advanced Study, Hong Kong University of Science and Technology, Clear Water Bay, Kowloon, Hong Kong; China.
- ⁶⁵Department of Physics, National Tsing Hua University, Hsinchu; Taiwan.
- ⁶⁶IJCLab, Université Paris-Saclay, CNRS/IN2P3, 91405, Orsay; France.
- ⁶⁷Centro Nacional de Microelectrónica (IMB-CNM-CSIC), Barcelona; Spain.
- ⁶⁸Department of Physics, Indiana University, Bloomington IN; United States of America.
- ⁶⁹(^a)INFN Gruppo Collegato di Udine, Sezione di Trieste, Udine;(^b)ICTP, Trieste;(^c)Dipartimento Politecnico di Ingegneria e Architettura, Università di Udine, Udine; Italy.
- ⁷⁰(^a)INFN Sezione di Lecce;(^b)Dipartimento di Matematica e Fisica, Università del Salento, Lecce; Italy.
- ⁷¹(^a)INFN Sezione di Milano;(^b)Dipartimento di Fisica, Università di Milano, Milano; Italy.
- ⁷²(^a)INFN Sezione di Napoli;(^b)Dipartimento di Fisica, Università di Napoli, Napoli; Italy.
- ⁷³(^a)INFN Sezione di Pavia;(^b)Dipartimento di Fisica, Università di Pavia, Pavia; Italy.
- ⁷⁴(^a)INFN Sezione di Pisa;(^b)Dipartimento di Fisica E. Fermi, Università di Pisa, Pisa; Italy.
- ⁷⁵(^a)INFN Sezione di Roma;(^b)Dipartimento di Fisica, Sapienza Università di Roma, Roma; Italy.
- ⁷⁶(^a)INFN Sezione di Roma Tor Vergata;(^b)Dipartimento di Fisica, Università di Roma Tor Vergata, Roma; Italy.
- ⁷⁷(^a)INFN Sezione di Roma Tre;(^b)Dipartimento di Matematica e Fisica, Università Roma Tre, Roma; Italy.
- ⁷⁸(^a)INFN-TIFPA;(^b)Università degli Studi di Trento, Trento; Italy.
- ⁷⁹Universität Innsbruck, Department of Astro and Particle Physics, Innsbruck; Austria.
- ⁸⁰University of Iowa, Iowa City IA; United States of America.
- ⁸¹Department of Physics and Astronomy, Iowa State University, Ames IA; United States of America.
- ⁸²Istinye University, Sariyer, Istanbul; Türkiye.
- ⁸³(^a)Departamento de Engenharia Elétrica, Universidade Federal de Juiz de Fora (UFJF), Juiz de Fora;(^b)Universidade Federal do Rio De Janeiro COPPE/EE/IF, Rio de Janeiro;(^c)Instituto de Física,

Universidade de São Paulo, São Paulo;^(d)Rio de Janeiro State University, Rio de Janeiro;^(e)Federal University of Bahia, Bahia; Brazil.

⁸⁴KEK, High Energy Accelerator Research Organization, Tsukuba; Japan.

⁸⁵Graduate School of Science, Kobe University, Kobe; Japan.

⁸⁶^(a) AGH University of Krakow, Faculty of Physics and Applied Computer Science, Krakow;^(b) Marian Smoluchowski Institute of Physics, Jagiellonian University, Krakow; Poland.

⁸⁷Institute of Nuclear Physics Polish Academy of Sciences, Krakow; Poland.

⁸⁸^(a) Khalifa University of Science and Technology, Abu Dhabi;^(b) University of Sharjah, Sharjah; United Arab Emirates.

⁸⁹Faculty of Science, Kyoto University, Kyoto; Japan.

⁹⁰Research Center for Advanced Particle Physics and Department of Physics, Kyushu University, Fukuoka ; Japan.

⁹¹L2IT, Université de Toulouse, CNRS/IN2P3, UPS, Toulouse; France.

⁹²Instituto de Física La Plata, Universidad Nacional de La Plata and CONICET, La Plata; Argentina.

⁹³Physics Department, Lancaster University, Lancaster; United Kingdom.

⁹⁴Oliver Lodge Laboratory, University of Liverpool, Liverpool; United Kingdom.

⁹⁵Department of Experimental Particle Physics, Jožef Stefan Institute and Department of Physics, University of Ljubljana, Ljubljana; Slovenia.

⁹⁶Department of Physics and Astronomy, Queen Mary University of London, London; United Kingdom.

⁹⁷Department of Physics, Royal Holloway University of London, Egham; United Kingdom.

⁹⁸Department of Physics and Astronomy, University College London, London; United Kingdom.

⁹⁹Louisiana Tech University, Ruston LA; United States of America.

¹⁰⁰Fysiska institutionen, Lunds universitet, Lund; Sweden.

¹⁰¹Departamento de Física Teórica C-15 and CIAFF, Universidad Autónoma de Madrid, Madrid; Spain.

¹⁰²Institut für Physik, Universität Mainz, Mainz; Germany.

¹⁰³School of Physics and Astronomy, University of Manchester, Manchester; United Kingdom.

¹⁰⁴CPPM, Aix-Marseille Université, CNRS/IN2P3, Marseille; France.

¹⁰⁵Department of Physics, University of Massachusetts, Amherst MA; United States of America.

¹⁰⁶Department of Physics, McGill University, Montreal QC; Canada.

¹⁰⁷School of Physics, University of Melbourne, Victoria; Australia.

¹⁰⁸Department of Physics, University of Michigan, Ann Arbor MI; United States of America.

¹⁰⁹Department of Physics and Astronomy, Michigan State University, East Lansing MI; United States of America.

¹¹⁰Group of Particle Physics, University of Montreal, Montreal QC; Canada.

¹¹¹Fakultät für Physik, Ludwig-Maximilians-Universität München, München; Germany.

¹¹²Max-Planck-Institut für Physik (Werner-Heisenberg-Institut), München; Germany.

¹¹³Graduate School of Science and Kobayashi-Maskawa Institute, Nagoya University, Nagoya; Japan.

¹¹⁴^(a) Department of Physics, Nanjing University, Nanjing;^(b) School of Science, Shenzhen Campus of Sun Yat-sen University;^(c) University of Chinese Academy of Science (UCAS), Beijing; China.

¹¹⁵Department of Physics and Astronomy, University of New Mexico, Albuquerque NM; United States of America.

¹¹⁶Institute for Mathematics, Astrophysics and Particle Physics, Radboud University/Nikhef, Nijmegen; Netherlands.

¹¹⁷Nikhef National Institute for Subatomic Physics and University of Amsterdam, Amsterdam; Netherlands.

¹¹⁸Department of Physics, Northern Illinois University, DeKalb IL; United States of America.

¹¹⁹^(a) New York University Abu Dhabi, Abu Dhabi;^(b) United Arab Emirates University, Al Ain; United

Arab Emirates.

¹²⁰Department of Physics, New York University, New York NY; United States of America.

¹²¹Ochanomizu University, Otsuka, Bunkyo-ku, Tokyo; Japan.

¹²²Ohio State University, Columbus OH; United States of America.

¹²³Homer L. Dodge Department of Physics and Astronomy, University of Oklahoma, Norman OK; United States of America.

¹²⁴Department of Physics, Oklahoma State University, Stillwater OK; United States of America.

¹²⁵Palacký University, Joint Laboratory of Optics, Olomouc; Czech Republic.

¹²⁶Institute for Fundamental Science, University of Oregon, Eugene, OR; United States of America.

¹²⁷Graduate School of Science, Osaka University, Osaka; Japan.

¹²⁸Department of Physics, University of Oslo, Oslo; Norway.

¹²⁹Department of Physics, Oxford University, Oxford; United Kingdom.

¹³⁰LPNHE, Sorbonne Université, Université Paris Cité, CNRS/IN2P3, Paris; France.

¹³¹Department of Physics, University of Pennsylvania, Philadelphia PA; United States of America.

¹³²Department of Physics and Astronomy, University of Pittsburgh, Pittsburgh PA; United States of America.

¹³³(^a)Laboratório de Instrumentação e Física Experimental de Partículas - LIP, Lisboa; (^b)Departamento de Física, Faculdade de Ciências, Universidade de Lisboa, Lisboa; (^c)Departamento de Física, Universidade de Coimbra, Coimbra; (^d)Centro de Física Nuclear da Universidade de Lisboa, Lisboa; (^e)Departamento de Física, Escola de Ciências, Universidade do Minho, Braga; (^f)Departamento de Física Teórica y del Cosmos, Universidad de Granada, Granada (Spain); (^g)Departamento de Física, Instituto Superior Técnico, Universidade de Lisboa, Lisboa; Portugal.

¹³⁴Institute of Physics of the Czech Academy of Sciences, Prague; Czech Republic.

¹³⁵Czech Technical University in Prague, Prague; Czech Republic.

¹³⁶Charles University, Faculty of Mathematics and Physics, Prague; Czech Republic.

¹³⁷Particle Physics Department, Rutherford Appleton Laboratory, Didcot; United Kingdom.

¹³⁸IRFU, CEA, Université Paris-Saclay, Gif-sur-Yvette; France.

¹³⁹Santa Cruz Institute for Particle Physics, University of California Santa Cruz, Santa Cruz CA; United States of America.

¹⁴⁰(^a)Departamento de Física, Pontificia Universidad Católica de Chile, Santiago; (^b)Millennium Institute for Subatomic physics at high energy frontier (SAPHIR), Santiago; (^c)Instituto de Investigación Multidisciplinario en Ciencia y Tecnología, y Departamento de Física, Universidad de La Serena; (^d)Universidad Andres Bello, Department of Physics, Santiago; (^e)Instituto de Alta Investigación, Universidad de Tarapacá, Arica; (^f)Departamento de Física, Universidad Técnica Federico Santa María, Valparaíso; Chile.

¹⁴¹Department of Physics, Institute of Science, Tokyo; Japan.

¹⁴²Department of Physics, University of Washington, Seattle WA; United States of America.

¹⁴³(^a)Institute of Frontier and Interdisciplinary Science and Key Laboratory of Particle Physics and Particle Irradiation (MOE), Shandong University, Qingdao; (^b)School of Physics, Zhengzhou University; China.

¹⁴⁴(^a)School of Physics and Astronomy, Shanghai Jiao Tong University, Key Laboratory for Particle Astrophysics and Cosmology (MOE), SKLPPC, Shanghai; (^b)Tung-Dao Lee Institute, Shanghai; China.

¹⁴⁵Department of Physics and Astronomy, University of Sheffield, Sheffield; United Kingdom.

¹⁴⁶Department of Physics, Shinshu University, Nagano; Japan.

¹⁴⁷Department Physik, Universität Siegen, Siegen; Germany.

¹⁴⁸Department of Physics, Simon Fraser University, Burnaby BC; Canada.

¹⁴⁹SLAC National Accelerator Laboratory, Stanford CA; United States of America.

¹⁵⁰Department of Physics, Royal Institute of Technology, Stockholm; Sweden.

- ¹⁵¹Departments of Physics and Astronomy, Stony Brook University, Stony Brook NY; United States of America.
- ¹⁵²Department of Physics and Astronomy, University of Sussex, Brighton; United Kingdom.
- ¹⁵³School of Physics, University of Sydney, Sydney; Australia.
- ¹⁵⁴Institute of Physics, Academia Sinica, Taipei; Taiwan.
- ¹⁵⁵^(a)E. Andronikashvili Institute of Physics, Iv. Javakhishvili Tbilisi State University, Tbilisi;^(b)High Energy Physics Institute, Tbilisi State University, Tbilisi;^(c)University of Georgia, Tbilisi; Georgia.
- ¹⁵⁶Department of Physics, Technion, Israel Institute of Technology, Haifa; Israel.
- ¹⁵⁷Raymond and Beverly Sackler School of Physics and Astronomy, Tel Aviv University, Tel Aviv; Israel.
- ¹⁵⁸Department of Physics, Aristotle University of Thessaloniki, Thessaloniki; Greece.
- ¹⁵⁹International Center for Elementary Particle Physics and Department of Physics, University of Tokyo, Tokyo; Japan.
- ¹⁶⁰Graduate School of Science and Technology, Tokyo Metropolitan University, Tokyo; Japan.
- ¹⁶¹Department of Physics, University of Toronto, Toronto ON; Canada.
- ¹⁶²^(a)TRIUMF, Vancouver BC;^(b)Department of Physics and Astronomy, York University, Toronto ON; Canada.
- ¹⁶³Division of Physics and Tomonaga Center for the History of the Universe, Faculty of Pure and Applied Sciences, University of Tsukuba, Tsukuba; Japan.
- ¹⁶⁴Department of Physics and Astronomy, Tufts University, Medford MA; United States of America.
- ¹⁶⁵Department of Physics and Astronomy, University of California Irvine, Irvine CA; United States of America.
- ¹⁶⁶University of West Attica, Athens; Greece.
- ¹⁶⁷Department of Physics and Astronomy, University of Uppsala, Uppsala; Sweden.
- ¹⁶⁸Department of Physics, University of Illinois, Urbana IL; United States of America.
- ¹⁶⁹Instituto de Física Corpuscular (IFIC), Centro Mixto Universidad de Valencia - CSIC, Valencia; Spain.
- ¹⁷⁰Department of Physics, University of British Columbia, Vancouver BC; Canada.
- ¹⁷¹Department of Physics and Astronomy, University of Victoria, Victoria BC; Canada.
- ¹⁷²Fakultät für Physik und Astronomie, Julius-Maximilians-Universität Würzburg, Würzburg; Germany.
- ¹⁷³Department of Physics, University of Warwick, Coventry; United Kingdom.
- ¹⁷⁴Waseda University, Tokyo; Japan.
- ¹⁷⁵Department of Particle Physics and Astrophysics, Weizmann Institute of Science, Rehovot; Israel.
- ¹⁷⁶Department of Physics, University of Wisconsin, Madison WI; United States of America.
- ¹⁷⁷Fakultät für Mathematik und Naturwissenschaften, Fachgruppe Physik, Bergische Universität Wuppertal, Wuppertal; Germany.
- ¹⁷⁸Department of Physics, Yale University, New Haven CT; United States of America.
- ¹⁷⁹Yerevan Physics Institute, Yerevan; Armenia.
- ^a Also at Affiliated with an institute formerly covered by a cooperation agreement with CERN.
- ^b Also at An-Najah National University, Nablus; Palestine.
- ^c Also at Borough of Manhattan Community College, City University of New York, New York NY; United States of America.
- ^d Also at Center for Interdisciplinary Research and Innovation (CIRI-AUTH), Thessaloniki; Greece.
- ^e Also at Centre of Physics of the Universities of Minho and Porto (CF-UM-UP); Portugal.
- ^f Also at CERN, Geneva; Switzerland.
- ^g Also at CMD-AC UNEC Research Center, Azerbaijan State University of Economics (UNEC); Azerbaijan.
- ^h Also at Département de Physique Nucléaire et Corpusculaire, Université de Genève, Genève; Switzerland.

- ⁱ Also at Departament de Fisica de la Universitat Autònoma de Barcelona, Barcelona; Spain.
- ^j Also at Department of Financial and Management Engineering, University of the Aegean, Chios; Greece.
- ^k Also at Department of Mathematical Sciences, University of South Africa, Johannesburg; South Africa.
- ^l Also at Department of Modern Physics and State Key Laboratory of Particle Detection and Electronics, University of Science and Technology of China, Hefei; China.
- ^m Also at Department of Physics, Bolu Abant İzzet Baysal University, Bolu; Türkiye.
- ⁿ Also at Department of Physics, King's College London, London; United Kingdom.
- ^o Also at Department of Physics, Stanford University, Stanford CA; United States of America.
- ^p Also at Department of Physics, Stellenbosch University; South Africa.
- ^q Also at Department of Physics, University of Fribourg, Fribourg; Switzerland.
- ^r Also at Department of Physics, University of Thessaly; Greece.
- ^s Also at Department of Physics, Westmont College, Santa Barbara; United States of America.
- ^t Also at Faculty of Physics, Sofia University, 'St. Kliment Ohridski', Sofia; Bulgaria.
- ^u Also at Faculty of Physics, University of Bucharest ; Romania.
- ^v Also at Hellenic Open University, Patras; Greece.
- ^w Also at Henan University; China.
- ^x Also at Imam Mohammad Ibn Saud Islamic University; Saudi Arabia.
- ^y Also at Institutio Catalana de Recerca i Estudis Avancats, ICREA, Barcelona; Spain.
- ^z Also at Institut für Experimentalphysik, Universität Hamburg, Hamburg; Germany.
- ^{aa} Also at Institute for Nuclear Research and Nuclear Energy (INRNE) of the Bulgarian Academy of Sciences, Sofia; Bulgaria.
- ^{ab} Also at Institute of Applied Physics, Mohammed VI Polytechnic University, Ben Guerir; Morocco.
- ^{ac} Also at Institute of Particle Physics (IPP); Canada.
- ^{ad} Also at Institute of Physics and Technology, Mongolian Academy of Sciences, Ulaanbaatar; Mongolia.
- ^{ae} Also at Institute of Physics, Azerbaijan Academy of Sciences, Baku; Azerbaijan.
- ^{af} Also at National Institute of Physics, University of the Philippines Diliman (Philippines); Philippines.
- ^{ag} Also at The Collaborative Innovation Center of Quantum Matter (CICQM), Beijing; China.
- ^{ah} Also at TRIUMF, Vancouver BC; Canada.
- ^{ai} Also at Università di Napoli Parthenope, Napoli; Italy.
- ^{aj} Also at University of Colorado Boulder, Department of Physics, Colorado; United States of America.
- ^{ak} Also at University of Sienna; Italy.
- ^{al} Also at Washington College, Chestertown, MD; United States of America.
- ^{am} Also at Yeditepe University, Physics Department, Istanbul; Türkiye.
- * Deceased